MECHANISMS BY WHICH CALCIUM REGULATES THE HUMAN CARDIAC

VOLTAGE-GATED SODIUM CHANNEL HH1

By

Vikas N. Shah

Dissertation

Submitted to the Faculty of the

Graduate School of Vanderbilt University

in partial fulfillment of the requirements

for the degree of

DOCTOR OF PHILOSOPHY

in

Biochemistry

August, 2005

Nashville, Tennessee

Approved:

Professor Walter Chazin

Professor Mark Anderson

Professor Richard Armstrong

Professor Andrzej Krezel

Professor Charles Sanders

For my mother and father,
whose courageous foray into a new country
allowed me to pursue my dreams.

ACKNOWLEDGEMENTS

This dissertation could not have been completed were it not for the scientific contributions and personal support of a great many people. First and foremost, I'd like to thank my mentor, Dr. Walter Chazin, for supporting me in pursuing a project new to the lab, for understanding and support when I needed to take a year off, for encouragement and experimental advice, and, yes, even for the swift kick in the pants when I needed it. I'd like to thank my committee members, Dr. Mark Anderson, Dr. Richard Armstrong, Dr. Andrzej Krezel, and Dr. Charles Sanders for providing me with good advice and clear goals for completing my dissertation work. Our collaboration with Dr. Jeffrey Balser, who served on my committee during the early part of my graduate training, allowed us to do some very exciting interdisciplinary work. Deserving special recognition is Dr. Tammy Wingo, who initially identified the EF-hand computationally and did all of electrophysiological experiments described in this dissertation. Susan "Chromatography" Meyn and Svetlana Stepanovic provided invaluable technical assistance. Finally, I'd like to thank the Vanderbilt Medical Scientist Training Program, without which I wouldn't be here today.

Those are the people who helped me with my science. I'd also like to thank everyone who kept me sane and human – in my opinion, a remarkable feat in graduate school: from New Jersey, Subir, Mike and Ivan; from my Michigan State days, Bennett, Mark, Joe, Ryan, Brian and the whole crew I've met since then; here in Nashville, Christina, Anna, Jeremy, Ben, Cameron, and Miriam.

And, of course, Leta. For the last two years, you've made everything better. Thank you for everything.

TABLE OF CONTENTS

Appendix

LIST OF TABLES

LIST OF FIGURES

LIST OF ABBREVIATIONS

ATP	adenosine triphosphate
bis-Tris	Bis(2-hydroxyethyl)iminotris(hydroxymethyl)methane
CaM	calmodulin
CaMKII	calmodulin-dependent protein kinase II
cAMP	cyclic adenosine-monophosphate
BAPTA	1,2-bis(2-aminophenoxy)ethane-N,N,N',N'-tetraacetic acid
BME	beta-mercapto-ethanol
DDT	4,4'-(2,2,2-trichloroethane-1,1-diyl)bis(chlorobenzene)
DTT	dithiothreitol
EDTA	ethylenediaminotetraacetic acid
EF-hand	common calcium-binding helix-loop-helix motif
EGTA	ethylenedioxy-diethylene-dinitrilo-tetraacetic acid
EKG	electrocardiogram
FBS	fetal bovine serum
FHF1b	fibroblast growth factor homologous factor 1b
GPCR	GTPase-protein coupled receptor
HEPES	4-(2-hydroxyethyl)-1-piperazineethanesulfonic acid
hH1	$Na_V1.5$, Scn5a; human cardiac voltage-gated sodium channel
hH1-CTD-93	a fragment of the hH1 channel comprised of residues E1773-S1865
hH1-CTD-120	a fragment of the hH1 channel comprised of residues E1773-I1892
hH1-CTD-148	a fragment of the hH1 channel comprised of residues E1773-S1920

hH1-CTD-153	a fragment of the hH1 channel comprised of residues E1773-S1925
HSQC	heteronuclear single-quantum correlation
IFM motif	isoleucine-phenylalanine-methionine tripeptide motif; III-IV linker of hH1; the inactivation gate of hH1
IPTG	isopropyl-beta-D-thiogalactopyranoside
IQ motif	calmodulin binding motif
ITC	isothermal titration microcalorimetry
LTCC	L-type calcium channel
MALDI-TOF MS	matrix-assisted laser desorption and ionization time-of-flight mass spectrometry
MBP	maltose binding protein
NMR	nuclear magnetic resonance
PCR	polymerase chain reaction
PDB	RSCB Protein DataBank
PDZ	protein-protein interaction motif commonly used by syntrophins
QT	the length of time between the QRS complex and the T-wave in an electrocardiogram
RP-HPLC	reversed phase high pressure liquid chromatography
RyR	ryanodine receptor
SDS-PAGE	sodium dodecyl sulfate polyacrylamide gel electrophoresis
SR	sarcoplasmic reticulum
TCA	trichloroacetic acid
TM	transmembrane helix
Tris	Tris(hydroxymethyl)aminomethane
V2R	V2 vasopressin GTPase-protein coupled receptor

CHAPTER I

INTRODUCTION

Introduction

The exciting field of ion channel biology has exploded in recent years. New structural techniques have yielded an amazing amount of information about the mechanisms of various aspects of channel function, including gating, selectivity, and drug/toxin interactions. The studies presented in support of this dissertation were undertaken to structurally and biochemically characterize the regulation of the human voltage-gated sodium channel hH1 ($Na_V1.5$) by calcium. The findings are interesting in that they are the first evidence that calcium directly regulates voltage-gated sodium channel function by binding to an element in the polypeptide chain of the channel itself. Moreover, they reveal crosstalk between this intrinsic calcium sensing pathway and an extrinsic calcium sensing pathway mediated by calmodulin. This introductory chapter is designed to convey a basic understanding of ion channel function at the molecular and cellular level. This chapter also summarizes some of the evolutionary and structural information currently known about ion channels, and discusses drugs, toxins, and proteins which are known to modulate hH1 function. Naturally occurring mutations in hH1 and their effects are examined. Finally, basic biochemical characteristics of a common calcium binding motif, the EF-hand, are discussed in detail. This background serves as a springboard for understanding the rationale behind the experiments described in the rest of the thesis.

Ion channels are responsible for mediating a wide range of normal physiology

Ionic currents mediate muscle and nerve cell excitability

It has been known since the late 1800's that ions are critical for, and can be used to manipulate, the normal functioning of nerve and muscle cells. A series of frog heart perfusion studies done by Sidney Ringer in the 1880's revealed that a mixture of sodium (Na^+), potassium (K^+), and calcium (Ca^{2+}) ions, each in a relatively narrow range, was required for maintaining heartbeat (Hille 1992). In the ensuing half-century, numerous hypotheses were developed and tested with regards to the nature of cellular electrophysiology. Julius Bernstein proposed early in the 20th century that resting cell membranes are selectively permeable to K^+ ion, and that excitation is both mediated by and results in changes to this selective permeability (Hille 1992). The work done by Hodgkin and Huxley in the early 1950's (Hodgkin and Huxley 1952a; Hodgkin and Huxley 1952b), using the squid giant axon as a model system, demonstrated specific Na^+-dependent and K^+-dependent currents across the cell membrane. These studies firmly established the concept that ion-selective channels exist and give rise to the excitability of muscle and nerve cells by producing an *action potential* across the cell membrane, and included a detailed model of the changes in selective permeability that occur over the course of an action potential.

Since the now classic work of Hodgkin and Huxley, advances in fields spanning genomics, electrophysiology, structural biology, and medicine have identified hundreds of these selective ion channels in humans, established the mechanism by which cells maintain ion gradients across the cell membrane and produce an action potential in re-

sponse to stimulation, and found that a large number of disease causing mutations affect these channels. A high visibility example of the latter is CFTR ("cystic fibrosis trans-membrane conductance regulator"); mutations in this secretory chloride channel result in cystic fibrosis, the most common fatal genetic disease (Quinton 1990).

Action potentials are the basic unit of excitability

Since the action potential is the basic currency of excitability in muscle and nerve cells, it is important to examine this process in more detail to provide a framework for the studies that will be described later. While the details of this process can be found in any basic physiology textbook, the description employed here is that of Bertil Hille in *Ionic Channels of Excitable Membranes* (Hille 1992).

Prior to an action potential, the cell is said to be at rest (Figure 1.1a,b). At rest, cells expend energy in the form of ATP to drive a Na^+/K^+ exchanger, which translocates 3 Na^+ ions from inside of the cell to the outside while simultaneously translocating 2 K^+ ions from outside to the inside. This exchanger is responsible for maintaining the high relative concentration of K^+ inside the cell (large K^+) and the high relative concentration of Na^+ outside the cell (large Na^+). At rest, the membrane experiences slight, selective leakage of K^+ ion, which establishes a *resting membrane potential* of approximately -90 mV (as can be calculated using the *Nernst equation* given the extracellular and intracellular concentrations of K^+). This resting membrane potential can vary from minute to minute or hour to hour in the same cell due to alterations in the ratio of intracellular to extracellular potassium. These variations in membrane potential are important for reasons that will be discussed shortly.
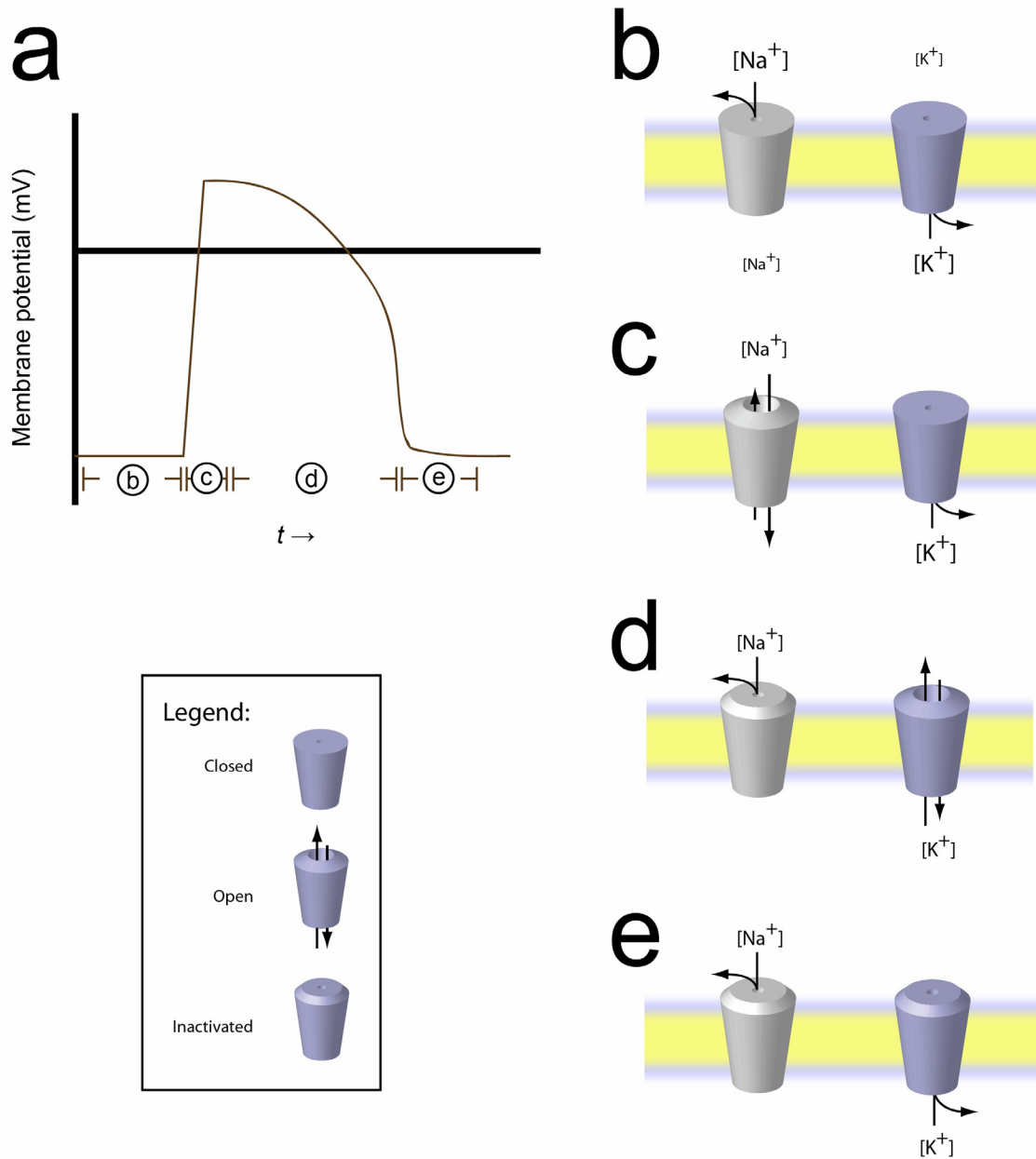
Figure 1.1: The roles played by voltage-gated sodium and potassium channels in the generation of an action potential. (*a*) Typical cardiac myocyte action potential showing transmembrane potential as a function of time. Baseline potential is around -90 mV, and peak positive potential can be as high as +40 mV. Circled letters show, generally, the relationship between the transmembrane potential shown in this panel and the channel states shown in panels b-e. (*b-e*) Open, closed, or inactivated state of sodium and potassium channels during an action potential. See text for details.

At rest, voltage-gated Na^+ and K^+ channels are in the *closed* state. An action potential is initiated by a small *depolarization* of the cell membrane, e.g. a change in the potential across the cell membrane from -80 mV to -40 mV. Following the initiation of the action potential, *voltage-gated Na^+ channels* "gate" open in response to the voltage change (Figure 1.1c), allowing Na^+ ions to rush into the cell across their concentration gradient. This results in further depolarization of the cell membrane, resulting in transmembrane potentials as high as +40 mV.

At this point in the process, Na^+ channels begin to *inactivate*, while voltage-gated K^+ channels, some of which gate slowly, begin to open. This reverses the direction of change in the transmembrane potentials and leads to *repolarization* of the cell membrane (Figure 1.1d). Another set of potassium channels also contributes to repolarization; these "fast delayed rectifier channels" gate open quickly with the Na^+ channels, but inactivate very quickly as well. Late in the action potential, these channels begin to recover from inactivation and contribute to repolarization. Repolarization may end in *undershoot*, which would be at the point shown in Figure 1.1e; it is not present here because cardiac ventricular myocytes do not typically exhibit undershoot. In undershoot, the cell is mildly hyperpolarized and is in a *refractory period* during which it cannot fire another action potential until channels recover from inactivation. The cell then re-establishes the resting membrane potential and readies itself for the next action potential. The entire cycle from beginning to end occurs in less than half a second in cardiac myocytes depending on heart rate; in neurons, at any point along an axon, the propagation of an action potential through that point can occur in under 5 milliseconds.

5

It is critically important to understand that "inactivated" channels are very different from "closed" channels in at least one fundamental respect: their ability to gate open in response to a voltage signal. As we saw earlier, closed channels gate open; inactivated channels DO NOT. Thus, in Figure 1.1 we differentiate between channels in the closed state (flat-top, small hole) versus channels in the inactivated state (beveled top, small hole). While the cell is repolarizing and during the undershoot phase, a preponderance of channels on the cell membrane are in the inactivated state. The cell is in a *refractory period*, unable to respond to a voltage pulse with an action potential.

With the difference between inactivated and closed channels well-defined, we must return to the point that the resting membrane potential can vary from minute to minute or hour to hour. It is important to note that even at rest, a proportion of channels are in the inactivated state (versus those in the closed state). The ratio is modulated in part by the resting membrane potential, a phenomenon termed *voltage-dependent steady-state availability*; this phenomenon will play a prominent role in the electrophysiological data to be described in this dissertation.

The Hodgkin/Huxley model was a groundbreaking analysis of the action potential, providing a rigorous mathematical description of this time-dependent phenomenon. Its importance for both describing and understanding the fundamental behavior of excitable membranes cannot be understated. An excellent overview of this model can be found in Hille's treatise (Hille 1992).

Where does the initiating voltage pulse originate? While there are many potential sources, it has been observed that *ligand-gated ion channels* are a common and important source for the initial depolarization. For example, the nicotinic acetylcholine (nAChR)

receptor is found at the neuromuscular junction and is stimulated to gate open by its ligand, the molecule acetylcholine. This channel nonspecifically conducts monovalent and divalent cations, including Ca^{2+}, Na^+ and K^+ (Takeuchi and Takeuchi 1960; Takeuchi 1963a; Takeuchi 1963b), providing the initial depolarization event leading to an action potential in muscle cells. The action potential across the myocyte then stimulates the phenomenon known as excitation-contraction coupling, in which muscle cells translate the biochemical changes caused by the action potential into muscular contraction.

Ligand- and voltage-gated ion channels can be contrasted with another class of membrane proteins called receptors. Unlike ion channels, receptors do not conduct ions. Rather, receptors bind their ligand and transmit a signal to the other side of the membrane. The signal is then propagated by second-messengers like adenosine 3',5'-monophosphate (cyclic AMP, cAMP) or inositol 1,4,5-triphosphate (IP_3). A widespread superfamily of receptors are G-protein coupled receptors (GPCRs), which bind a variety of ligands and mediate, among other things, a diverse set of hormonal responses. GPCRs can, in some cases, modulate the function of ion channels (Kim et al. 1989; Kurachi et al. 1989), adding to the complexity of excitable systems.

Evolutionary analysis of genetic data reveals families of ion channels

A large number of voltage-gated ion channels, primarily conducting Na^+, K^+, and Ca^{2+}, can be found in the human genome. These genes share significant homology with one another and likely result from gene duplication events allowing for specialized expression, subcellular localization, and regulation of channels able to conduct the same ion.

Potassium channels are generally formed by homotetrameric α_4 structures in which each α subunit contains six transmembrane (TM) spanning helices. These channels are thought to be the oldest, evolutionarily speaking. In many cases, the homotetramer is tightly associated with a β subunit which modulates function.
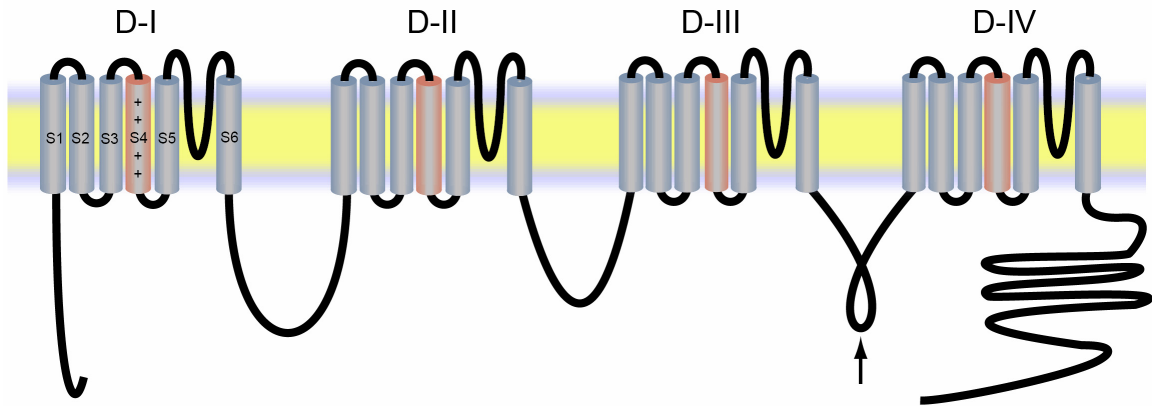
Figure 1.2: Overall domain structure and transmembrane topology of voltage-gated sodium and calcium channels. The location of the IFM motif is indicated by an arrow.

The primary α subunits of sodium and calcium channels, on the other hand, are about four times larger than the potassium channel and are basically the equivalent of a potassium homotetramer, linked into a single polypeptide chain by hydrophilic loops. The predicted domain structure and transmembrane topology of the alpha subunits of these channels are identical across all human members of this family (Figure 1.2). The alpha subunit is a single large polypeptide (~2000 residues) with four transmembrane domains connected by cytoplasmic (intracellular) linkers of varying length. The N- and C-termini are also on the cytoplasmic side of the cell membrane. Each transmembrane domain is denoted by a Roman numeral (I, II, III, IV) and is comprised of six transmembrane helices. There is also a pore-forming loop, conformationally found in the plane of

the membrane, between transmembrane helix 5 (also known as segment 5 or S5) and transmembrane helix 6 (S6). The S4 helices are indicated as a red TM helices in Figure 1.2. These are arginine and lysine rich helices, giving each S4 a net positive charge. There is substantial evidence that these charges act as the voltage sensor of the channel, causing, in response to changes in transmembrane potential, the conformational changes that result in channel opening (Bezanilla 2005).
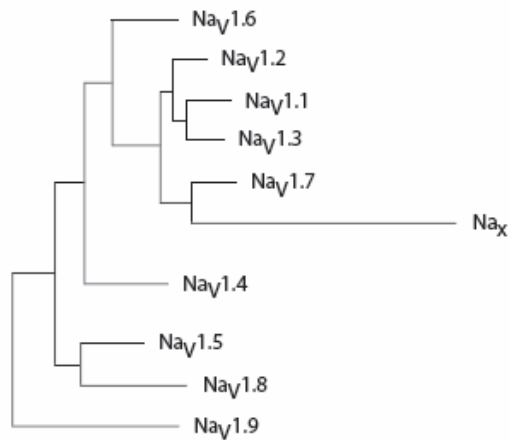
Figure 1.3: The phylogenetic relationship between voltage-gated sodium channel iso-forms found in humans. Adapted from (Catterall et al. 2003).

Although the channels are able to function in heterologous expression systems when only the alpha subunit is expressed, all have associated secondary subunits that modulate their function. Sodium channels have two beta subunits, and calcium channels have secondary alpha, beta, and delta subunits. The mechanism by which these associated subunits operate is unclear, but the number and ubiquitous presence of these subunits suggest an important role for these subunits in fine tuning channel behavior in different cellular contexts.

There are nine human voltage-gated sodium channel isoforms. These channels have been given a systematic designation $Na_V1.1$ through $Na_V1.9$, though each member of the family has a number of other, older designations as well. A tenth member of the sodium channel family, designated Na_x, has been tentatively identified based on sequence homology, but the protein has not been shown to conduct ions in heterologous expression systems and further characterization is required. Figure 1.3 illustrates the phylogenetic relationship between these isoforms (Catterall et al. 2003).

Ion channels transition through a series of states during gating

While it is certainly possible to imagine a large number of ways in which channels gate open and then inactivate, most of these can be ruled out by inference from electrophysiological, biophysical, and structural information acquired over the past forty years.

Perhaps the most important and controversial contribution to our current understanding of channel structure and function comes from a pair of studies done by the MacKinnon group in 2003 (Jiang, Lee et al. 2003; Jiang, Ruta et al. 2003). One of these papers reported the X-ray crystal structure of a voltage-gated potassium channel, KvAP, from *Aeropyrum pernix*, an archaean hyperthermophilic microbe. The accompanying paper reported the use of an elegant but ultimately flawed antibody-based structural immobilization technique used to elucidate information about the molecular mechanism of voltage gating. Based on their data, Jiang and colleagues hypothesized that the positively charged S4 segments act together with part of the S3 segment as a helix-turn-helix "paddle" which traverse as much as 15 Å during activation gating, partially through the mem-

brane lipid bilayer. This movement causes conformational changes throughout the channel that result in channel opening.

The structure itself generated quite a bit of controversy, and it is now generally accepted that the published structure is distorted and does not represent the conformation of the channel in the lipid bilayer (Bezanilla 2005). For example, in the KvAP structure, the N-terminus and the S1-S2 linker are buried. This information contradicts years of biophysical and mutational work which indicate that the N-terminus is cytoplasmic, and the S1-S2 linker extracellular.

This paddle hypothesis remains controversial and has stimulated a number of follow up studies (Cuello et al. 2004; Bezanilla 2005). Most of the available evidence supports a model in which the movement of the S4 segments upon activation gating is relatively small. Additionally, the energetic costs of ionic movement through even part of the lipid bilayer are quite large, and changes in transmembrane potential may not supply enough energy to support such a large movement. Shielding of the S4 charges by burying them in protein and in hydrated crevasses alleviates the theoretical energetic cost, but also changes the model so that it looks more like traditional proposals about the mechanism of activation gating (Ahern and Horn 2004). Competing hypotheses based on mutational studies have been around for years, and new data will certainly shed further light on the subject.

Inactivation gating is a poorly understood phenomenon

The field of activation gating has advanced quite rapidly as a result of the MacKinnon group's work and the follow up work it has stimulated. The mechanism of

11

inactivation gating, on the other hand, remains quite opaque. There is evidence, discussed below, that in sodium and calcium channels, inactivation is mediated in part by the cytoplasmic loops and termini. Jiang and colleagues removed these cytoplasmic domains in order to crystallize KvAP.

The limited information that we do have about inactivation gating comes primarily from mutational studies. A prime contributor to our understanding of inactivation gating has resulted from genetic analysis and identification of disease causing mutations. These studies have revealed, for example, that a critical component of the fast inactivation gate resides in the tripeptide motif `-IFM-` found in the III-IV linker of $Na_V1.5$ (West et al. 1992). The location is indicated in Figures 1.2 and 1.4. The structure of this short cytoplasmic domain has been determined by solution state NMR spectroscopy (Rohl et al. 1999).

In addition to fast inactivation, sodium channels experience slow inactivation, a process of inactivation that builds up over multiple activation-inactivation cycles. One hypothesis is that extended exposure to depolarized potentials results in additional conformational changes which lock the molecule into a "deeper" inactivated state; this lock can be released by exposure to hyperpolarized potentials. We note, however, that slow inactivation is even more poorly understood than fast inactivation (Goldin 2003).

The conformational changes associated with slow and fast inactivation have yet to be identified. The molecular details of inactivation are important not only to understand normal physiological processes, but also to understand the mechanism of disease-causing mutations and open new therapeutic avenues for those who suffer from these mutations. In other words, a better understanding of inactivation may lead to new, better drugs with

cardiac and neurological applications. These drugs could target specific aspects of the inactivation machinery to alter electrophysiological properties of cells. Moreover, isoform specific targeting could also result in fewer side effects associated with these powerful and dangerous drugs.

hH1 is a critical voltage-gated sodium channel with cardiac localization

hH1 is an important drug target

Na$_V$1.5 is a critically important human voltage-gated sodium channel. This channel is also referred to in the literature as Scn5a, hH1, and LQT3. Its gene is found on chromosome 3 (locus 3p21) and is expressed primarily in heart muscle cells, where the protein is localized to the intercalated discs. The protein is responsible for the primary sodium influx during the depolarization phase of cardiac muscle cell excitation (Figure 1.1b). Highlighting the importance of this protein is the fact that a number of drugs and toxins target this channel.

In the family of voltage-gated sodium channels, nine classes of compounds (encompassing both toxins and therapeutic drugs) that alter or block their function have been identified. They have been classified on the basis of the putative site of interaction as determined by the electrophysiological effects of these compounds combined with site-directed mutagenesis to identify disruption of these effects (Wang and Wang 2003). These compounds include tetrodotoxin (TTX), conotoxins, scorpion toxins (α and β), DDT, and a wide variety of antiarrhythmic, antidepressant and local anaesthetic drugs. While not all of these compounds target hH1 (e.g. antidepressants target neural isoforms),

13

many are thought to bind at similar sites across different isoforms in the sodium channel family. This results in cross-reactivity by drugs which act to modulate sodium channel function; cardiac drugs can have severe neurological side effects, for example. Interestingly, many of these compounds target the S6 segments of some or all of the domains, possibly indicating that the effects stem from interference with sodium permeation or channel gating (Wang and Wang 2003).
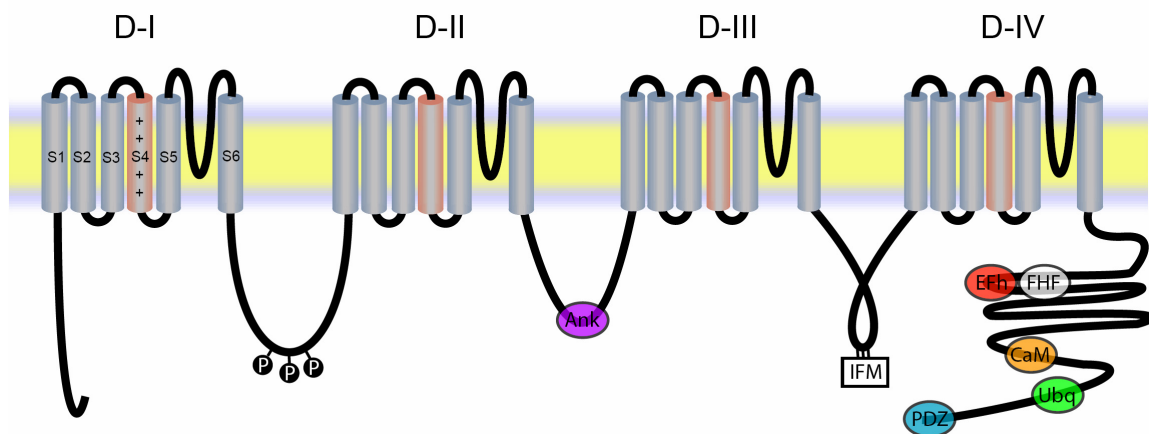
Figure 1.4: Sites of interaction between hH1 and its known binding partners. Phosphorylation sites in the I-II linker are also indicated, as is the fast-inactivation gate ("IFM") in the III-IV linker. From left to right, "Ank" indicates the ankyrin G interaction site. "EFh" indicates the putative EF-hand in hH1. "FHF" indicates the FHF1b interaction site. "CaM" represents the IQ-motif calmodulin interaction site. "Ubq" indicates a ubiquitination site, mediated by the Nedd4-like E3 ligase. "PDZ" indicates the syntrophin interaction site. Each of these features are described in more detail in the accompanying text. Adapted from Abriel and Kass 2005.

As mentioned, drugs that target ion channels are both powerful and dangerous. Most of these compounds have significant dose-dependent effects which can result, paradoxically, in fatal responses. For example, Class I anti-arrhythmic drugs such as quinidine (I-A), lidocaine (I-B), and encainide (I-C) slow cardiac conduction by blocking hH1. While these drugs were initially hailed by the medical community, it has since been

shown that use of these drugs to suppress arrhythmias may actually cause an increase in mortality, as a result of proarrhythmic side effects of these compounds. In other words, the drugs can actually *cause* the effect that they were administered to prevent!

A better mechanistic understanding of channel and drug behavior will hopefully lead to better compounds for the treatment of arrhythmias. Some of the mechanics are already understood. For example, many of the current generation of antiarrhythmics act in a "use-dependent" manner, i.e. these drugs bind only when the channel is in the open state, and therefore act in a cumulative manner over time even at steady-state drug concentrations. Further mechanistic insights will require better understanding of both (a) the molecular mechanisms of single channel behavior and (b) how alterations to single channel behavior translate to organ-level changes in function.

hH1 interacts with many proteins

In addition to interactions with many drugs and toxins, the channel interacts with a large number of cellular proteins. As mentioned earlier, the channel itself has a beta subunit, of which there are four isoforms (β1-β4). All are expressed in the heart. The role of the beta subunits is to fine-tune channel function. Further details will not be discussed here, as all of the gating and pore machinery necessary for voltage-gated sodium ion flux can be found in the α subunit, which is the focus of this dissertation. Other proteins that interact with hH1 are indicated in Figure 1.4 (Abriel and Kass 2005). Many of these binding partners have only been identified in the past few years, as new information and new tools accelerate the pace of research. In some cases, the functional relevance of the interacting protein has yet to be identified. Current information suggests that five

proteins interact with hH1: ankyrin-G, syntrophins, Nedd4-like E3 ubiquitin ligases, fibroblast growth factor homologous factor 1b (FHF1b), and calmodulin (Abriel and Kass 2005).

<u>Ankyrins</u>

Ankyrins are cytoskeletal adapter proteins that play an important role in anchoring membrane proteins and possibly in trafficking/targeting as well. Of the three mammalian isoforms (ankyrin-B, ankyrin -G, and ankyrin –R), only ankyrin-G has been shown to directly interact with hH1. This interaction is mediated by the nonapeptide sequence `VPIAVA``E``SD` in the II-III linker, encompassing residues 1047-1055 (Lemaillet et al. 2003). As will be discussed later in this Chapter, a number of disease causing mutations occur in hH1, one of which occurs in this site. The mutation E1053K (highlighted in red in the nonapeptide; see also Figure 1.5) causes Brugada syndrome. This mutation has been shown to abolish interactions between ankyrin-G and hH1 and disrupt normal channel trafficking (Mohler et al. 2004).

<u>Syntrophins</u>

The syntrophin family of proteins are also adapter proteins, functioning to localize a number of protein targets to the muscle protein dystrophin. There are five known isoforms (α1, β1, β2, γ1, γ2) which are coded for on separate genes and exhibit tissue-specific expression (Albrecht and Froehner 2002). Interaction with protein targets is mediated through a PDZ domain ("<u>p</u>ostsynaptic density-95/<u>d</u>iscs large/<u>z</u>ona occludens-1"), which binds to PDZ binding motifs. The consensus PDZ binding motif consists of the C-terminal tripeptide `-SIV-COOH`, found in a wide variety of proteins including protein kinases and membrane proteins. This motif is found in hH1 ($Na_V1.5$). One other mem-

ber of the human sodium channel family, Na$_V$1.4, has a slightly modified PDZ binding motif (`-SLV-COOH`). None of the other family members have similar sequences. Both hH1 and Na$_V$1.4 have been shown to bind syntrophins and can be copurified in complex with syntrophin and dystrophin (Gee et al. 1998). The specific syntrophin isoforms that are involved in the interaction have not been fully characterized. However, the γ2 isoform has been specifically shown to interact with hH1, and both are co-expressed in intestinal smooth muscle cells (Ou et al. 2003). Likewise, the functional importance of this interaction has not yet been pinned down; various studies have come to different conclusions about the electrophysiological effects of this interaction (Zhou et al. 2002; Ou et al. 2003).

Nedd4-like E3 ubiquitin ligase

hH1 is ubiquitinated *in vivo* to regulate membrane turnover of the protein (van Bemmelen et al. 2004). Ubiquitin is a 7 kDa protein found in all animal cells; this protein is covalently attached to a wide variety of cytoplasmic and membrane proteins ("ubiquitination"). This process can regulate trafficking and internalization, and can also tag a protein for lysosomal or proteasomal degradation.

Ubiquitination, reviewed elsewhere (Vander kooi 2004), is carried out in a cascade of transfer reactions involving, sequentially, E1, E2 and E3 ubiquitin ligases. These reactions activate ubiquitin for attachment to target proteins. The attachment of ubiquitin occurs via a covalent bond between its highly conserved C-terminal glycine and a lysine on the target protein. Ubiquitin is first recruited by and attached via a thioester bond to the E1 ligase in an ATP-dependent reaction. The molecule is then transferred to an E2 ligase, also via thioester linkage, for presentation to the target protein, which is bound to

E3 ligase. The activated ubiquitin may be transferred directly to the E3 ligase or positioned by the E3 ligase to bring the E2-ubiquitin complex into close proximity with the target. Either way, E3 ligases play a critical role in positioning the activated ubiquitin and the target. The relative roles played by E1, E2 and E3 ligases are reflected in number of isoforms of each found in animals; most organisms contain only one E1 ligase, a few E2 ligases, but hundreds of E3 ligases.

The Nedd4-like family of E3 ligases have two to four WW domains that interact with the consensus sequence PPxY (PY motif) on its substrates (Staub et al. 1996). These PY motifs are found in the C-termini of almost all voltage gated sodium channels, including hH1 (Abriel and Kass 2005). The human Nedd4-2 E3 ligase has been shown to directly bind the hH1 PY motif and ubiquitinate the channel in mammalian cells (van Bemmelen et al. 2004). Furthmore, ubiquitinated hH1 has been detected in cardiac tissue, and the presence of Nedd4-2 in HEK293 cells increases the rate of internalization of coexpressed hH1 likely as a result of ubiquitination (Rougier et al. 2005). With nine Nedd4-like isoforms, five of which have been demonstrated to be expressed in the heart, it is likely that this is a physiologically relevant mechanism of channel regulation.

Fibroblast growth factor homologous factor 1b (FHF1b)

FHF1b is a recently discovered member of the fibroblast growth factor family that is expressed in the cytoplasm and is not secreted (Liu et al. 2001). The crystal structure of this protein has been recently determined and, as expected, showed high structural homology to other members of the fibroblast growth factor family (Olsen et al. 2003). Key sequence differences, however, prevent it from being secreted (Liu et al. 2001). Recent studies have shown that the protein interacts with the C-terminal cytoplasmic do-

mains of hH1 and other voltage-gated sodium channels (Liu et al. 2001; Liu et al. 2003). These studies have also shown that coexpression of FHF1b with hH1 results in changes to steady state inactivation. Though the functional role of FHF1b in modulation of hH1 has been characterized (Liu et al. 2003), the molecular details have yet to be explored.

<u>Calmodulin (CaM)</u>

Calmodulin is a ubiquitous calcium sensor protein, mediating the calcium-dependent regulation of a large number of cellular proteins. These include regulation of brush border myosin I heavy chain, calcium/calmodulin dependent kinase II, phosphati-dyl-inositol-3 kinase, and nicotinamide dinucleotide kinase (Nelson and Chazin 2005). It is highly conserved from bacteria to mammals, and is 148 residues long in most higher organisms including humans. The protein consists of two domains connected by a flexi-ble linker. Each domain contains a pair of EF-hands, the calcium-sensing elements of the protein. EF-hands are discussed in detail later in this Chapter.

Calmodulin binds to hH1 in the C-terminal cytoplasmic domain in the region R1897-S1925 via an IQ-motif. The IQ motif is a common calmodulin binding motif first identified in neuromodulin (Alexander et al. 1988) and first characterized in myosins (Cheney and Mooseker 1992). The consensus sequence of the IQ motif is **δQxxxβGxxxβxxδ**, where **δ** represents any of Phe/Ile/Leu/Val and **β** represents either Lys or Arg (Bahler and Rhoads 2002). The Gly at position 7 is only loosely conserved, as is the final hydrophobic residue. These relaxed requirements are reflected in the defi-nition of an "IQ-like" motif with the consensus sequence **δQxxxβxxxxx** (Bahler and Rhoads 2002). In most cases, the IQ motif is able to bind apo (Ca^{2+}-free) calmodulin and binding of calcium to calmodulin either maintains or weakens this interaction. It is

commonly held that the function of the IQ motif is to localize calmodulin at basal calcium levels, so that the local concentration is high near a site where calmodulin is to perform a calcium-dependent role. This interaction between CaM and hH1 is one of the focuses of this dissertation; further details can be found in Chapter IV.

Mutations in hH1 lead to arrhythmogenic disease syndromes

A large number of arrythmogenic mutations have been identified in hH1, as shown in Figure 1.5 (Balser 2001). Most commonly, these mutations lead to long QT syndrome subtype 3 (LQT3) or Brugada syndrome (BrS). These genetic diseases are often insidious in their presentation, silent until they result in sudden collapse or death. For example, patients with Brugada syndrome commonly die in their sleep, secondary to ventricular fibrillation.
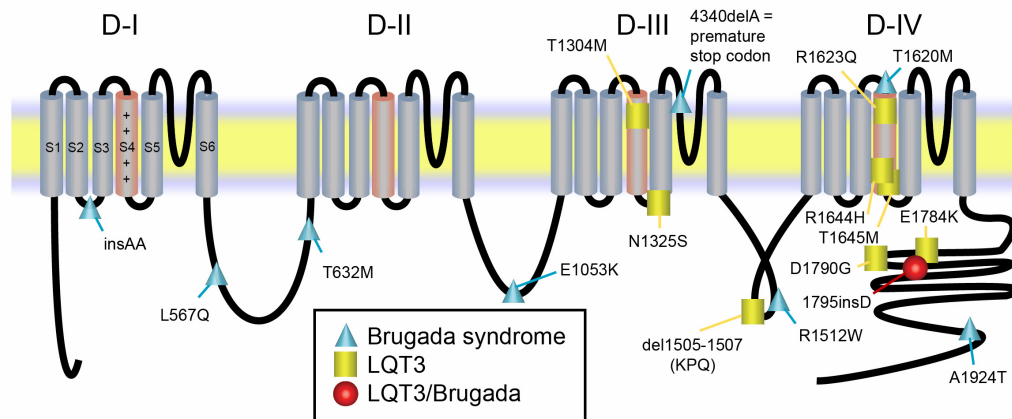
Figure 1.5: Arrhythmogenic mutations in hH1 can be found throughout the protein. Adapted from Balser 2001.

Most of these mutations have a definite electrophysiological profile, and the dysfunctional aspects of individual channel behavior can be modeled to explain the macro-

scopic problems linked to these mutations. In LQT3, reopening of inactivated sodium channels results in prolonged ventricular repolarization (Li et al. 2000; Kass and Moss 2003). This manifests as a lengthening of the Q-T interval in an EKG. Resting $QT_{corrected}$ > 460 milliseconds is diagnostic of long QT syndrome, as compared with control $QT_{corrected}$ of 436 ± 19 ms (Ackerman et al. 2002). The lengthened Q-T interval substantially raises the risk of arrhythmias, though the mechanisms behind this risk remain unclear. In Brugada, on the other hand, the sodium current density is lower (Naccarelli et al. 2002). Thus, some areas may not depolarize ("fire" an action potential) at all, also raising the risk of arrhythmias. This leads to an increased risk of so-called "reentrant" arrhythmias caused by regions which, after failing to fire with the rest of the heart tissue, fire inappropriately during mid-cycle. Thus, both gain of function and loss of function mutations are arrhythmogenic – revealing the fine-tuned nature of this system.

Two mutations which have stubbornly defied electrophysiological characterization are the D1790G and 1795insD mutations. Both of these mutations occur in the proximal part of the C-terminal cytoplasmic tail, as indicated in Figure 1.5.

Analysis of the hH1 amino acid sequence has been performed in an attempt to determine the nature of the disruptions caused by these disease-associated mutations. As will be detailed in Chapter II, a putative consensus EF-hand calcium binding loop was identified in the twelve residue stretch D1788-E1799. This led to the hypothesis that the proximal part of the hH1 C-terminus contains a functional EF-hand domain, and that disruption of the EF-hand by D1790G and 1795insD is able to cause changes in the electrophysiological behavior of the channel. This was an exciting idea, because calcium-

dependent regulation of voltage-gated sodium channels had not been observed previously.

The EF-hand is a ubiquitous calcium-binding motif

EF-hands are found in a diverse set of calcium sensors and modulators

Since a significant portion of the experiments in this dissertation involve the hH1 EF-hand directly or tangentially, it is important to understand the nature and role of EF-hands in normal physiology. The EF-hand is a very common calcium binding motif; over 1000 have been identified in animal genomes from their unique sequence signatures (Henikoff et al. 1997). Calcium levels are known to regulate many processes in biology (Berridge 1997), including excitation-contraction coupling in heart and skeletal muscle (Celio et al. 1996). The intracellular concentration of calcium is tightly regulated, with a low basal concentration of approximately ~100 nM (Braveny 2002), and release of calcium from intracellular stores during a signaling event can result in intracellular calcium concentrations as high as 10 μM, and local concentrations in subcellular compartments may be orders of magnitude higher than this. The EF-hand motif is a structural element of proteins used to transduce changes in calcium concentration into a biochemical signal.

Acidic residues in the EF-hand loop are critical for calcium-chelation

Structurally, the EF-hand is a helix-loop-helix motif first identified in parvalbumin (Kretsinger and Nockolds 1973). The "EF" refers to the two helices in the motif. It is called a "hand" because, if thumb and index finger are used to form an "L" shape and

the other three fingers curled inward so the fingertips touch the palm, the two extended

fingers approximately represent the helices of the motif and the curled fingers together

with the palm approximately represent the calcium binding loop. The angle between

thumb and index finger, representing the interhelical angle, can be variable; calcium

binding can cause changes in this interhelical angle, resulting in widespread conforma-

tional changes which can then transduce the calcium signal into a biochemical event by

altering the binding surface presented by the protein.
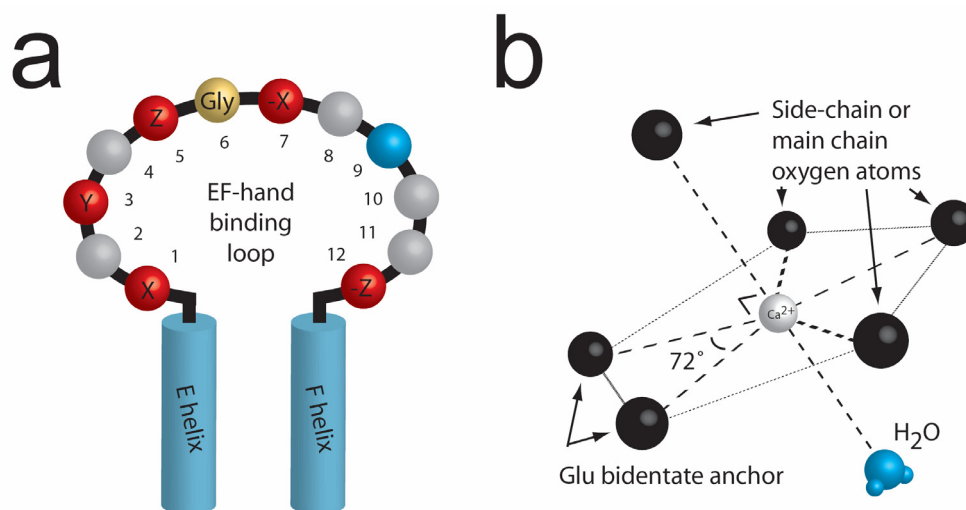
Figure 1.6: EF-hand calcium binding loop coordinates the calcium (II) ion with pentagonal bipyramidal geometry. (*a*) Consensus EF-hand calcium binding loop sequence. Residues 1, 3, 5, 7, and 12, indicated in red, contribute oxygens for calcium coordination; see text for details. Position 6 Gly is strongly conserved for steric/conformational reasons. Position 9, shown in blue, participates in coordination by hydrogen bonding with a water molecule needed to complete the coordination sphere. (*b*) Pentagonal bipyramidal geometry of calcium coordination in an EF-hand. All of the peripheral large spheres (black and blue) represent oxygen atoms participating in coordination.

The consensus loop of the EF-hand is comprised of twelve residues (Figure 1.6a)

that surround the bound calcium (II) ion, coordinating the ion with oxygen atoms ar-

ranged in a pentagonal bipyramidal geometry (Drake et al. 1997; Yang et al. 2002), as

shown in Figure 1.6b. The side chains of residues at positions 1, 3, and 5 each provide one oxygen ligand, thus Asn, Asp, Gln, or Glu are most frequently found at these positions. The main chain oxygen of residue 7 provides a fourth ligand. In order to attain appropriate positioning of residues 5 and 7, the residue in position 6 must occupy an unusual backbone conformation favorable only for glycine, resulting in strong conservation of Gly in this position. The Glu residue at position 12 is strictly conserved because it provides two coordination sites for a critical bidentate ligand. Residue 9 is also involved in coordinating the calcium ion by hydrogen bonding the water molecule that chelates the ion, completing the coordination sphere.

Given the complexity of the calcium coordination geometry, it seems likely that if an EF-hand calcium binding domain is present in hH1, mutations in and around the calcium binding loop may well perturb its calcium binding activity. Indeed, the D1790G mutant associated with long QT subtype 3 removes the oxygen atom used for calcium coordination at position 3. Such a mutation is predicted to reduce calcium affinity by an order of magnitude or more. The 1795insD Brugada mutation would likewise shift the register of at least one ligand, and is anticipated to reduce or abolish calcium binding function.

Given the available evidence for the presence of an EF-hand domain in hH1, we set out to test whether there is biophysical or electrophysiological evidence of calcium binding to hH1, and if mutations in the calcium binding loop could diminish or abolish calcium-dependent properties of the channel that were found. These findings are discussed in Chapter II. Chapter III discusses work that was done to characterize the precise residues in the C-terminus that are involved in calcium binding and to refine our under-

standing of this EF-hand domain, which has both canonical and unique aspects to its sequence signature. That chapter describes the surprising result that the folded EF-hand core has a substantially lower calcium affinity than a construct containing both the EF-hand and the downstream IQ motif. This leads to the work described in Chapter IV, which describes characterization of the IQ motif and exploration of cross-talk between the two calcium sensing pathways. Chapter V describes a model based on this data and, in addition, takes a broad view of the literature to examine the role of calcium in the regulation of ion channels. Chapter VI discusses the further implications of this work, preliminary data, and future directions.

CHAPTER II

AN EF-HAND IN THE SODIUM CHANNEL COUPLES INTRACELLULAR
CALCIUM TO CARDIAC EXCITABILITY

Introduction

As discussed in Chapter I, life-threatening arrhythmias have been demonstrated to arise from inherited Na^+ channel dysfunction (Bennett et al. 1995; Chen et al. 1998). Mutations throughout hH1 have been implicated in arrhythmia syndromes; a number of these reside within the C-terminal cytoplasmic domain. These mutations alter functional properties of channel gating (Dumaine et al. 1996; Wang et al. 1996; Benhorin et al. 1998; Bezzina et al. 1999). One of these mutations, D1790G, has been associated with long QT syndrome subtype 3 (An et al. 1998; Wehrens et al. 2000). Analysis of the hH1 C-terminus revealed an ordered, helical domain (Cormier et al. 2002a), but localization of structural and functional components of channel gating has proven difficult.

This chapter reports a series of studies, conducted in collaboration with Dr. Tammy Wingo and Dr. Jeff Balser and previously published (Wingo et al. 2004). These studies identified the structural motif underlying D1790G-mediated LQT3. To accomplish this goal, we made use of computational methods, patch-clamp electrophysiology, and a variety of spectroscopic tools. These approaches uncovered the presence of an intrinsic EF-hand calcium binding site in the polypeptide chain of the hH1 α subunit, specifically in the C-terminal domain. D1790G perturbs normal calcium binding to this motif and alters calcium-dependent functional properties of the channel. This intrinsic calcium binding site is just upstream of a calmodulin binding site, an interesting coincidence

26

which will be explored in later chapters. In addition to examining the molecular patho-physiology associated with D1790G, these results provide an improved understanding of the functional role of the Na$^+$ channel C-terminus in cardiac rhythm and add to our understanding of the role of Ca^{2+} in cellular regulation.

Results

hH1 contains a putative EF-hand in the C-terminal cytoplasmic domain

Analysis of the hH1 C-terminus using the NCBI PSI-BLAST program (Altschul et al. 1990; Altschul et al. 1997), Figure 2.1a, revealed homology to EF-hand helix-loop-helix motifs in a number of Ca^{2+}-binding proteins, such as calmodulin. As discussed in Chapter I, EF-hand proteins mediate the transduction of Ca^{2+} signals in cellular responses, including regulation of ion channels (Peterson et al. 2000). Remarkably, the EF-hand was found approximately 120 residues upstream from an "IQ-domain" calmodulin binding site identified previously, in the region I1908-R1919 (Deschenes et al. 2002b; Tan et al. 2002a). A structure-based multiple sequence alignment with several of the highest scoring hits from the PSI-BLAST search, all proteins with EF-hands whose 3D structures are known (1C07, 1C7V, 1EXR, 1BJF, 1TRF; Figure 2.1a), provided further support for this structural class assignment.

A single EF-hand motif is not an intrinsically stable structure, and is always found at least in pairs (Shaw et al. 1990; Lewit-Bentley and Rety 2000). A pair of EF-hands forms the minimal stable structural unit—a four-helix bundle (Strynadka and James 1989; Linse and Forsen 1995). According to our multiple sequence alignments, the hH1

C-terminus has a pair of EF-hands in the region E1773-D1852. A Ca^{2+} binding site is found in the first EF-hand sequence, based on the close fit to the consensus binding loop (cyan box, Figure 2.1a).
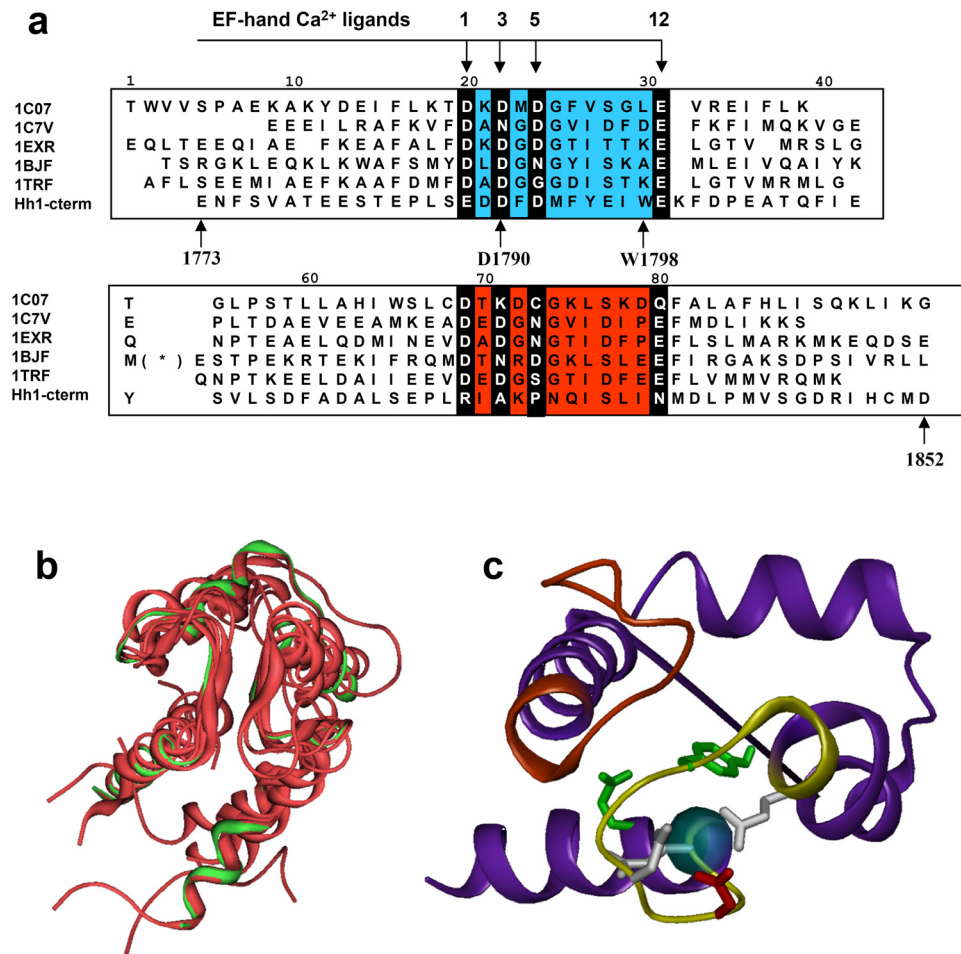
Figure 2.1: Structure based sequence alignment and model of the proximal region of the hH1 C-terminus (residues 1773-1852). This region was aligned with Ca^{2+}-binding proteins identified using PSI-BLAST (PDB identifiers indicated at left; see text). (*a*) Bolded blocked regions indicate key residues responsible for Ca^{2+} ion coordination (designated as positions 1, 3, 5, 12) in EF-hand loops. The cyan box identifies an EF-hand predicted to have a strong Ca^{2+} binding site; the orange box identifies a second EF hand that could serve to stabilize the requisite paired structure. (*b*) Energy-minimized model of the hH1 C-terminus (green) superimposed on the backbone structure of the Ca^{2+}-binding proteins used as templates in model construction (red). (*c*) Predicted model for the hH1 proximal C-terminus highlighting features of the EF-hand loop. The functional EF-hand loop is shown in yellow, and the distal putative loop in orange. Key residues are color-coded for clarity and shown in ball-and-stick representation. The residue highlighted in red represents residue D1790, which is in position 3 for Ca^{2+} ion coordination. Mutation of this residue (D1790G) results in long QT syndrome. Other residues important for Ca^{2+} ion coordination (position1: E1788, position 5: D1792, position 12: E1799) are highlighted in white. Additional positions where mutations elicit arrhythmia phenotypes (e.g. E1784; see text) are indicated in green. A translucent cyan sphere represents bound Ca^{2+} ion. Model constructed by Tammy Wingo. Taken from Wingo et al 2004.

The second EF-hand loop is not expected to bind Ca^{2+} because it lacks key consensus side chains involved in chelating the ion. The lack of a competent Ca^{2+} site in the second EF hand (orange box, Figure 2.1a) is not atypical, and binding of a single Ca^{2+} ion is known to be sufficient to activate several EF-hand Ca^{2+} sensor domains. Examples of the latter include the N-terminal domain of cardiac troponin C and the C-terminal domain of centrin.

Threading calculations for hH1 (1773-1852) against a library of all structurally characterized tertiary fold templates confirmed that a paired EF-hand motif is a highly plausible 3D structure for this sequence. A structural model (Figure 2.1b,c) was therefore constructed using a structure-based sequence alignment with the five EF-hand protein templates listed in Figure 2.1a. The presence of an ordered structure is consistent with prior work showing the C-terminus contains helical secondary structure (Cormier et al. 2002a).

hH1 exhibits Ca^{2+}-dependent changes in voltage-dependent availability

Like most voltage-gated ion channels, hH1 can occupy an open (Na^+ conducting) state, as well as two distinctive non-conducting states, termed "closed" and "inactivated". These states are discussed in detail in Chapter I. Briefly, channels in the closed state can open and generate Na^+ current (I_{Na}) in response to a stimulus, whereas channels in the inactivated state cannot open and are functionally unavailable. Under resting conditions, the potential across the membrane determines the ratio of closed to inactivated channels in a population of Na^+ channels. Depolarization of the membrane potential, i.e. potentials that are closer to 0 mV, shifts the balance to favor the inactivated state. Because this

"availability curve" is steepest at voltages that approach the cardiac myocyte maximum diastolic membrane potential (resting membrane potential $V_{rest} \sim -90$ mV), the population of Na^+ channels available to open is sensitive to even modest changes in V_{rest}. Pathologic conditions which alter V_{rest} can markedly change hH1 availability, modifying I_{Na} and destabilizing the cardiac rhythm (Shaw and Rudy 1997). Ischemia and acidosis are conditions which have been previously described to alter V_{rest}.

The potential for a functional EF-hand domain in hH1 led us to investigate the effects of intracellular Ca^{2+} on the voltage-dependence of Na^+ channel availability (Figure 2.2). These studies were conducted by Tammy Wingo working under the mentorship of Dr. Jeffrey Balser. For these studies, whole-cell Na^+ currents (I_{Na}, see top inset, Figure 2.2), were recorded in voltage-clamped tsA201 cells transiently transfected with wild type (WT) hH1 cDNA. Voltage-dependent channel availability was assessed by quantifying the I_{Na} magnitude during an activating pulse to -20 mV (see bottom inset, Figure 2.2a) as a function of various "test" resting membrane voltages. Figure 2.2a indicates that raising free Ca^{2+} concentrations from 0 to 10 μM caused a rightward shift in availability, with the effect saturating at ~ 1 μM. The observed change is consistent with a destabilizing effect on inactivation gating: the membrane potential at which 50% of the Na^+ channels were available to open ($V_{1/2}$) was -98.3 ± 1.5 mV in Ca^{2+}-free conditions, but was -87.2 ± 1.0 mV in 1 or 10 μM Ca^{2+} ($p < 0.001$). A dose-response curve fitted to the $V_{1/2}$ data (Figure 2.2c) yields an EC_{50} of 175 nM, a value consistent with a physiological and structural role for Ca^{2+}-binding to the EF-hand (Linse and Forsen 1995). Other gating processes, including activation and recovery from inactivation, were evaluated as described previously (Veldkamp et al. 2000), and did not respond to added Ca^{+2}.

Although studies have identified effects of the Ca^{2+}-dependent cofactor calmodulin on Na^+ channel gating (Deschenes et al. 2002b; Tan et al. 2002a), direct effects of Ca^{2+} on Na^+ channel availability have not been described. However, an important change in the present studies was to utilize BAPTA as a Ca^{2+} buffer in the patch electrode solution. Over the range of free Ca^{2+} concentrations tested (0 to 10 μM), the $V_{1/2}$ values for the hH1 availability curve (−87 to −98 mV) bracket the value obtained in prior studies using 10 mM EGTA and no added Ca^{2+} (−93.5 mV) (Deschenes et al. 2002b; Tan et al. 2002a). In fact, the $V_{1/2}$ of the availability curve in nominally Ca^{2+} free solutions containing EGTA is quite close to the $V_{1/2}$ measured at the EC_{50} Ca^{2+} concentration when BAPTA is used, suggesting EGTA is not as effective as BAPTA in maintaining Ca^{2+} at low (nM) levels. Hence, with EGTA as the calcium buffer, detection of Ca^{2+} effects on Na^+ channel availability would be difficult, since the $V_{1/2}$ dynamic range would be no greater than 5 mV (from −93 to −98 mV). Overall, our findings suggest that the selection of metal ion buffer is critical when evaluating the function of the hH1 EF-hand in cellular preparations.

In prior work describing Ca^{2+}-CaM mediated effects on Na^+ channel inactivation, we and others have noted changes in the rate of fast Na^+ current decay that appear to be mediated by Ca^{2+} (Deschenes et al. 2002b; Tan et al. 2002a). However, with BAPTA substituted for EGTA, we find the hH1 I_{Na} decay rate (Figure 2.2a, inset) does not change appreciably with added Ca^{2+} (fitted I_{Na} decay time constants provided in Figure 2.2, legend). Recognizing that BAPTA provides more stringent Ca^{2+} buffering conditions, and more rapid Ca^{2+} binding kinetics (Tsien 1980), we speculate that the small Ca^{2+}-dependent effect previously noted on hH1 I_{Na} decay (Tan et al. 2002a) may result from

activation of Ca^{2+}-signalling pathways that modulate hH1, but are less tightly controlled by EGTA than BAPTA.
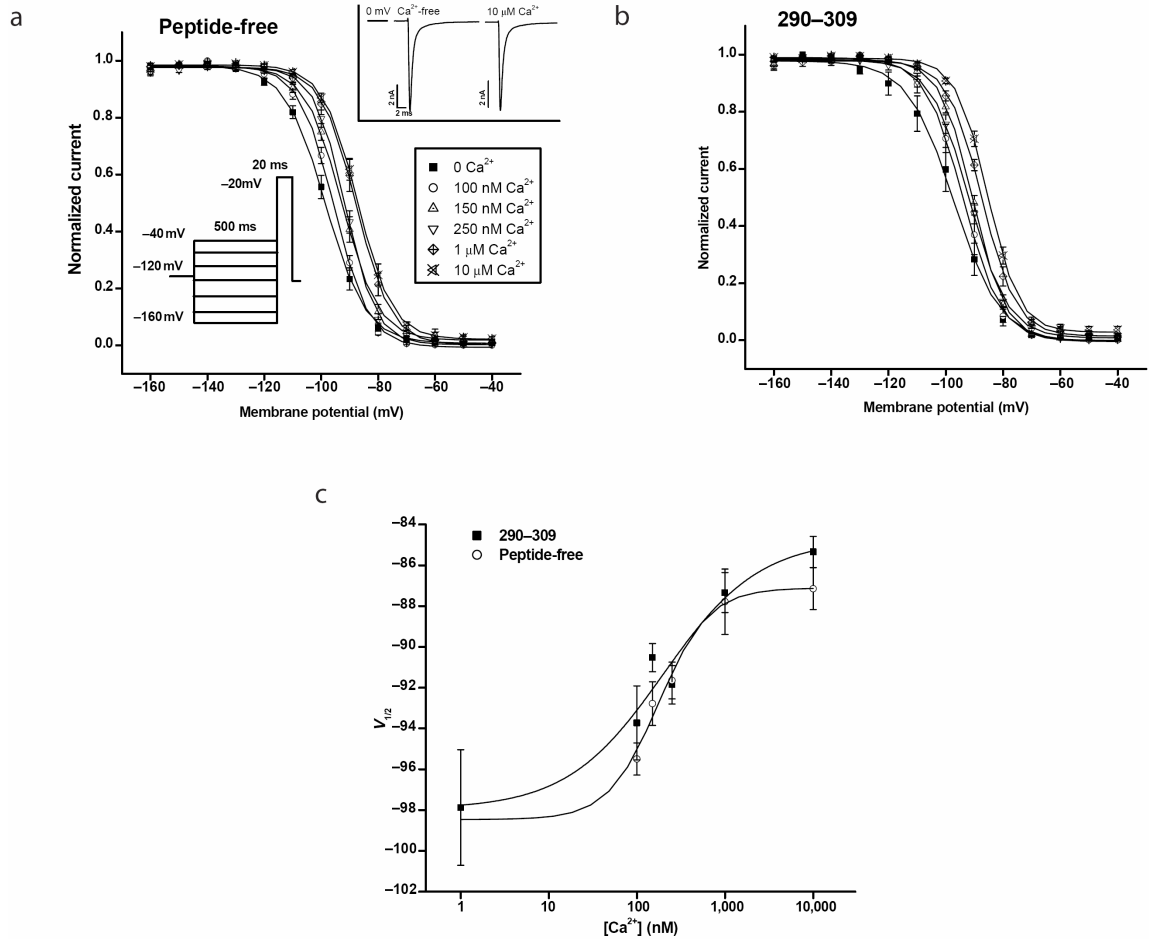
Figure 2.2: Inactivation gating of wild-type hH1 channels is Ca^{2+} sensitive. (*a*) Solid lines indicate a least-squares fit of a Boltzmann function to the data. The membrane potential of 50% channel availability ($V_{1/2}$) was: -98.3 ± 1.5 (n=11), -95.4 ± 0.8 (n=4), -92.8 ± 1.1 (n=8, $p < 0.05$), -91.6 ± 0.9 (n=8, $p < 0.01$), -87.8 ± 1.6 (n=7, $p < 0.001$), and -87.1 ± 1.0 mV (n=17, $p < 0.0001$) for 0, 100, 150, 250 nM, 1 μM, and 10 μM Ca^{2+}, respectively. Slope (k) factor in zero free Ca^{2+} decreased slightly in 10 μM Ca^{2+}: 6.38 ± 0.24 (n=11) versus 5.54 ± 0.23 (n=17), respectively ($p < 0.05$). (*a, inset*) Representative I_{Na} measured at -20 mV after holding at -120 mV in 0 and 10 μM free Ca^{2+} reveals no appreciable change in current magnitude or inactivation kinetics. (*b*) Voltage-dependence of inactivation dose response analysis with CaM inhibitory peptide 290-309, as above. $V_{1/2}$ values: -97.6 ± 1.9 (n=4), -93.7 ± 1.8 (n=4), -90.5 ± 0.7 (n=4, $p < 0.05$), -91.6 ± 0.9 (n=4, $p < 0.05$), -87.3 ± 1.0 (n=3, $p < 0.01$), -85.3 ± 0.8 (n=6, $p < 0.001$). Significant differences indicate comparisons to the 0 Ca^{2+} condition. (*c*) Dose-response analysis of data represented in panels (*a*) and (*b*). EC_{50} values, with and without the CaM inhibitory peptide 290-309, were 175 and 199 nM respectively. Work done by Tammy Wingo. Taken from Wingo et al 2004.

32

The hH1 C-terminal domain contains a structured domain

To assess whether the consensus EF-hand motif is capable of binding Ca^{2+}, we characterized a bacterially expressed construct containing the first 148 residues of the C-terminal region (hH1-CTD-148). Circular dichroism (CD) was used to examine secondary structure, nuclear magnetic resonance (NMR) to probe tertiary structure, and fluorescence spectroscopy to directly monitor the binding of Ca^{2+}. The profile of the CD spectrum of hH1-CTD-148 has the characteristic minimum at 222 nm indicative of significant helical content (Figure 2.3a). NMR signals are relatively narrow and are widely dispersed across the NMR spectrum, particularly in the ^{1}H dimension (Figure 2.3b, Figure 2.4a). The dispersion of ^{1}H signals from 6.5-11.5 p.p.m. in the 2D ^{15}N-^{1}H HSQC NMR spectrum of Ca^{2+}-loaded hH1-CTD-148 is clear evidence of a well-folded structural domain.
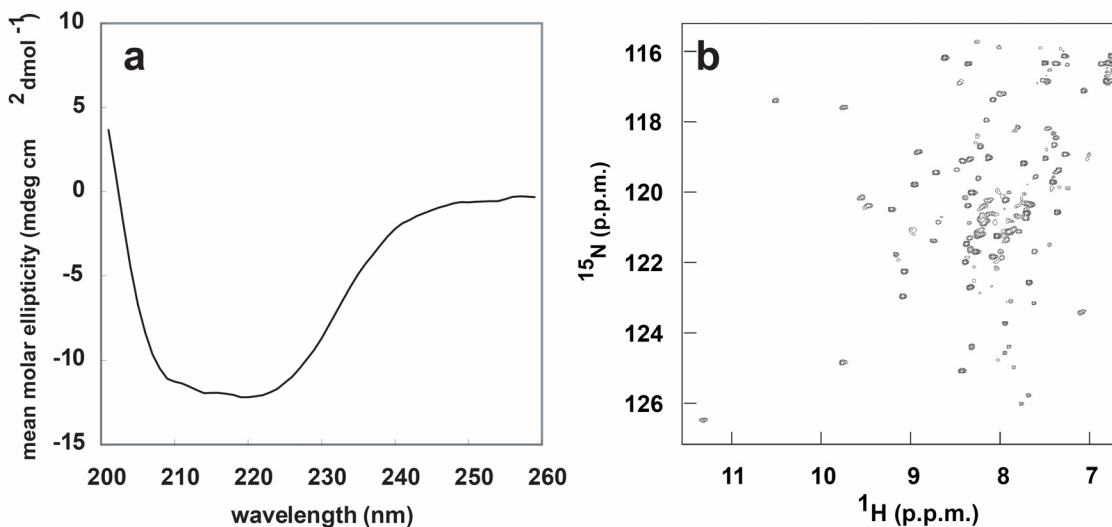
Figure 2.3: hH1-CTD-148 is a well-folded helical protein. (*a*) CD and (*b*) ^{15}N-^{1}H HSQC NMR spectra of hH1-CTD-148.

The hH1 C-terminal domain has µM calcium affinity

Trp1798 in position 11 of the first EF-hand loop (Figure 2.1) serves as a convenient fluorescent probe to monitor Ca^{2+} binding since this is the only tryptophan in hH1-CTD-148. A significant (~20%) quenching of fluorescence accompanied by a small blue shift in the spectrum is observed upon addition of Ca^{2+} to the protein (Figure 2.4b). Fitting a plot of fluorescence intensity versus Ca^{2+} concentration (Figure 2.4c) provides an estimate of the Ca^{2+} dissociation constant (K_d) of 1.3 µM, within the range expected for a Ca^{2+} sensor domain *in vitro* (Linse and Forsen 1995).

D1790G disrupts calcium-dependent properties of hH1

The LQT3 mutation D1790G resides at a position where the native aspartic acid side chain directly coordinates Ca^{2+} in consensus EF-hand loops (position 3; Figure 2.1a). Based on extensive prior mutational analysis on EF-hand proteins (Linse and Forsen 1995), the D1790G mutation would be predicted to reduce Ca^{2+} affinity approximately one order of magnitude. Such an effect could conceivably alter inactivation gating in hH1, and at least partly explain the LQT phenotype (Wehrens et al. 2000).

As predicted, D1790G significantly impairs the inactivation-destabilizing effect of Ca^{2+} on hH1 (Figure 2.4d). In D1790G, 10 µM Ca^{2+} only shifts the $V_{1/2}$ positively by 6.1 mV, versus 11.1 mV in WT (p < 0.0001 vs. D1790G, see Figure 2.2 and 2.4 legends for absolute $V_{1/2}$ values). The availability curves for D1790G and WT in 0 Ca^{2+} did not differ significantly, suggesting the mutation does not cause an allosteric effect on channel structure. However, in nearly all non-zero Ca^{2+} concentrations, the voltage-dependent availability of the mutant is left-shifted (hyperpolarized) relative to WT (Figure 2.4d), as

noted previously in studies employing less stringent Ca^{2+}-buffering conditions, but utilizing β1 subunit coexpression (An et al. 1998; Wehrens et al. 2000). Here we find that under more tightly-controlled Ca^{2+} buffering conditions, co-expression of β1 is not required to identify a hyperpolarizing shift in D1790G availability relative to WT.
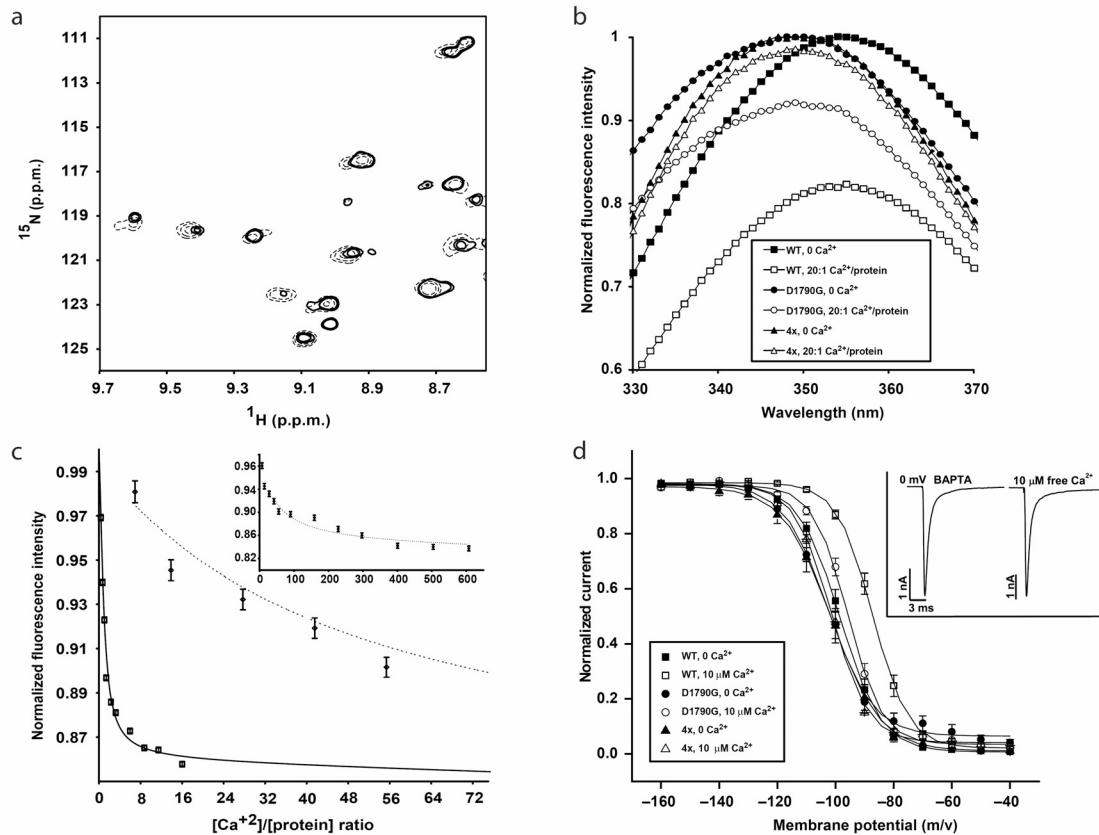
Figure 2.4: Structural characterization and calcium binding to hH1-CTD-148. (*a*) Close-up view of the down-field shifted region of hH1-CTD-148 wild type spectrum acquired at 28 ºC (dashed contours) with the corresponding region of the spectrum acquired under identical conditions for the D1790G mutant (solid contours). (*b*) Calcium dependence of the intrinsic tryptophan fluorescence spectrum of hH1-CTD-148 wild type, and the D1790G and 4X mutants. See legend. Filled symbols are for the apo state and open symbols for a solution containing ~20 μM Ca^{2+}. (*c*) Plot of fluorescence intensity versus added Ca^{2+} for hH1-CTD-148 (solid line) and the D1790G mutant (dotted line). The line through the points is the best fit to a single-site standard binding curve. Since the binding to the mutant is incomplete in the main panel, an inset is included to show the full binding curve (to 600-fold excess). (*d*) Voltage dependence of availability for D1790G and the 4X mutant. For reference, the wild type data is also included. For D1790G, the $V_{1/2}$ was -101.9 ± 1.7 (n=4) and –95.8 ± 1.0 mV (n=7) for 0 Ca^{2+} and 10 μM Ca^{2+} respectively (p < 0.01). k values were: 7.55 ± 0.14 (n= 4) and 5.68 ± 0.219 (n = 7) for 0 Ca^{2+} and 10 M Ca^{2+}, respectively (p < 0.001). For 4X, $V_{1/2}$ were -101.3 ± 2.2 mV in 0 Ca^{2+} (n = 9) and -101.1 ± 1.1 in 10 μM Ca^{2+} (n = 9) (p = N.S.). k values were: 7.58 ± 0.43 (n= 9) and 6.28 ± 0.276 (n = 9) for 0 Ca^{2+} and 10 μM Ca^{2+}, respectively (p < 0.01). Electrophysiological work in panel d done by Tammy Wingo. Taken from Wingo et al 2004.

The impact of a hyperpolarizing shift in availability due to D1790G has been mathematically modeled in detail (An et al. 1998; Wehrens et al. 2000). The reduced availability of Na^+ channels at the resting membrane potential leads to a diminished Na^+ current during the initiation of the action potential, which triggers a cascade of changes in the kinetics of multiple ionic currents during the action potential. This prolongs the cardiac action potential, increasing the likelihood of cardiac arrhythmias as seen in LQT3 (An et al. 1998; Wehrens et al. 2000). A recent study of D1790G has also detected a PKA-sensitive increase in sustained, "bursting" Na^+ channel activity during sustained depolarization (Tateyama et al. 2003), a gating behavior that also provokes LQT3 (Bennett et al. 1995; Chen et al. 1998). In our studies, addition of 10 μM intracellular Ca^{2+} did not increase the magnitude of the plateau current in either the wild-type (0.24 ± 0.14%, n = 11, plateau current relative to peak inward current) or D1790G (0.24 ± 0.057%, n = 7). Hence, we postulate that D1790G evokes LQT3 by prolonging the cardiac action potential through two complementary mechanisms: 1) a protein kinase A-dependent, Ca^{2+}-independent increase in channel bursting that increases the plateau current (Tateyama et al. 2003), and 2) disruption of Ca^{2+}-binding in the hH1 EF-hand, causing a hyperpolarizing shift in hH1 voltage-dependent availability (Figure 2.4d).

Biophysical analysis of hH1-CTD-148 containing the D1790G mutation reveals that the mutation does not cause significant changes to the NMR and CD spectra of the domain. Superimposing the down-field region of the 2D ^{15}N-^1H HSQC NMR spectra to compare the mutant and WT proteins provides convincing evidence that the mutation does not alter the protein structure (Figure 2.4a). In contrast, measurements of tryptophan fluorescence reveal Ca^{2+} binds more weakly to the mutant (Figure 2.4b,c) with a K_d

of 27 μM, ~20-fold lower than hH1-CTD-148. This reduction in affinity is consistent with the effects of mutations in other EF-hand Ca^{2+} binding proteins (Linse and Forsen 1995) and is sufficient to reduce the ability of the EF-hand domain to act as a Ca^{2+} sensor. Together, the patch-clamp and biophysical data suggest that D1790G causes LQT3 by weakening Ca^{2+}-dependent regulation of hH1 availability. This weakening is accomplished by disruption of Ca^{2+} binding to the EF-hand.

A "4X" mutant abolishes calcium-dependent properties of hH1

To further test this hypothesis, a mutant hH1 was designed to completely eradicate Ca^{2+} binding to the functional EF-hand. The first EF-hand binding loop contains the consensus acidic side chains at positions 1, 3, and 5, and the highly conserved glutamic acid at position 12 (Figure 2.1a), all of which directly chelate Ca^{2+}. The corresponding "4X" mutant (E1788A, D1790A, D1792A, E1799A) was prepared and examined electrophysiologically (whole channel) and *in vitro* (hH1-CTD-148 construct).

Raising free Ca^{2+} from 0 to 10 μM did not change "4X" voltage-dependent availability (Figure 2.4d). Moreover, the "4X" availability curve in 0 Ca^{2+} was similar to WT (Figure 2.4d), as was the I_{Na} decay rate (Figure 2.4d, inset), suggesting that the quadruple substitution does not induce marked structural changes in the C-terminus. Like WT, the "4X" response to Ca^{2+} was not altered by the CaM inhibitory (290-309) peptide (Figure 2.4d legend).

The results from biophysical analysis of hH1-CTD-148 containing the "4X" mutation were fully consistent with the electrophysiological observations. Ca^{2+} titrations monitored by fluorescence showed almost no response, even at a thousand-fold excess of

Ca^{2+} (Figure 2.4b), indicating that 4X-hH1-CTD-148 does not bind Ca^{2+} with any detectable affinity. The CD spectrum of 4X-hH1-CTD-148 confirmed the helical structure of the wild-type protein was retained. These results strongly imply that the "4X" mutation results in loss of Ca^{2+} binding activity without loss of overall structure.

Discussion

Ca^{2+} modulation of ion channels

Multiple sequence alignment, homology modeling and biophysical data on hH1-CTD-148 constructs leave virtually no doubt as to the presence of an EF-hand domain in hH1 that binds Ca^{2+} with affinity well within the range of known Ca^{2+} sensors. Binding of Ca^{2+} to this EF-hand domain has a role in a critical hH1 gating function: increasing channel activity by inducing a depolarizing shift in the voltage-dependence of channel availability.

While the effects of mutations in the EF-hand were consistent between the electrophysiologic and spectroscopic analyses, there was a ~7-fold difference in the apparent Ca^{2+} affinities: the EC$_{50}$ for the gating effect of Ca^{2+} on WT channels was 175 nM, while the Kd for Ca^{2+} in the C-terminal fragment binding studies was 1.3 μM. We ascribe these differences to the very different contexts under which the measurements were conducted. The Kd was measured using a Ca^{2+} binding domain (hH1-CTD-148) extracted from the channel, whereas the EC$_{50}$ was determined from measuring a voltage-dependent gating process in a population of channels within the intact cell. While the Ca^{2+} binding event is coupled to interactions that lead to changes in the gated state of the channel, the latter

38

(EC_{50}) measurement incorporates factors beyond the Ca^{2+} affinity alone. Hence, while the absolute values differ, the parallel changes in Ca^{2+} sensitivity induced by the EF-hand mutations lend strong evidence to support the proposal that the Ca^{2+} effect can be assigned to the EF-hand domain in the proximal C-terminus.

Recent studies (Deschenes et al. 2002b) have described indirect effects of Ca^{2+} on multiple Na^+ channel isoforms, through the actions of both CaM and CaM kinase. Inhibition of CaM altered both the voltage-dependent availability and the fast current decay of skeletal muscle Na^+ channels (Deschenes et al. 2002b). CaM was not observed to have this effect on hH1, but was found to inhibit a slowly-inactivating kinetic component evoked by sustained depolarization. Inhibition of CaM kinase was found to slow both the rate of current decay and the rate of entry into inactivation, and also induce the voltage-dependence of hH1 availability; notably, all three effects were found to be independent of CaM, and did not extend to the skeletal muscle isoform (Deschenes et al. 2002b). Similarly, the direct effects of Ca^{2+} observed on hH1 voltage-dependent availability through the EF-hand are CaM-independent: the 290-309 CaM-inhibitory peptide did not diminish the Ca^{2+}-dependent effects measured on hH1 availability (Figure 2.2b). Since 290-309 is a highly specific inhibitor of CaM but not CaM kinase, the use of this peptide should not confound our results by influencing CaM kinase regulation.

It remains unclear whether Ca^{2+} can directly modulate noncardiac Na^+ channel isoforms through the C-terminal EF-hand. A prior report found that intracellular addition of 10 mM BAPTA eliminated the Ca^{2+}-dependent CaM-induced hyperpolarizing shift in availability of the skeletal muscle isoform. This finding is not sufficient to exclude the possibility that Ca^{2+} alone may regulate the skeletal muscle isoform; however, given that

the Ca^{2+}-dependent CaM effect on the skeletal muscle isoform is directionally opposite to the EF-hand mediated effect we observe on the cardiac isoform, direct Ca^{2+} regulation of the EF-hand in skeletal muscle Na^+ channels may prove difficult to distinguish because the gating effects of Ca^{2+} in skeletal muscle channels may counterbalance, leading to a more subtle net effect. Numerous single amino acid C-terminal sequence changes, both within and outside the EF-hand region, are known to significantly influence Na^+ channel inactivation gating. These differences could well explain the isoform differences observed in Ca^{2+}-dependent gating effects. It is increasingly clear that several aspects of Na^+ channel gating are regulated by intracellular Ca^{2+}, and that mechanisms mediating these effects involve both direct (EF-hand mediated) and indirect (CaM (Tan et al. 2002a) and CaM kinase (Deschenes et al. 2002b)) actions by Ca^{2+}.

Implications for cardiac arrhythmia syndromes

Our findings suggest the C-terminal EF-hand domain plays a modulatory role in an inherited form of the long QT syndrome (D1790G; Figure 2.4). While the putative loci regulating fast and slow inactivation in the Na^+ channel were originally localized to the domain III-IV linker and P-segments, respectively, additional loci throughout the channel were eventually shown to influence both gating processes. Several inherited mutations in the hH1 C-terminus are associated with defects in either fast or slow inactivation, and the insertion mutant (1795insD) evokes defects in both gating processes, causing both the long QT and Brugada syndromes in the same family. It is noteworthy that both the IQ and EF hand motifs in the C-terminus are adjacent to many of these arrhythmia-related loci. As such, it is possible that inherited mutations in the C-terminus may modulate hH1

inactivation gating through altering the function of these two, adjacent Ca^{2+} regulatory elements, either separately or in combination.

The structural model of the EF hand domain (Figure 2.1c) serves as a point of reference for generating initial hypotheses to unravel molecular mechanisms that underlie disease-causing mutations in the hH1 C-terminus. For example, the model suggests the insertion within the Ca^{2+}-binding loop (1795insD) associated with both LQT3 and the Brugada arrhythmia syndromes (Veldkamp et al. 2000) will alter the register of side chains coordinating the Ca^{2+} ion. E1784K, another LQT3 mutation (Wei et al. 1999), is located adjacent to the Ca^{2+}-binding loop, and the model suggests this mutation could disrupt the network of hydrogen bonds critical to the structural stability of the binding loop (Strynadka and James 1989). Electrophysiologic, biophysical, and structural studies of hH1 constructs carrying these disease-linked mutations should provide insight into how modified Ca^{2+} binding in the EF-hand region influences hH1 dysfunction, and thereby shed light on the mechanisms of these inherited arrhythmia syndromes.

Therefore, we undertook to first characterize the precise stretch of residues defining the folded core of the proximal hH1 C-terminus containing the EF-hand and calcium binding activity. We also designed a series of mutations in the EF-hand to characterize unique aspects of the binding loop. These results are described in Chapter III.

CHAPTER III

REMOVAL OF THE IQ-MOTIF FROM HH1 RESULTS IN SIGNIFICANTLY RE-
DUCED CALCIUM AFFINITY IN THE HH1 C-TERMINUS

Introduction

As described in Chapter II, it has been established with a high level of confidence that calcium binds directly to the hH1 C-terminus, causing functional changes in channel behavior. Mutations in the EF-hand calcium binding loop disrupt this binding and reduce or abolish calcium-dependent functional effects. On the basis of these findings, further characterization of the EF-hand core in the hH1 C-terminus was undertaken. Two approaches were taken.

First, truncation mutants were generated in order to further define the folded region of the hH1 C-terminus. Observations while working with hH1-CTD-148 suggested that this 148 residue construct is proteolytically sensitive at the C-terminus. This observation is consistent with previous observations published in the literature (Zwerling et al. 1991), and led to the hypothesis that further truncations could be made without adverse effect on folding of the EF-hand core.

Second, mutational studies were undertaken in order to study the role of specific residues in the calcium binding loop. Four single mutations that fall within the loop were designed for examination: D1790G, F1791A, M1793G, and E1799A. Based on the properties of canonical EF-hand calcium binding loops, the two mutations involving acidic residues (D1790G and E1799A) were expected to lower calcium affinity. F1791A is a control and was expected to have no effect on affinity. M1793G was expected to either

increase calcium affinity or have no effect (Nelson and Chazin 1998). As discussed in Chapter I, in canonical EF-hands the position 7 residue contributes its main chain oxygen to the chelation of calcium ion. Since position 5 contributes an oxygen from its side chain, the position 6 residue must adopt an unusual backbone conformation favorable only for glycine, leading to strong conservation of glycine in this position. Calcium binding in an EF-hand with a methionine at position 6, as there is in hH1, suggests that a higher energetic penalty is being paid during a calcium binding event for this site relative to a canonical EF-hand. Mutation of position 6 from methionine to glycine would therefore possibly reduce or abolish this extra energetic penalty, a reduction which may translate into an increased calcium affinity.

The studies in this chapter confirm and extend our previous findings with regard to the presence and role of an intrinsic calcium sensing EF-hand motif in the proximal hH1 C-terminus. Specifically, these experiments show that the stably folded component of hH1-CTD-148 can be found within the 93-residue region E1773-S1865, but that intermediate (sensor-range) calcium affinity requires the presence of downstream residues.

Results

The proximal 93-residues of the hH1 C-terminus are stably folded

In order to determine the stretch of residues that defines the folded core of the calcium binding motif, two significantly truncated constructs (hH1-CTD-93, E1773-S1865; hH1-CTD-120, E1773-I1892) relative to the one previously used (hH1-CTD-148, E1773-S1920) were generated. The truncations were based on previously published sec-

ondary structure predictions (Cormier et al. 2002b) and multiple sequence alignment, re-moving the predicted 6th, or 5th and 6th, helices from the construct. ^{15}N-^{1}H HSQC NMR spectra were collected for these proteins in the presence of saturating calcium. Figure 3.1 shows ^{15}N-^{1}H HSQC spectra of hH1-CTD-93, hH1-CTD-120, and hH1-CTD-148. Note especially the downfield regions of the spectra containing signals that are highly sensitive to the tertiary structure. These overlays demonstrate that all of the downfield shifted peaks characteristic of the globular core are preserved even in the shortest construct. The very small chemical shift differences imply that there is at most a minor conformational effect of leaving off the predicted fifth and sixth helices of the C-terminus. Thus, the truncations do not adversely affect the folded core containing the globular EF-hand do-main, which implies that the core is within hH1-CTD-93.

Calcium binding to hH1-CTD-93 is observable by NMR

^{15}N-^{1}H HSQC spectra of hH1-CTD-93 in the absence (2 mM BAPTA) and pres-ence (20 mM CaCl$_2$) of calcium revealed a significant number of calcium-dependent chemical shift perturbations (Figure 3.2a). While the number of perturbations is large, it is clear from the magnitude of these changes that the conformational effect of calcium binding is significantly milder than that seen for a typical calcium sensor such as calmodulin. Calcium-dependent changes in the ^{15}N-^{1}H spectra for these proteins are much more substantial, indicating more significant reorganization of the tertiary structure in these cases (e.g. Ikura et al. 1990; Skelton et al. 1992; Ishida et al. 2002).
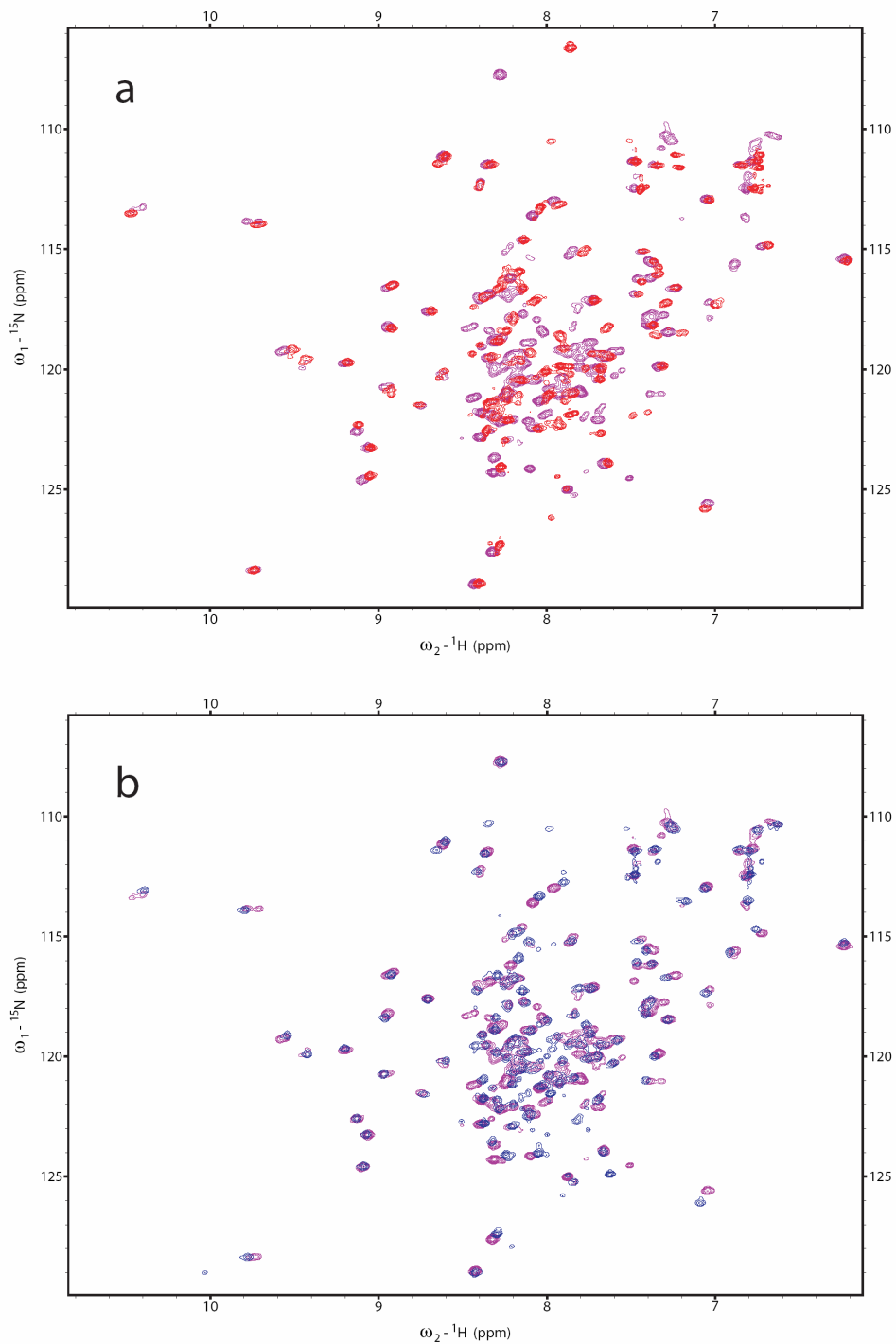
Figure 3.1: NMR reveals that truncation to hH1-CTD-93 do not disrupt the folded EF-hand core. Shown here are zoomed regions of the ^{15}N-^{1}H HSQC NMR spectrum of ^{15}N-nat-hH1-CTD-148 (purple, both panels) with the spectra of (*a*) ^{15}N-nat-hH1-CTD-93, red and (*b*) ^{15}N-nat-hH1-CTD-120, blue. All proteins were expressed without any tags and were exchanged into buffer containing 20 mM Tris, 5 mM BME, 20 mM CaCl$_2$ at pH 7.5. See Appendix C for further details on the Materials and Methods. Full spectra are included in Appendix D.
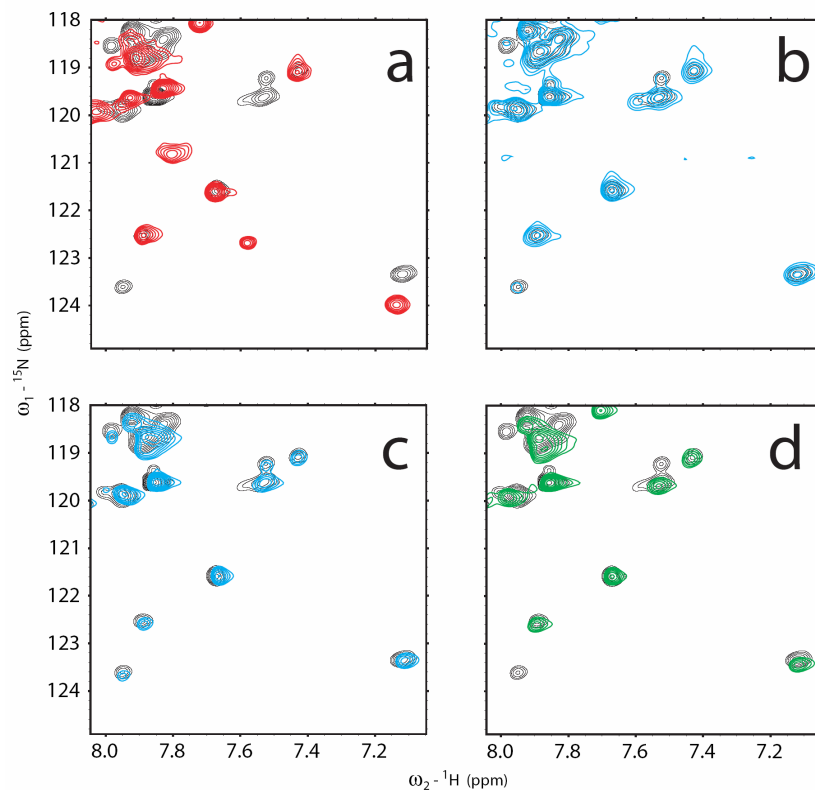
Figure 3.2: Calcium-dependent changes in the NMR spectrum of hH1-CTD-93. Shown are zoom regions of the ^{15}N-^{1}H HSQC NMR spectrum of ^{15}N-His-hH1-CTD-93 in BAPTA (black, all panels) with spectra of the protein under the following conditions: (*a*) in CaCl$_2$, red; (*b*) in EGTA, light blue; (*c*) TCA precipitated, light blue; (*d*) in MgCl$_2$, green. Full spectra are included in Appendix D.

In order to verify that the chemical shift perturbations in hH1-CTD-93 are specifi-

cally related to the binding of calcium and not to changes induced by binding of BAPTA,

protein was decalcified using two other protocols and also exchanged into calcium-free

buffer containing 20 mM MgCl$_2$ (Figure 3.2b-d; see Methods). ^{15}N-^{1}H HSQC spectra of

the proteins decalcified in different ways overlay with the BAPTA spectrum (Figure

3.2b,c), confirming that the observed chemical shift changes are not caused by BAPTA

and are specifically related to the presence of the divalent ion. The spectrum of the mag-

nesium loaded sample (Figure 3.2d) largely overlays with the BAPTA spectrum, indicat-

ing that the chemical shift perturbations are specifically related to the presence of cal-

cium. The small changes induced by magnesium are attributed to the fact that magnesium can bind in calcium binding sites with weak affinity, but without causing the conformational effects associated with calcium binding (Andersson et al. 1997). The lack of conformational effect is suggested by the fact that a majority of peaks that shift significantly in the presence of calcium do not shift at all in the presence of magnesium. Those peaks that do shift upon binding magnesium are found, in part, to disappear (Figure 3.2d), presumably due to line broadening associated with chemical exchange.

EF-hand mutations in hH1-CTD-93 did not disrupt structure

The four EF-hand calcium binding loop mutations (D1790G, F1791A, M1793G, and E1799A) discussed above were introduced into hH1-CTD-93. Our strategy was to first assay the structural integrity of each mutant protein, then measure calcium affinity. CD and ^{15}N-^{1}H heteronuclear NMR were used for structural characterization. To facilitate the analysis, the more stable and soluble His$_6$-tagged constructs were used for these experiments. Due to the potential for interference from the His$_6$-tag, some of the calcium affinity measurements were performed using protein expressed without the tag and purified by other means (see Materials and Methods). Figure 3.3 shows the CD and ^{15}N-^{1}H HSQC NMR data for the wild-type protein and each mutant. The CD data indicates that the secondary structure content of each of these constructs is highly similar to that of the wild-type protein. While there is a detectable difference in the CD spectrum of D1790G in the region between 220 and 230 nm as compared to the other constructs, the effect is not large enough to conclude that the structure of this mutant is significantly different.
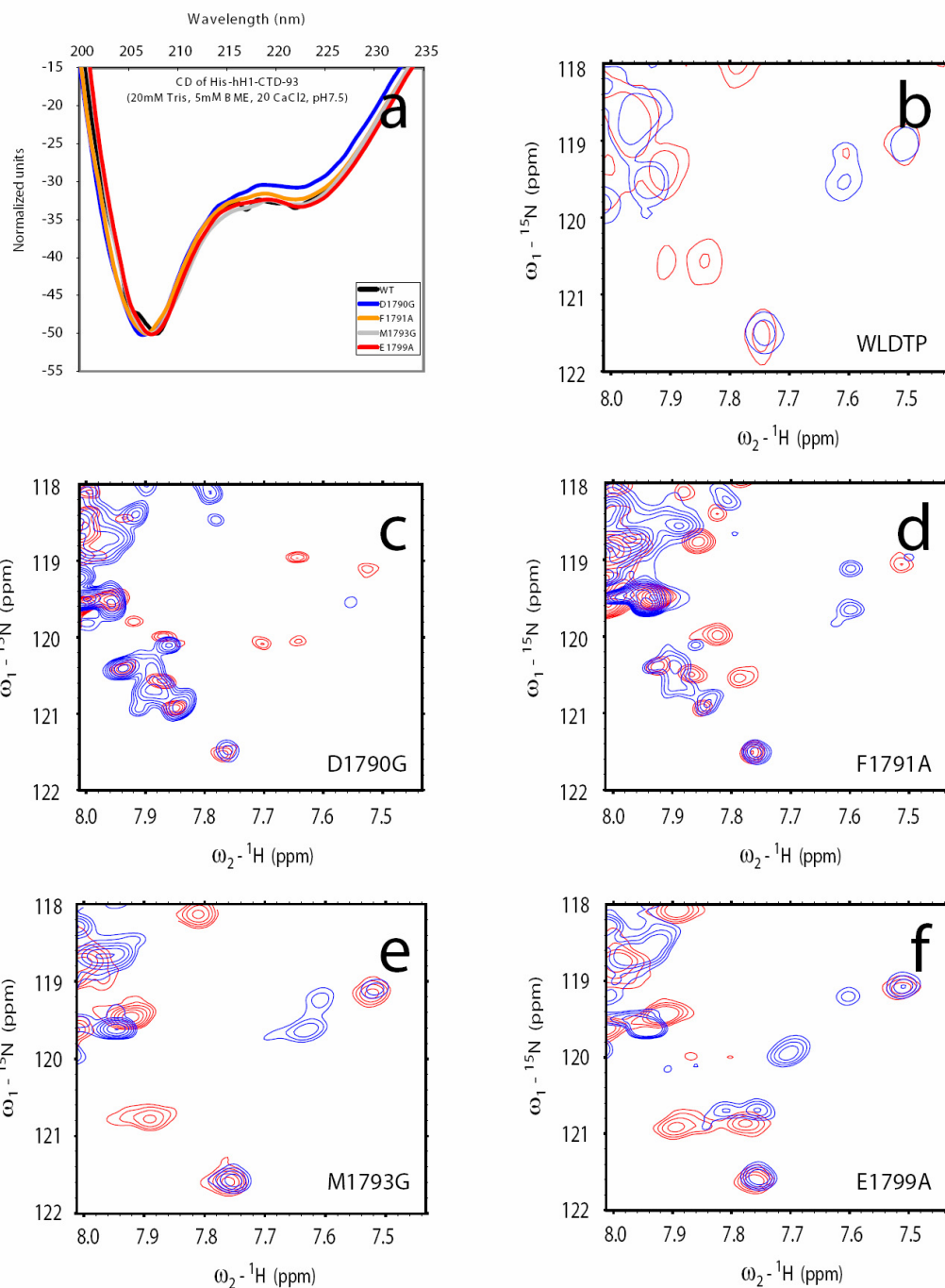
Figure 3.3: Mutations in the hH1 EF-hand do not disrupt secondary or tertiary structure. (*a*) CD spectra of wild-type and all mutations show helical characters with characteristic minimum at 222 nm. (*b-f*) Overlays of zooms of ^{15}N-^{1}H HSQC NMR spectra collected for wild-type or mutant protein, as indicated in the panel, under apo (blue) or Ca^{2+}-loaded (red) conditions. These indicate preservation of tertiary structure; some chemical shift perturbations versus wild-type are expected simply due to the introduction of mutations. Full spectra are included in Appendix D.

The NMR data confirms that the tertiary structure of each of the mutants is retained, as reflected in the overlap of signals in the spectrum of each mutant with signals in the wild-type protein.

Calcium binds to hH1-CTD-93 with mM affinity

The calcium affinity of hH1-CTD-93 was determined by titration of calcium into calcium-free, BAPTA-free protein. Attempts to monitor the titration by fluorescence and isothermal titration microcalorimetry were unsuccessful because, unknown at the time the measurement were undertaken, the calcium affinity of the 93-residue construct was much weaker than the calcium affinity of the 148-residue construct.
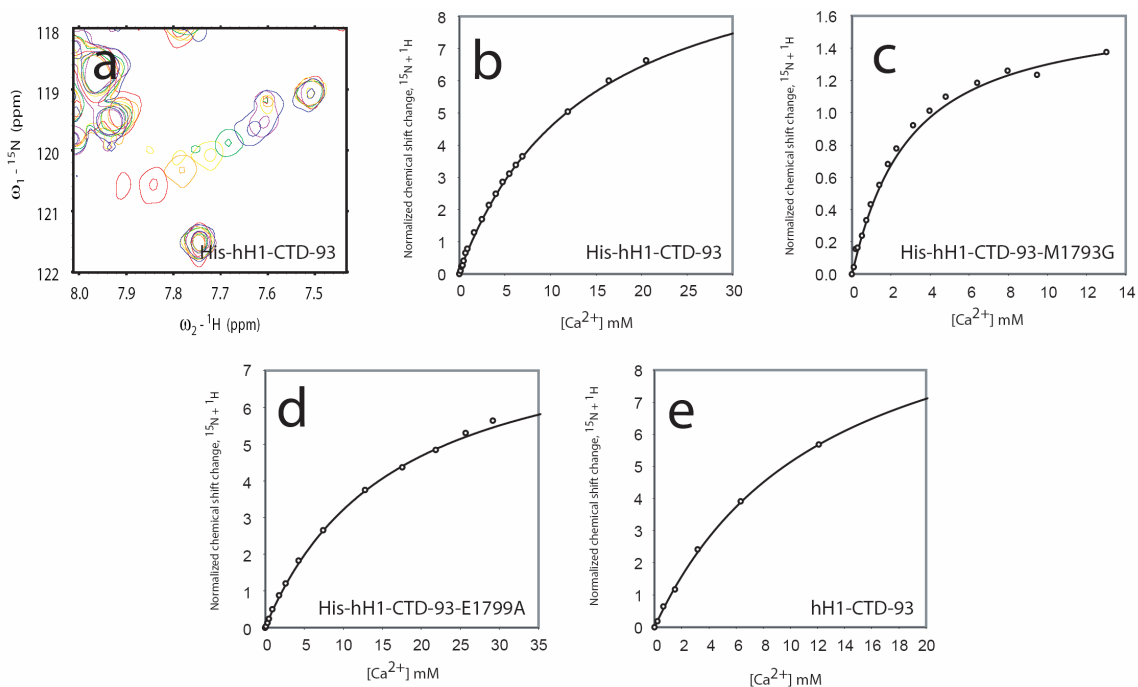
Figure 3.4: Calcium titrations of hH1-CTD-93 monitored by NMR. Changes in selected signals from the ^{15}N-^{1}H HSQC spectra of (*a,b*) wild-type ^{15}N-His-hH1-CTD-93, (*c*) M1793G ^{15}N-His-hH1-CTD-93, (*d*) E1799A ^{15}N-His-hH1-CTD-93, and (*e*) wild-type ^{15}N-nat-hH1-CTD-93. See text for affinity values. Full spectra for panel a are included in Appendix D.

Based on the observed calcium-dependent chemical shift changes, NMR was used to monitor the calcium titration. The titration of a representative peak in the ^{15}N-^{1}H HSQC spectrum of His-hH1-CTD-93 is shown in Figure 3.4a. Calculation of the binding constant (average binding constant for 8 residues with significant chemical shift perturbations) using this data revealed an extremely weak binding interaction (7.5 ± 0.6 mM; fit shown in Figure 3.4b). This affinity is far weaker than the affinity measured previously for the longer hH1-CTD-148 construct (1.3 ± 1.2 μM), and is well outside the range of calcium affinity expected for a physiologically relevant calcium sensor.

The accuracy of this dissociation constant was verified by repeating the calcium titration several times with wild-type protein. Moreover, titrations of calcium into His-M1793G and His-E1799A mutant protein (Figure 3.4c,d) provided similar results with K_d values of 4.7 ± 0.6 mM and 7.3 ± 0.9 mM, respectively. Finally, to ensure that the reduced affinity was not caused by the His$_6$-tag, a calcium titration was performed with hH1-CTD-93 construct expressed without the tag (Figure 3.4e). Similar low affinity K_d values were measured, confirming that the EF-hand domain is insufficient on its own to attain high affinity calcium binding.

In light of the weak calcium binding affinity measured for hH1-CTD-93, the calcium binding affinity measurement of hH1-CTD-148 reported in Chapter II was repeated. These new measurements took advantage of improved expression, purification, and de-calcification protocols and provided binding constants with significantly higher precision than those reported in Chapter II. Improved sample preparation also allowed recording of ^{15}N-^{1}H HSQC spectra for both apo and calcium-loaded hH1-CTD-148. These spectra confirm that the calcium-dependent chemical shift perturbations observed in hH1-CTD-

93 are comparable to those seen in hH1-CTD-148 (Figure 3.5b). Titration of calcium into hH1-CTD-148, monitored by NMR, provided an estimate of affinity (K_d < 10 μM) (Figure 3.5b). A more accurate value of the dissociation constant was determined by monitoring calcium-dependent changes in intrinsic tryptophan fluorescence, yielding a value of 5.8 ± 0.3 μM (Figure 3.5a), fully consistent with our previous findings. These results confirm the potential of the EF-hand domain of hH1 to serve as an effective calcium sensor.
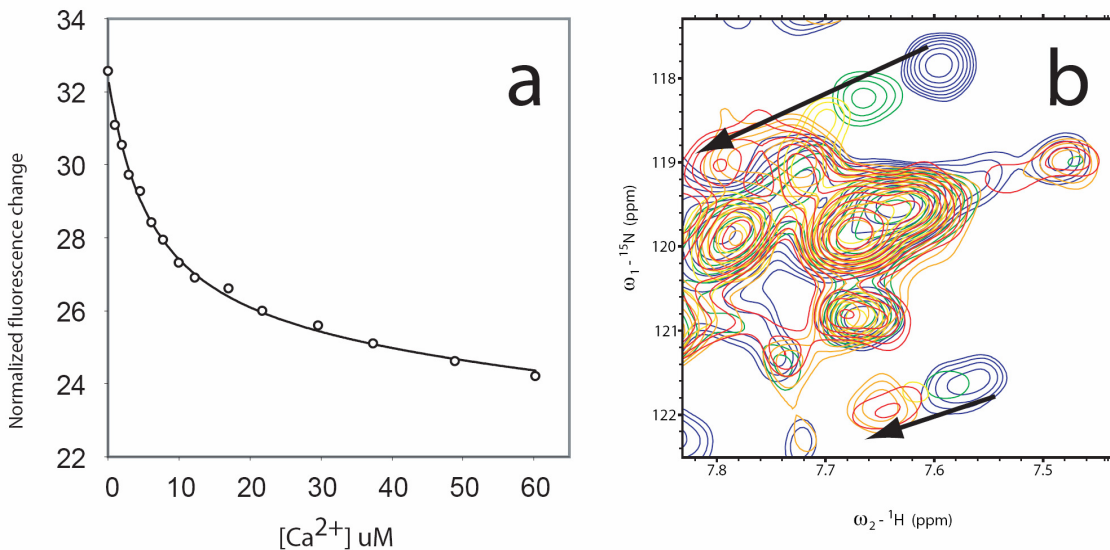
Figure 3.5: Titration of calcium into ^{15}N-hH1-CTD-148 monitored by ^{15}N-^{1}H HSQC NMR and by intrinsic tryptophan fluorescence reveal high affinity calcium binding. (a) Titration of Ca^{2+} into nat-hH1-CTD-148 monitored by intrinsic tryptophan fluorescence. (b) [Ca^{2+}] was 0 μM, 200 μM, 500 μM, 630 μM, 1800 μM for blue, green, yellow, orange, and red respectively; protein concentration approximately 500 μM. Note that the shift change is virtually saturated at 630 μM, indicating an affinity much stronger than the protein concentration (see Appendix B). Full spectra are included in Appendix D.

Discussion

The observation of weak (mM range) calcium affinity in hH1-CTD-93 was not anticipated. Our initial assumption was that the folded EF-hand core would retain full

calcium-binding capability; the fact that it does not, and that the additional 55 residues are necessary for high affinity calcium binding without playing a significant structural role, is highly provocative. It suggests cross-talk between two calcium-dependent hH1 regulatory pathways since both involve the IQ calmodulin-binding motif. This type of direct communication between calcium sensors may function as some sort of detector for firing rate and/or intracellular calcium buildup, depending on the kinetics governing the various interactions.

It is important to note that the NMR and fluorescence experiments reconfirmed our previous observation of high affinity calcium binding in hH1-CTD-148. A recent report noted an inability to reproduce the calcium dependent changes in intrinsic tryptophan fluorescence even though the investigators were using a construct similar to ours (Kim, Ghosh, Liu et al. 2004). However, although this team used a standard protocol for decalcification, no evidence was provided that the samples were fully decalcified. Our previous observations showed that standard decalcification procedures are not always fully effective at decalcifying the hH1 EF-hand domain. Hence, we believe that the high affinity calcium binding site remained occupied in their experiments, and consequently no calcium-dependent spectral changes were observed.

When this group measured the intrinsic tryptophan fluorescence of their hH1-CTD construct, they found an extremely blue-shifted tryptophan fluorescence emission maximum of approximately 325 nm, as compared to the maximum which we observed to occur at approximately 345 nm. They suggest that this difference may indicate partial unfolding in our samples. However, the dispersion of ^{15}N-^{1}H HSQC chemical shifts in our samples, reported both here and in Chapter II, unambiguously demonstrates the pres-

ence of folded globular protein (Cavanagh 1996). Our new results show calcium-dependent NMR chemical shift perturbations and high affinity calcium binding in hH1-CTD-148 by intrinsic tryptophan fluorescence and by NMR. The affinity reported here is nearly identical to that obtained previously using a different construct, a different purification protocol, and a different decalcification protocol. These facts suggest that other factors, such as the aforementioned incomplete decalcification, may be involved in the inability of Kim et. al. to reproduce our results.

The experiments reported here established the minimum region necessary for high affinity calcium binding in hH1. More importantly, they suggest a potentially new and exciting role for the sixth helix in hH1-CTD-148, which contains an IQ motif. This prompted a series of complementary spectroscopic and electrophysiologic studies related to the IQ motif region, which are described in Chapter IV.

CHAPTER IV

THE HH1 C-TERMINAL IQ MOTIF PLAYS A DUAL ROLE
IN CALCIUM-DEPENDENT REGULATION

Introduction

Chapter II provides detailed evidence that calcium is able to bind to an EF-hand found in the region E1788-E1799 of the hH1 C-terminal domain, and that arrhythmogenic mutations in the EF-hand disrupt both the binding of calcium and the functional effects of calcium on the channel. The experiments described in Chapter III revealed that while the region containing the proximal 93 residues of the C-terminal domain preserved the folded EF-hand core, this region is not sufficient for high affinity calcium binding. Truncation of the 55 residues C-terminal to the EF-hand domain results in a three order of magnitude drop in calcium affinity.

The region R1897-S1925 at the C-terminus of hH1-CTD-148 contains an IQ-type calmodulin (CaM) binding motif (Tan et al. 2002b; Mori et al. 2003). The evidence provided in Chapter III suggests that this may be the component needed for high affinity calcium binding in the EF-hand. The IQ motif is a common calmodulin binding motif (see Chapter I). Briefly, the consensus sequence of the IQ motif is **δQxxxβGxxxβxxδ**, where **δ** represents any of Phe/Ile/Leu/Val and **β** represents either Lys or Arg (Bahler and Rhoads 2002). The Gly at position 7 is only loosely conserved; while it is found is some human isoforms of the sodium channel, it is not present in hH1. The final hydrophobic residue is likewise variably conserved, but it is found in all human sodium channel isoforms. It is commonly held that the function of the IQ motif, which can bind apo-CaM, is to localize calmodulin at basal calcium levels so that the local concentration of CaM is

high near sites where it is to perform a calcium-dependent role (Alexander et al. 1987; Jurado et al. 1999). It may also function to modulate the kinetics of calcium binding by increasing the off-rate of calcium, allowing more rapid responsiveness to calcium signals (Putkey et al. 2003).

CaM has been reported to bind to the hH1 IQ-motif in a calcium-independent manner, i.e. it binds CaM in the absence of calcium (Mori et al. 2003), but the functional effect of CaM binding remains unclear. The initial report described an enhancement of slow inactivation by the binding of Ca^{2+}-CaM to the hH1 IQ motif (Tan et al. 2002b), but others have found different effects or no effect of CaM on hH1, though some have found that CaM may modulate other isoforms of the voltage-gated sodium channel family (Deschenes et al. 2002a; Herzog et al. 2003). Further complicating the picture is a recent report suggesting that all calcium-dependent changes experienced by hH1 are mediated by CaM and that calcium does not bind directly to the EF-hand domain (Kim, Ghosh, Liu et al. 2004).

Even absent conflicting reports, it remains difficult to understand the role of various regulators (e.g. Ca^{2+}, CaM, FHF1b, and Nedd; see Chapter I), given the critical lack of information about the mechanisms that underlie steady-state availability and slow inactivation. Characterization of arrhythmogenic mutations have uncovered regions of the channel that are important for various channel functions, and have in that way contributed to advances in understanding these mechanisms. Since it is known that calcium is playing a critical and possibly anti-arrhythmic role in channel function based on the data in Chapters II and III, further examination of this pathway may lead to important insights into the mechanisms of both normal and aberrant channel behavior.

This chapter describes the combination of electrophysiology, fluorescence and NMR approaches that were used to characterize one aspect of this pathway. Interactions between the IQ motif and both calmodulin and the hH1 EF-hand domain are characterized. Mutations in the IQ motif which disrupt calcium-dependent function of the channel are then introduced and characterized spectroscopically and electrophysiologically, revealing that mutations in the IQ motif can indeed significantly disrupt calcium binding in the upstream EF-hand. A mechanistic model for the regulation of hH1 by calcium is then explored in Chapter V.

Results

The IQ motif binds to hH1-CTD-93 in a Ca^{2+}-dependent manner

Given the significant difference in calcium affinity between hH1-CTD-148 and hH1-CTD-93, as described in Chapter III, we hypothesized that the sixth ("IQ") helix is acting to tune the calcium affinity of the folded domain (hH1-CTD-93) during a calcium signaling event, even though, based on the truncation NMR data, this region is not playing a significant structural role in the folding of the EF-hand domain.

```
                 δQxxxRxxxxRxxδ          canonical IQ
RRKHEEVSAMVIQRAFRRHLLQRSLKHAS  hH1 IQ peptide
...........AA................  IQ/AA mutant
...........................T.  A1924T mutant
```

Figure 4.1: Canonical IQ motif sequence compared with the hH1 IQ motif. Also indicated are the locations of two IQ motif mutations introduced to ascertain their effect on calcium and calmodulin affinity.

To explore this hypothesis, a 31-residue peptide corresponding to the region R1897-S1925 of hH1, centered on the putative IQ motif in the hH1-C-terminus, was generated. This peptide was used in chemical shift perturbation assays to probe binding to ^{15}N-labeled hH1-CTD-93. Figure 4.1 shows the primary sequence of the IQ motif peptide.

Based on chemical shift perturbations, the IQ motif binds hH1-CTD-93 in both apo and calcium-loaded states; addition of the peptide causes selective broadening and/or shifting of a significant number of peaks (Figure 4.2). Remarkably, many peaks that change upon the addition of peptide are also peaks that shift upon the addition of calcium, and the perturbations in some cases differentially affect the proton and/or nitrogen resonance frequencies. For example, a peak at 122 ppm in ^{15}N and 8.4 ppm in ^{1}H appears to shift primarily in the ^{1}H dimension upon the addition of calcium, but primarily in ^{15}N dimension upon the addition of peptide. This observation suggests that IQ motif binding promotes the conformational change needed to bind calcium. Thus, the peptide seems to play a role either in direct chelation of the calcium ion or in a conformational change in the EF-hand core that facilitates calcium binding. It is also interesting to note that under calcium-loaded conditions, addition of the peptide causes the protein to precipitate significantly. This suggests that the presence of both peptide and calcium results in a conformational change that promotes aggregation of this protein construct.

The affinity of the IQ motif for hH1-CTD-93 was not determined, for both theoretical and practical reasons. The measurement of the affinity as a bimolecular event would not accurately reflect the association of these two species because they are covalently linked *in vivo* in the same polypeptide chain. This results in a dramatic increase in

the local concentration of the IQ motif vis-à-vis the EF-hand. Due to these considerations, an *in vitro* bimolecular affinity measurement would dramatically underestimate the actual ratio of bound to free species in the channel. From a practical standpoint, addition of the peptide causes precipitation of hH1-CTD-93. During experiments, this results in an inability to hold the protein relatively constant while measuring the response of the system at various ligand concentrations, a critical requirement for accurate determination of K_d (see Appendix B). Finally, the observation of intermediate and fast exchange phenomena in the spectra allows us to coarsely estimate the bimolecular affinity as between 50 μM and 500 μM. While weak on its own, by factoring in the effect of covalent linkage we conclude that interaction is likely to be physiologically relevant.
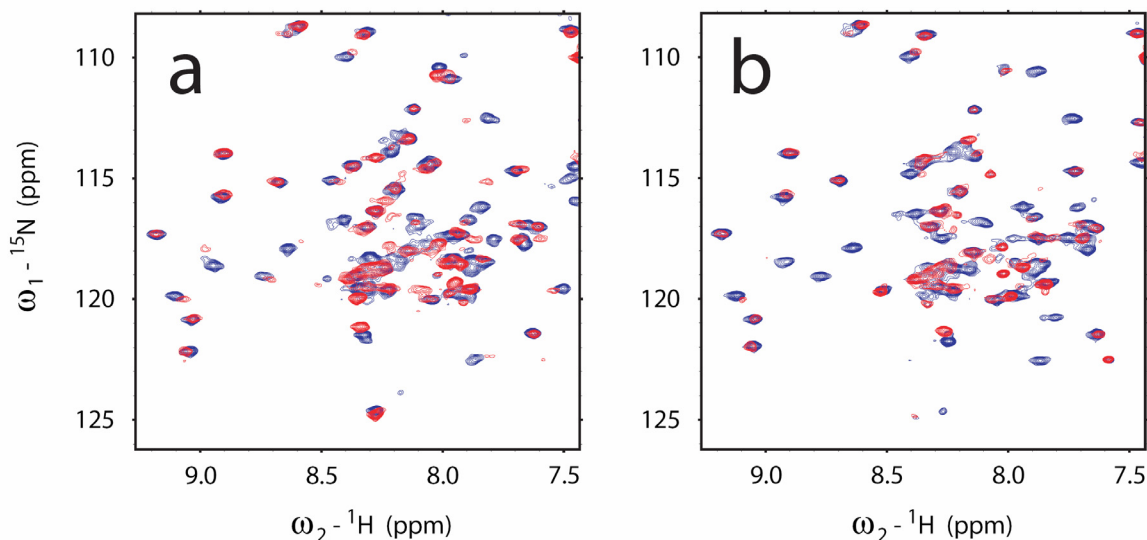
Figure 4.2: IQ motif peptide binds to both apo- and Ca^{2+}-hH1-CTD-93. (*a*) The overlay of apo-hH1-CTD-93 in the absence (blue) and presence (red) of saturating peptide. (*b*) Corresponding spectra for Ca^{2+}-hH1-CTD-93. The effects of the IQ motif are more pronounced in presence of calcium as evidenced by greater selective exchange broadening in panel b. Calcium-dependent chemical shift perturbations are not directionally the same as IQ-dependent perturbations. Full spectra are included in Appendix D.

IQ motif mutations alter calcium affinity

In order to further characterize the role of the IQ motif in Ca^{2+}-dependent regulation of channel function, a collaboration with the laboratory of Dr. Jeffrey Balser was initiated to characterize the properties of IQ motif region mutations using electrophysiological and spectroscopic techniques.

Two mutations were selected for characterization: a naturally occurring arrhythmogenic mutation is found in the distal part of the IQ motif at position 1924, resulting in an alanine to threonine mutation (A1924T). This mutation is known to cause Brugada syndrome and was observed to disrupt Ca^{2+}-CaM interactions with the hH1 IQ motif by Tan and colleagues (Tan et al. 2001). Another IQ mutation, I1908A/Q1909A (IQ/AA), was also examined because it had been previously used by others in the characterization of CaM interactions. Figure 4.1 shows the location of these mutations in context of the wild-type IQ motif sequence.
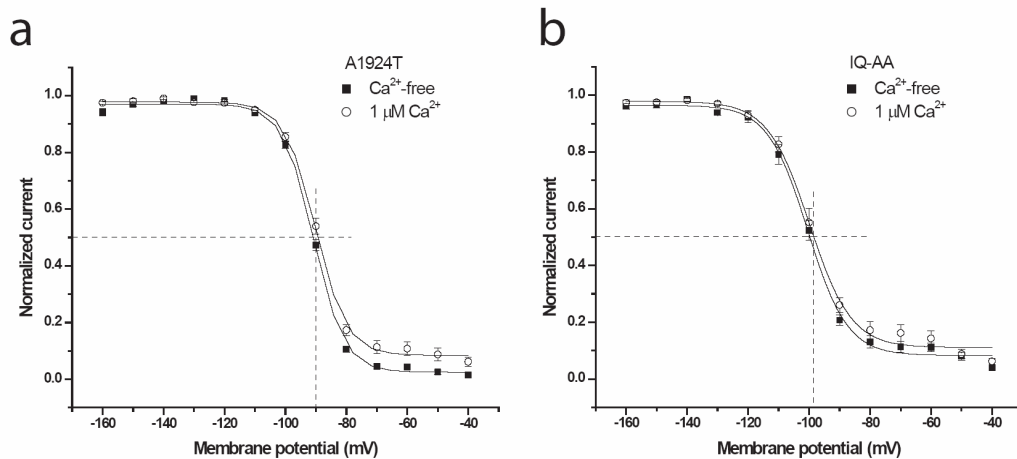
Figure 4.3: Mutations in the IQ motif diminish calcium-dependent changes in steady-state availability. (a) $V_{1/2}$ for A1924T was: -90.87 ± 0.44 (n = 12) for Ca^{2+}-free conditions and -90.18 ± 0.71 (n = 13) for 1 μM Ca^{2+}. (b) $V_{1/2}$ for IQ/AA was: -100.76 ± 1.05 (n = 9) for virtually Ca^{2+}-free conditions, and -100.03 ± 1.44 (n = 9), for 1 μM Ca^{2+}. Data was collected by Tammy Wingo.

Interestingly, these mutations have very different effects on the electrophysiological properties of the channel. A1924T was found to cause a rightward shift of the steady-state availability curve at basal calcium levels, recapitulating the $V_{1/2}$ observed for calcium-loaded wild-type channel (Figure 4.3a). In contrast, the IQ/AA mutation caused a shift in the availability curve to the left, in a manner similar to that observed for the 4X mutation discussed in Chapter II (Figure 4.3b). In both cases, however, mutant channels failed to exhibit a the significant calcium-dependent shift in steady-state availability observed in wild-type hH1 (Figure 2.2a).
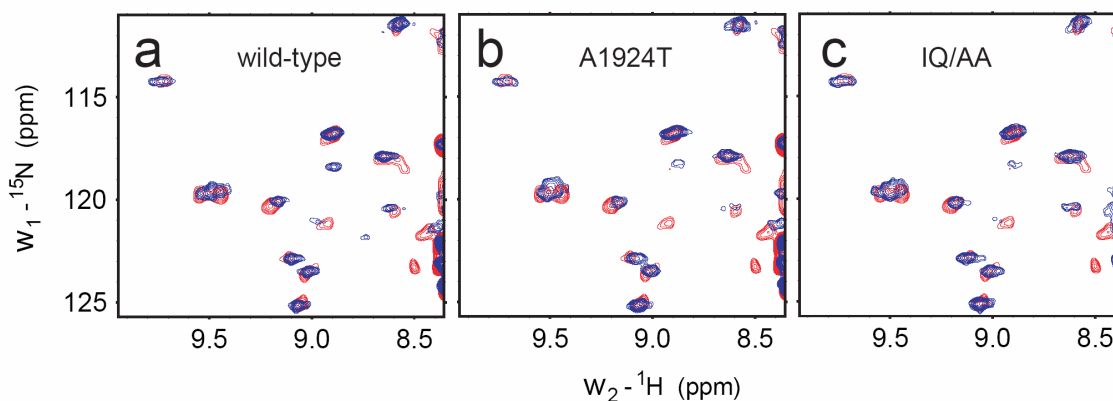
Figure 4.4: Mutations in the IQ motif of hH1-CTD-153 do not disrupt the structure of the EF-hand domain as compared to hH1-CTD-148. Regions of the ^{15}N-^{1}H HSQC spectra of (a) wild-type hH1-CTD-153 (blue), (b) hH1-CTD-153-A1924T (blue), and (c) hH1-CTD-153-IQAA (blue) overlayed with the spectrum of hH1-CTD-148 (red). Full spectra are included in Appendix D.

In order to characterize the biophysical and structural effects of these mutations, a slightly longer construct of the hH1 C-terminus was required, extending from residues E1773-S1925 (hH1-CTD-153). This construct was expressed without any tags and purified by standard methods. The IQ-motif region mutations were introduced into hH1-CTD-153 by site-directed mutagenesis.

^{15}N-^{1}H HSQC NMR spectra of protein expressed from these constructs indicate that the hH1-CTD-153 wild-type and mutant constructs retain the same tertiary structure as hH1-CTD-148 (Figure 4.4). Of note, point mutations normally cause at least one or two significant chemical shift perturbations in ^{15}N-^{1}H HSQC spectra, but none are observed for the IQ motif mutants. This observation suggests that the IQ region in this construct is in chemical exchange and not visible in the NMR spectra, although it is possible that the resonances that are perturbed are buried in the crowded central region of the spectrum (7.5 to 8.5 ppm in ^{1}H, 118 to 125 ppm in ^{15}N).
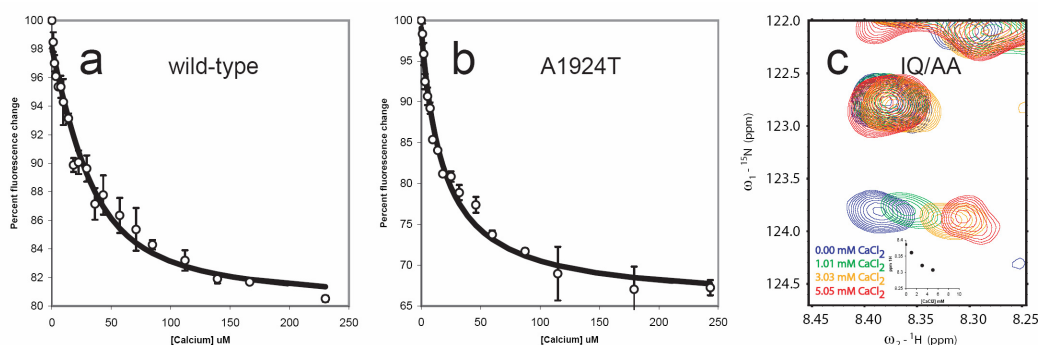
Figure 4.5: Titration of calcium into hH1-CTD-153 wild-type and mutants reveals significantly reduced affinity in the IQ/AA mutant. Binding affinity for hH1-CTD-153-WT was 15 ± 5 μM, and for hH1-CTD-153-A1924T was 18 ± 5 μM. These values were not significantly different from one another. The IQ/AA mutant showed affinity in the mM range, comparable to the affinity observed for the hH1-CTD-93 truncation mutant.

In order to confirm the biochemical function of the hH1-CTD-153 construct, calcium affinity measurements were performed as described previously and a K_d value of 15 ± 5 μM was obtained (Figure 4.5a). This affinity, is approximately tenfold weaker than the hH1-CTD-148 affinity reported in Chapter II and threefold weaker than the hH1-CTD-148 affinity reported in Chapter III. Although this value is outside the accepted range of affinities for calcium sensors, it is sufficiently close. The origin of this effect

remains unknown. However, as discussed in Chapter II, none of the *in vitro* affinity measurements are likely to reflect the actual calcium affinity *in vivo*. Moreover, calcium need not saturate binding sites to have a functional effect on ion channels. Because hundreds or thousands of ion channels work in concert to produce ionic currents, partial saturation of binding sites – and commensurate changes in the behavior of only a proportion of the channel population – may be enough to alter the macroscopic ion flow at the cellular level.

The effect of the mutations on calcium affinity was also measured. hH1-CTD-153-A1924T bound calcium with a K_d of 18 ± 5 µM, not significantly different from the affinity measured for wild-type (Figure 4.5b). However, initial attempts to measure the calcium affinity of hH1-CTD-153-IQAA using tryptophan fluorescence failed – no consistent change in fluorescence intensity as a function of calcium concentration could be measured. On the suspicion that the affinity was much weaker than wild-type, a calcium titration was performed, monitoring changes by ^{15}N-^{1}H HSQC NMR spectroscopy in a manner analogous to that used in Chapter III for hH1-CTD-93 (Figure 3.4). This titration confirmed our suspicions (Figure 4.5c); hH1-CTD-153-IQAA binds calcium with an affinity similar to that observed for hH1-CTD-93 and a thousand-fold weaker than wild-type. A coarse estimate of the K_d from these data yielded a value of 4.2 ± 2.3 mM.

The IQ motif binds to calmodulin in a Ca^{2+}-dependent manner

Previous studies have shown that calmodulin binds to the hH1 IQ motif. Combined with the data on the interaction of the IQ motif with hH1-CTD-93, this suggests that there may be competition with calmodulin for the IQ motif. Thus, it may be impor-

tant compare the relative strength of the IQ motif interaction with calmodulin versus hH1-CTD-93. Although direct, quantitative measurement of the affinity of the IQ motif for hH1-CTD-93 is not possible for the reasons outlined above, the affinities for apo and calcium-loaded calmodulin provide insight into the overall mechanism of calcium-dependent regulation of hH1.

To this end, titrations of IQ motif peptide into solutions of apo and calcium-loaded CaM were performed, monitored by ^{15}N-^{1}H HSQC NMR spectroscopy (Figure 4.6). These titrations revealed that apo-CaM binds the peptide with slow exchange kinetics on the NMR timescale, but Ca-CaM binds with intermediate to fast exchange kinetics. Since the binding constant K_d can be expressed as the ratio of the off-rate (k_{off}) to the on-rate (k_{on}) and assuming that the on-rate is diffusion limited, this change in kinetics implies that Ca^{2+}-CaM has a lower affinity for the peptide than apo-CaM.
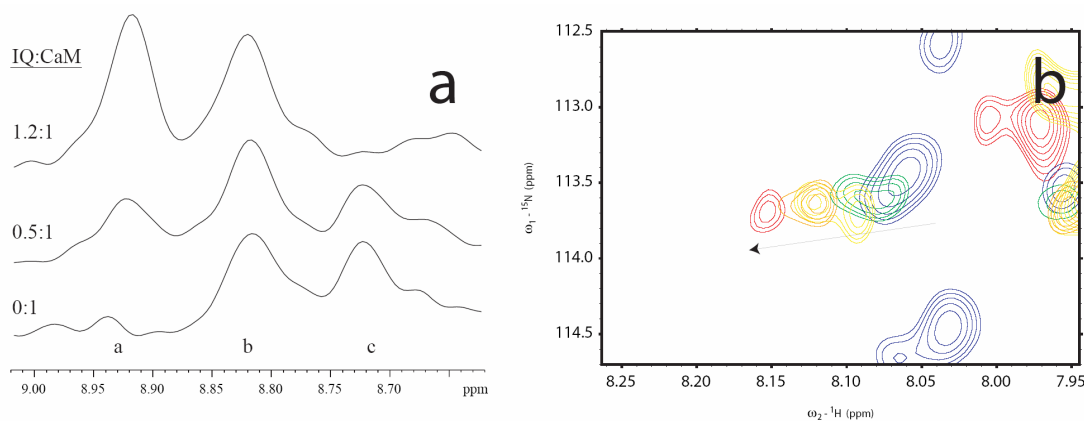
Figure 4.6: IQ motif peptide binds apo-CaM in slow exchange, and Ca^{2+}-CaM in intermediate to fast exchange. (a) 1D slices of 2D ^{15}N-^{1}H HSQC NMR spectra collected while titrating peptide into apo-CaM. These slices clearly demonstrate that the binding interaction is in slow exchange; peak a grows in volume as peptide is added while peak c diminishes in volume. (b) Chemical shift perturbations induced in the 2D ^{15}N-^{1}H NMR spectrum of Ca^{2+}-CaM as peptide is titrated in. The chemical shift perturbation indicates fast or intermediate exchange; the broadening of this and other peaks at intermediate points in the titration confirm that the interaction is governed by intermediate exchange kinetics. Full spectra are included in Appendix D.

The binding affinity was quantified by monitoring the intrinsic tyrosine fluorescence of CaM during the titration of peptide into the protein. This method has been used previously to monitor the binding of calcium to CaM (VanScyoc et al. 2002). The titrations revealed a weakening of affinity by more than tenfold in the calcium-loaded state (Figure 4.7a,b), with K_d values of 0.16 ± 0.04 μM for the apo-state versus 2.0 ± 0.3 μM for the Ca^{2+}-loaded state.

The NMR spectra of the complex of the IQ motif with calmodulin could be used to localize the peptide binding site on calmodulin. Chemical shift perturbations were interpreted using previously published assignments of Ca^{2+}-CaM from the BioMagRes-Bank (http://www.bmrb.wisc.edu) and unpublished assignments of apo-CaM kindly provided by Dr. Ad Bax. These results showed that apo-CaM (Appendix D) binds the IQ motif primarily via the C-lobe, whereas in the presence of calcium there is a shift in the mode of binding and interactions with both lobes of Ca^{2+}-CaM are observed (Appendix D). Although the assignments did not match perfectly with our spectra (caused by variations in the construct and/or conditions), these observations are consistent with the findings of Mori et al., where the authors used circular dichroism to determine that the hH1 IQ motif enhanced the helicity of only the C-lobe of apo-CaM, but enhanced the helicity of both lobes of Ca^{2+}-CaM (Mori et al. 2003).

IQ motif mutations affect calmodulin affinity

In order to confirm the important of the IQ motif, the IQ/AA and A1924T mutations were introduced into the peptide construct using site-directed mutagenesis. These peptides were prepared for binding studies to calmodulin monitored by changes in the
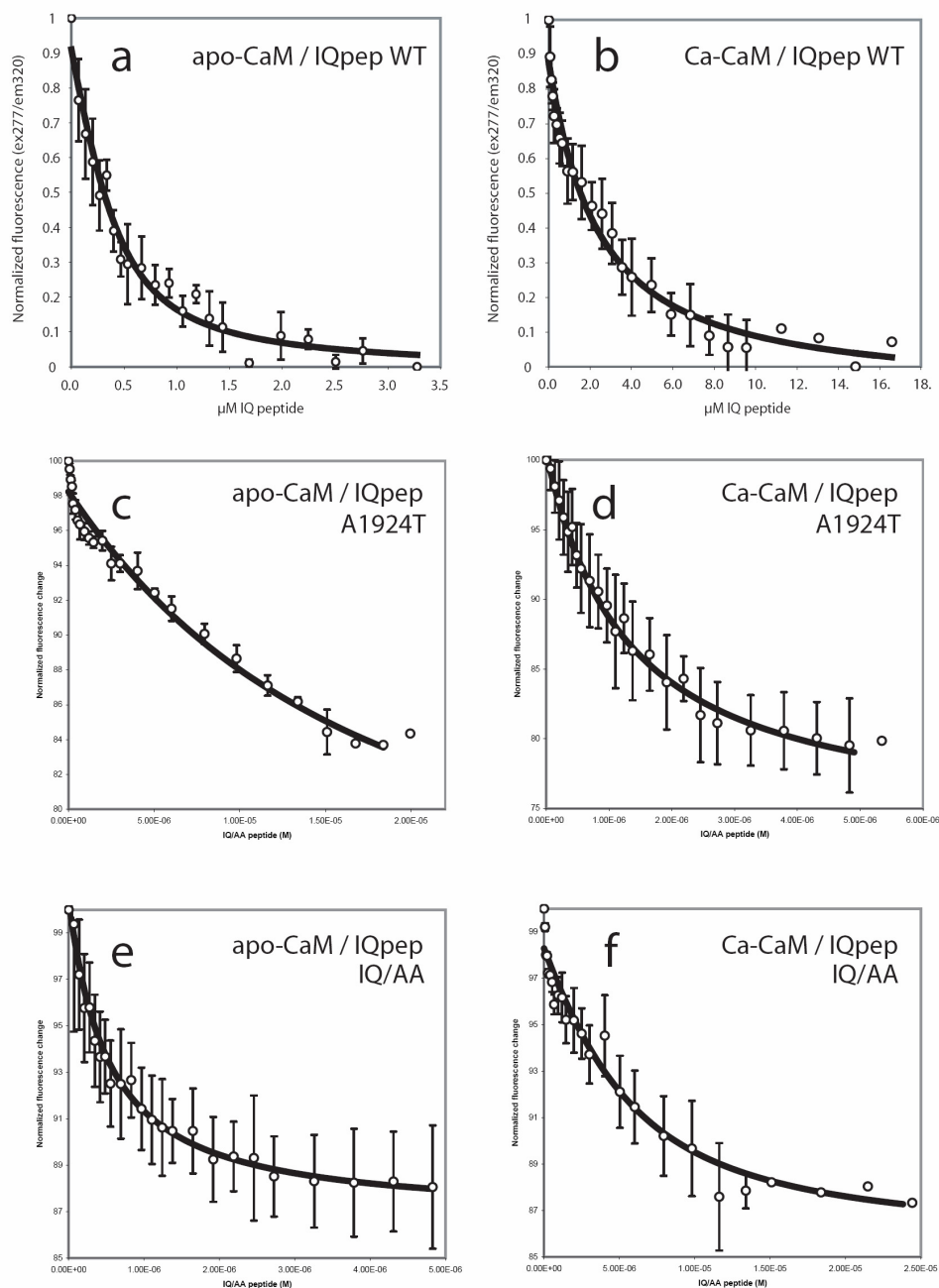
Figure 4.7: The hH1 IQ motif binds calmodulin, and IQ motif mutations can disrupt this interaction. (a,b) Binding of the hH1 IQ motif peptide to apo and Ca^{2+}-CaM. (c,d) Binding of the hH1 IQ motif peptide mutant A1924T to apo and Ca^{2+}-CaM. (e,f) Binding of the hH1 IQ motif peptide mutant IQ/AA to apo and Ca^{2+}-CaM. The wild-type IQ motif peptide bound to apo-CaM with a K_d of 0.16 ± 0.04 μM and to Ca^{2+}-CaM with a K_d of 2.0 ± 0.3 μM. The A1924T IQ peptide bound apo-CaM with a K_d of 1.3 ± 0.1 μM and Ca^{2+}-CaM with a K_d of 15 ± 5 μM. The IQ/AA peptide bound apo-CaM with a K_d of 0.49 ± 0.05 μM, and Ca^{2+}-CaM with a K_d of 3.4 ± 1.0 μM.

intrinsic tyrosine fluorescence of calmodulin. Both mutations were found to reduce the affinity of the peptide for calmodulin, and in both the apo- and calcium loaded states (Figure 4.7c-f). However, in contrast the effect of the mutations on calcium affinity, A1924T has a much larger effect on calmodulin affinity for the peptide than the IQ/AA mutation. The A1924T IQ peptide bound apo-CaM with a K_d of 1.3 ± 0.1 μM and Ca^{2+}-CaM with a K_d of 15 ± 5 μM, in both cases about a ten-fold weaker affinity than wild-type. In contrast, the IQ/AA peptide bound apo-CaM with a K_d of 0.49 ± 0.05 μM, and Ca^{2+}-CaM with a K_d of 3.4 ± 1.0 μM, approximately two-fold weaker than the wild-type IQ peptide.

Discussion

It is clear from the data presented in this chapter that the hH1 IQ motif can bind both calmodulin and the hH1 EF-hand. This data is consistent with our findings, described in Chapter III, that residues downstream of the EF-hand are necessary for high affinity binding of calcium. The observation that the IQ/AA mutation knocks down calcium affinity 1000-fold supports the hypothesis that the IQ motif is playing a critical role in tuning the calcium affinity of the EF-hand.

It is complicated to compare the qualitative affinity of the IQ motif peptide for the EF-hand domain versus the quantitive affinity for calmodulin. We believe that both the drop in affinity for calmodulin and the shift in the binding mode when calmodulin is calcium loaded are significant. In the apo-state, calmodulin is tightly bound to the IQ motif, and the interaction is mediated almost exclusively by the C-lobe. However, upon calcium loading, the overall affinity is more than ten-fold weaker and involves both lobes.

66

Because the interaction involves both lobes, the so-called "linkage effect" comes into play, i.e. two fairly weak interactions involving both the interaction with the N-lobe and the C-lobe mediate the synergistically stronger overall affinity. Thus, it is very likely that the affinity of the C-lobe for the IQ motif has dropped significantly more than ten-fold. This also means that the off-rate of each of the lobes from the IQ motif from is significantly higher than implied by the 2 μM K_d.

We also believe it is significant that the interaction between the IQ motif and Ca^{2+}-CaM is in intermediate/fast exchange, just as the bimolecular interaction between the EF-hand and the IQ motif is in intermediate/fast exchange. This implies that the affinities are in the same range, and the effective increase in the local concentration of the EF-hand as a result of covalent linkage likely means that the EF-hand is able to effectively compete for the IQ motif when calmodulin becomes calcium loaded.

The studies described show that IQ motif mutations can significantly affect calmodulin affinity. This is unsurprising, given what is known about IQ motifs and their ability to bind calmodulin. What is surprising, however, is fact that the A1924T mutation causes a greater disruption than IQ/AA mutation. A1924T is outside of the consensus sequence, but only just; it is three residues downstream of the final hydrophobic residue **δ** in the consensus sequence **δQxxxβGxxxβxxδ**. IQ/AA on the other hand, disrupts residues thought to be central to the binding motif; indeed, the motif is named for this dipeptide. While these findings bear out observations by some that residues upstream and downstream of the IQ motif are also important for calmodulin binding, that should also lead us to more closely examine different IQ motifs and how sequence might specify differences in calmodulin affinity or function.

It is provocative that the leftward shift of the steady-state availability curve of the IQ/AA mutant, similar to the shift observed for EF-hand knockout mutations, is accompanied by a strong effect on calcium affinity but a weak effect on calmodulin affinity, while the rightward shift of the steady-state availability curve of the A1924T mutant is accompanied by a weak effect on calcium affinity but a strong effect on calmodulin affinity. While this observation is correlative, it suggests that the mechanisms by which these mutations disrupt the underlying calcium-dependent effects on steady-state availability are tied to differential effects on two different calcium-sensing elements: the hH1 EF-hand hand and calmodulin.

In summary, these data, combined with the data presented in Chapter II and III, provide evidence of a complex mechanism governing the calcium-dependent regulation of hH1. In Chapter V, calcium-dependent regulation of other ion channels involved in excitability are presented with the goal of developing a model for the mechanism of regulation of hH1.

CHAPTER V

REVIEW OF CALCIUM-DEPENDENT REGULATION OF ION CHANNELS

Introduction

As discussed in Chapter I, calcium plays an important role in hundreds of biological processes as one of the most ubiquitous second messengers. Intracellular calcium concentrations are tightly regulated to very low levels (~100 nM); the general mechanism by which calcium alters cellular biology involves a transient spike in calcium concentration, reaching over 10 μM and possibly much higher in certain local environments (Martonosi and Pikula 2003). This represents a 100-fold change in calcium concentration. As a rough approximation, this means that a calcium binding protein at 1 μM concentation with an affinity (K_d) of 1 μM will go from less than 10% saturated to over 85% saturated due to this change in calcium concentration. (These numbers are highly dependent on the concentration of the calcium-binding protein in question as well as the concentration of other proteins competing for calcium. See Appendix B for a detailed discussion of binding constants.)

The EF-hand is the most common signal transduction element for translating this abrupt rise in calcium concentration into a biochemical signal. Though EF-hands were described in detail in Chapter I and will not be reviewed again here, it is important to understand that calcium affinity is tuned not only by the calcium binding loop but also by many other elements of the EF-hand structural domain (Nelson et al. 2002; Bunick et al. 2004). This is observed, for example, in the difference between calmodulin and calbindin

D$_{9k}$. These two proteins have reasonable sequence homology, but the former has an affinity in the μM range, while the latter has calcium affinity in the nM range.

The mechanisms for regulating intracellular calcium concentrations in excitable cells involve, in part, feedback mechanisms where calcium acts directly or indirectly on ion channels. Other mechanisms, such as those involving ion exchangers or GPCR's, are important but outside the scope of the current discussion. (Appendix A describes work done to characterize the calmodulin mediated calcium-dependent regulation of the G-protein coupled vasopressin receptor V2R.) The purpose of this chapter is to briefly survey these ion channel feedback mechanisms in order to gain some appreciation of the variations and commonalities in calcium-dependent regulation of these channels.

Calcium appears to regulate the function of nearly every channel involved in excitation. To briefly review the events of an action potential in myocytes: voltage-gated sodium channels open following an initial depolarization event, leading to rapid depolarization. The data in support of this thesis strongly suggest that sodium channels are regulated by calcium and calmodulin. Dihydropyridine sensitive L-type calcium channels (LTCC) on the cell surface open concurrently, resulting in an inward rush of calcium ions. T-tubules transmit the depolarization to the interior, where more LTCC's also open, resulting in further calcium release into the cytoplasm (Sperelakis 2001). The LTCC's interact with ryanodine receptors (RyR), which are found on the sarcoplasmic reticulum (SR). Activation of LTCC's leads to activation of RyR's, releasing calcium stored in the SR into the cytoplasm. Both of these calcium-conducting membrane proteins are tightly regulated by calcium, resulting variably in positive or negative feedback regulation of calcium release, depending on calcium concentration. Throughout this process, espe-

70

cially towards the middle and late stages of the action potential, potassium channels open, resulting in repolarization of the cell membrane. Certain members of the potassium channel family are regulated by calcium. The contributions of various currents to the overall action potential are shown in Figure 5.1 (Tamargo et al. 2004).
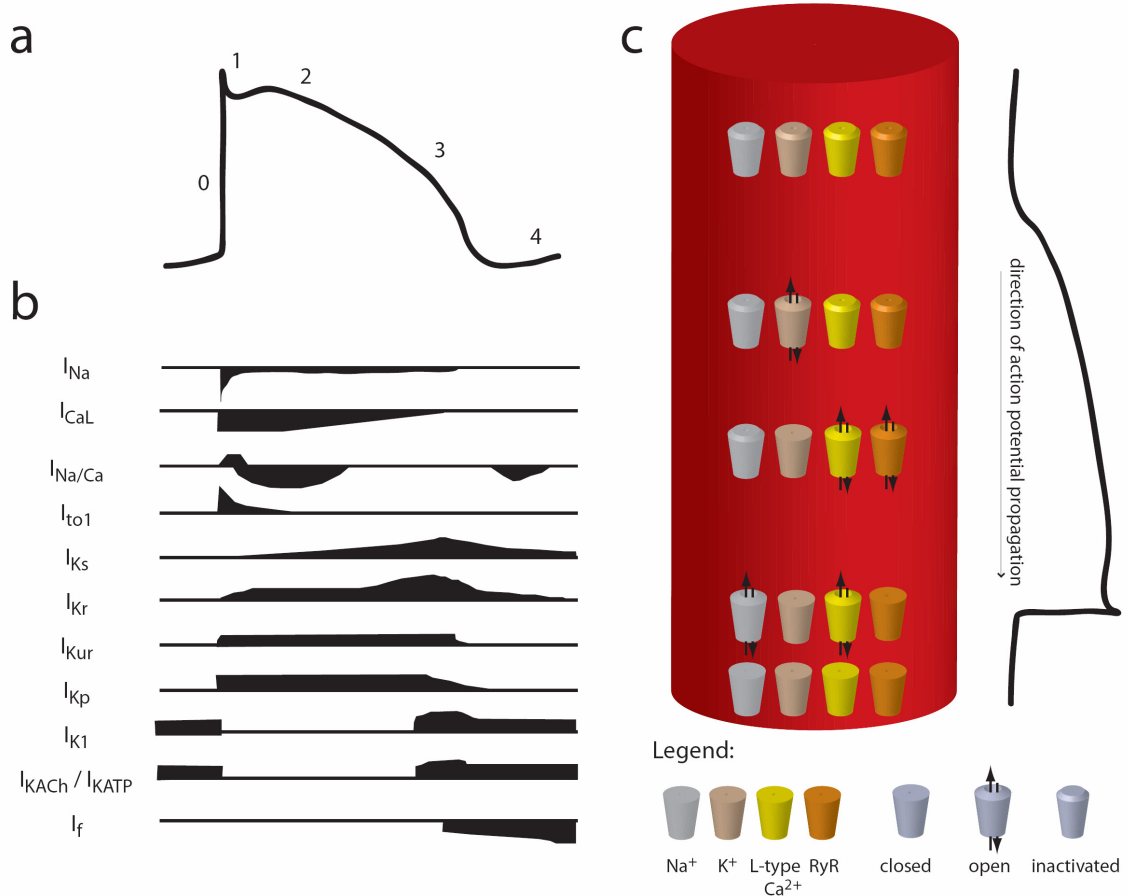
Figure 5.1: The contributions of various ionic currents to an action potential. Panel a demonstrates the changes in transmembrane potential that occur during an action potential (also shown in Figure 1.1). Panel b indicates the currents of sodium (I_{Na}), calcium (I_{CaL}), and potassium ($I_{K...}$) that occur during the course of the action potential. Panel c diagrams in a very general way the channel openings, closings, and inactivations that occur during an action potential, where the red cylinder represents a single myocyte. Panels a and b adapted with permission from Tamargo et al 2004.

This chapter reviews calcium dependent mechanisms of ion channel regulation in greater detail, culminating in a proposed model for the calcium-dependent regulation of hH1 based on the evidence provided in this thesis and other information that has been published.

Voltage-gated sodium channel

Prior to the publication of the data presented in Chapter II (Wingo et al. 2004), the presence of an EF-hand in hH1 and other voltage-gated sodium channels was completely unknown. The IQ motif had been reported in the literature, and because of the well-known role of the IQ motif in mediating calmodulin interactions, a number of groups have published data on the role of calmodulin in the regulation of sodium channel function.

The first report related to the IQ motif was published by Dr. Jeffrey Balser and colleagues in 2002 (Tan et al. 2002a). The main data presented were electrophysiological results showing the effect of exogenous Ca^{2+}-calmodulin added to the pipette solution on hH1, enhancing its entry into a slow inactivated state. The study also presented gel shift data indicating that the IQ motif produces a gel shift of CaM in the presence of calcium, but not in the absence of calcium. We now know that this doesn't reflect whether or not the peptide is able to bind calmodulin, since there are data in this thesis and in a published paper (Mori et al. 2003) reporting lobe specific binding of calmodulin to the IQ motif, in both the presence and absence of calcium. The latter reports CD measurements indicating that the IQ peptide enhances the helicity of only the C-lobe of calmodulin in the absence of calcium, but enhances the helicity of both lobes in the presence of cal-

cium. These data are fully consistent with the detailed NMR structural analysis reported in Chapter IV, which found the same calcium-dependent lobe specificity.

Contradictory to both of these studies was a previous report that calmodulin had no effect on hH1, although a CaM-dependent effect was found for hSkm1, the skeletal muscle isoform of the channel (Deschenes et al. 2002a). These authors also detected that inhibition of CaM-dependent kinase II affected channel function. Interestingly, close examination of the data uncovers an effect not noticed by the authors – namely that calcium has a direct effect on channel function. A second group failed to detect an interaction between hH1 and calmodulin (Herzog et al. 2003).

As is clear from this discussion, the state of knowledge regarding calcium-dependent regulation of voltage-gated sodium channels was still in its infancy prior to the studies reported in Chapter II. In order to better understand the context of the findings reported in this thesis, the mechanisms that underlie calcium-dependent regulation of other channels have been examined in the anticipation that some commonalities may emerge.

L-type calcium channel

The dihydropyridine sensitive L-type calcium channel ($Ca_V1.2$, LTCC) is an interesting case study in the regulation of ion channels by calcium because it exhibits strong calcium-dependent behavior. This protein has the layout of a prototypic voltage-gated calcium channel, containing four domains of six transmembrane helices each. The channel undergoes inactivation with a fairly slow (~1000 ms) rate constant in the pres-

ence of barium, a divalent commonly used to mimic calcium, but inactivation speeds up five-fold (~200 ms) in the presence of calcium.

It has been long recognized that the channel contains an EF-hand in the proximal part of the C-terminus (Babitch 1990). This region was initially proposed (de Leon et al. 1995) to mediate calcium-dependent inactivation of this channel, but subsequent studies have ruled this out (Zhou et al. 1997; Peterson et al. 2000). Sequence analysis suggests that this EF-hand may not even bind calcium with any significant affinity; there is a proline at position 2, and position 5 is a lysine instead of an acidic residue (Zhou et al. 1997).

In light of these and other revelations, the calcium-dependent behavior of the channel is now attributed to a calmodulin-mediated mechanism. It has been discovered that a number of noncontiguous sites in the C-terminus provide binding sites for calmodulin, including a canonical IQ-type motif (Pitt et al. 2001; Erickson et al. 2003; Xiong et al. 2005). These motifs were discussed in the introduction to Chapter IV, and are known to bind apo (calcium-free) calmodulin. It is commonly held that a major role for IQ motifs is to recruit calmodulin at basal calcium levels, which then serves as the calcium sensor for local calcium-dependent events; this appears to be the case for L-type calcium channels.

A number of proposals have been made for the mechanism of calcium-dependent behavior in this channel. The most recent, proposed by Geoffrey Pitt and colleagues (Kim, Ghosh, Nunziato et al. 2004), integrates data related to calcium-dependent binding of calmodulin sites in the LTCC C-terminus with new mutational data and newly uncovered interactions between the C-terminus and the I-II linker "inactivation particle".

74
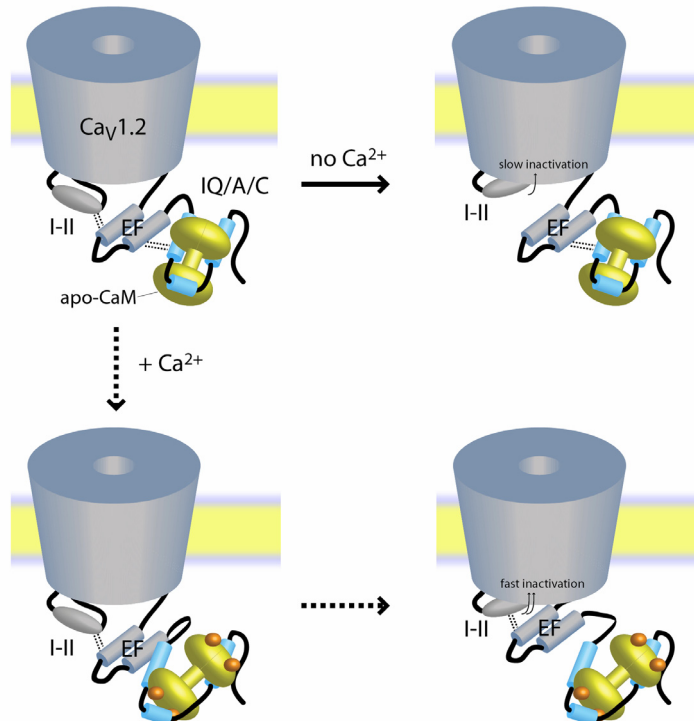
Figure 5.2: The proposed mechanism of calcium-dependent inactivation in Ca$_V$1.2. Top left figure shows the channel in the open state. Dotted lines from the EF-domain to the I-II region and to the IQ/A/C region indicate binding interactions. In the absence of calcium, these interactions must be interrupted for I-II mediated inactivation. In the presence of calcium, conformational changes allow the I-II to inactivate while preserving the I-II/EF interaction, speeding the process fivefold. Figure based on Kim et al 2004.

The authors propose that the EF-hand region serves a structural role in calcium-dependent channel behavior. According to their proposal, the complex of calmodulin and the calmodulin-binding-region in the C-terminus interacts constitutively with the EF-hand. The EF-hand, in turn, interacts with the I-II linker in a way which inhibits I-II mediated channel inactivation. Under basal calcium conditions, this results in slowing of I-II mediated inactivation. During conditions of elevated calcium, however, conformational changes in calmodulin release the EF-hand and allow the I-II linker to inactivate the channel more quickly. The proposed model elegantly ties voltage-dependent inactivation and calcium-dependent inactivation into a single mechanism, providing a mecha-

nistic model for calcium-dependent effects on both of these supposedly independent types of inactivation. The proposed mechanism of action is summarized in Figure 5.2.

Ryanodine receptors

L-type calcium channels found in the transverse (T) tubule system of myocytes play a key role in stimulating calcium release from the sarcoplasmic reticulum (SR) of muscle cells (Marx et al. 2001). The T-tubule system, formed by invaginations of the cell membrane, conducts depolarizations on the surface deep into the interior. Depolarization activates LTCC's. As discussed, this results in calcium flow from the T-tubule system into the cytoplasm. This process also activates ryanodine receptors (RyR). These receptors are found on the SR membrane at locations physically proximate to the T-tubule (Franzini-Armstrong et al. 1999; Bers 2004). Ryanodine receptors are massive (~5000 amino acid) proteins with four to twelve transmembrane helices that form tetrameric structures that are able to conduct calcium (stored in the SR lumen under resting conditions) when activated by LTCC (Bers 2004). Most of the bulk of the protein is on the cytoplasmic face of the SR membrane, forming 27 nm x 27 nm x 14 nm "feet," which can be visualized by electron microscopy (Sharma et al. 1998; Samso and Wagenknecht 2002; Wagenknecht and Samso 2002) in close association with L-type calcium channels (more so in skeletal than in cardiac muscle) as shown in Figure 5.3.

Three isoforms of RyR are found in mammals (Bers 2004). RyR1 is found predominantly in skeletal muscle, and RyR2 in cardiac muscle. RyR3 has more widespread distribution but is also found in muscle. These channels are activated by ATP and low µM cytoplasmic calcium (calcium-induced calcium release), but inhibited by calmodulin

and mM range cytoplasmic calcium (Martonosi and Pikula 2003). These receptors contain two low-calcium-affinity EF-hands, only one of which is thought to bind calcium (Hamada et al. 2002). Because the affinity is low, it is assumed that this EF-hand is involved somehow in channel inactivation, but little is known about the mechanisms by which calcium-dependent activation and inactivation occur.
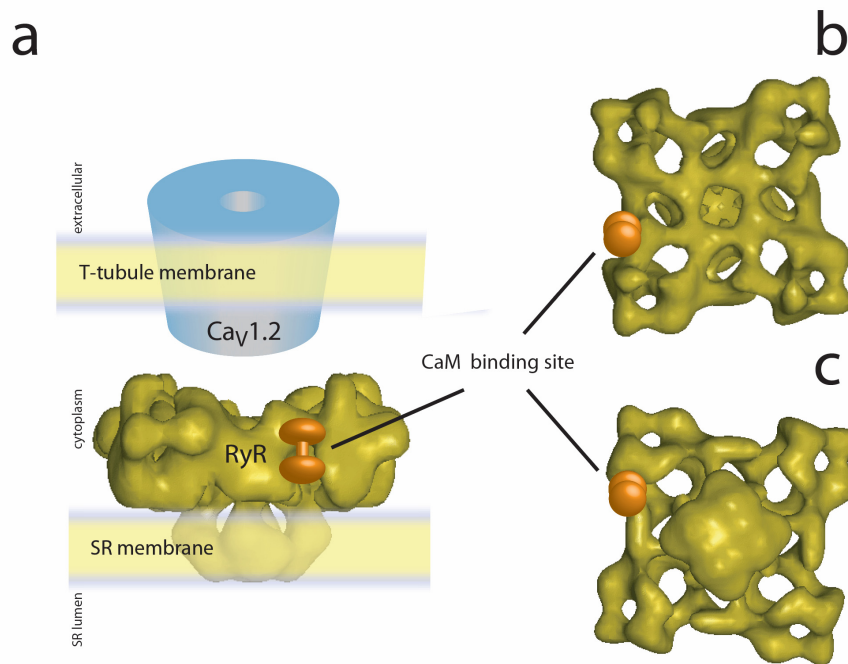
Figure 5.3: Three-dimensional reconstruction of the structure of the ryanodine receptor (RyR) tetramer by high-resolution electron microscopy. Panel a shows a side view and emphasizes the proximity of RyR to L-type calcium channels in the T-tubule system. Panel b shows a view from the cytoplasmic perspective, and panel c shows a view from the SR lumen perspective. The location of calmodulin binding on a single subunit of the tetramer is indicated. Figure modified with permission from Bers 2004.

Not much is known about the calmodulin dependent processes regulating the protein, either. Calmodulin binding sites have been characterized by high resolution electron microscopy, which have elucidated a pocket on the massive cytoplasmic "foot" where calmodulin binds (Samso and Wagenknecht 2002). Apo-calmodulin is able to bind to the

RyR, and the conformational changes accompanying the calcium-loading of calmodulin are thought to cause the calmodulin binding site to shift by a few amino acids; the change in position of calmodulin is observable by high resolution EM. Calmodulin is known to have different effects on the different isoforms of the RyR, but in all cases inhibits calcium release at higher calcium concentrations. A significant amount of work remains to be done to understand these and other mechanisms that regulate these channels.

Potassium channels

Potassium channels play an important role in the action potential cycle by repolarizing the cell membrane to complete the action potential, preparing the cell for the next action potential. A large number of potassium channels also act during various phases of the action potential to modulate membrane potential shifts caused by the flux of sodium and calcium ions as well. As discussed in Chapter I, some voltage-gated potassium channels open slowly compared to sodium channels, with the result that they begin to act just as sodium channels inactivate. Another subset of potassium channels, the so-called inward rectifiers, activate and then inactivate extremely rapidly during initial depolarization, resulting in little to no conduction of potassium ion. During the course of the action potential, however, these channels recover from inactivation and are able to activate again if the membrane potential is more positive than -30 mV. During this second activation, the channels will remain open longer if the membrane potential is between 0 mV and -30 mV. This results in increased potassium current and acceleration of repolarization.

A third subset of potassium channels, the focus of the discussion here, are the so-called calcium-activated potassium channels (K_{Ca}). These channels open in response to calcium and act in the late phase of the action potential to contribute potassium currents towards repolarization of the cell in response to elevated intracellular calcium. Three different subtypes of K_{Ca} have been identified on the basis of conductance: big conductance (BK_{Ca}), intermediate conductance (IK_{Ca}), and small conductance (SK_{Ca}) (Stocker 2004).

<u>BK_{Ca} channels</u>

BK_{Ca} channels are expressed in smooth muscle (Brayden and Nelson 1992) and nerve cells (Robitaille et al. 1993; Moczydlowski 2004). Recently, they have also been implicated in functions as diverse as innate immunity in neutrophil leukocytes (Ahluwalia et al. 2004) and protection against ischemia in cardiac myocyes (Xu et al. 2002). The channels appear to have the canonical 6-transmembrane topology, with a number of positively charged residues in the S4 segment. Interestingly, however, hydropathy plots indicate that there may be as many as five more transmembrane helices, one amino-terminal to the S1 segment (termed S0) and four distal to S6 (termed S7-S10). The channels are able to respond to both voltage signals and calcium signals (Cox 2005).

At the present time, there remains quite a bit of controversy over the number, affinity, and location of calcium binding sites in BK_{Ca}. What is clear is that there are no canonical calcium binding sites anywhere in the protein; the mechanisms of calcium binding are hotly disputed. Domain swapping studies across species have uncovered that transfer of the distal transmembrane segments can transfer calcium dependent properties across species (Wei et al. 1994), and others have shown by alanine-scanning mutagenesis that an acid-rich region in the intracellular S9-S10 loop is important for calcium binding

(Bao et al. 2004). This region has been termed the "calcium-bowl" and likely serves as one of the calcium binding sites in the protein.

Others have shown, however, that most of the voltage- and calcium-dependent properties of the channel are retained even when the last four transmembrane helices S7-S10 are truncated (Piskorowski and Aldrich 2002). This, combined with the lack of hard, direct evidence of calcium binding in the calcium-bowl, confirms that many questions about calcium binding in BK_{Ca} channels remain to be explored.

<u>SK_{Ca} and IK_{Ca} channels</u>

SK_{Ca} channels are expressed throughout the body in muscle and nerve cells (Vergara et al. 1998; Bond et al. 2005). In humans, this family is comprised of four members encoded by the genes *SK1, SK2, SK3,* and *IK1* (Bond et al. 2005). Note that the intermediate conductance channel is included in this family; although it has a larger single-channel conductance and different drug sensitivity than the other members of the family, sequence homology indicates that this channel functions in a similar manner and is closely related to SK_{Ca} channels. The initial separation of these channels into a separate classification stemmed from the fact that SK isoforms were sensitive to the bee venom toxin apamin, whereas the IK isoforms were not. SK_{Ca} channels are the only known target of apamin (Bond et al. 2005).

Each of these channels has the canonical transmembrane topology of potassium channels, namely, each channel has six transmembrane helices and tetramerizes to form a functional channel. The S4 segments in voltage-gated potassium channels (K_V) carry positively charged residues important for voltage-dependent gating. In SK_{Ca} channels five of these residues are mutated, likely explaining the voltage-independent behavior of

these channels (Stocker 2004). The focus of research on the three SK isoforms of this channel has been mainly restricted to their function in neural contexts, but it has been demonstrated that the SK2 isoform is expressed in the atria and ventricles of both human and mouse heart (Xu et al. 2003). Apamin blockade results in substantially longer lasting plateau and repolarization phases of the cardiac action potential. This and other observations in this report revealed both the presence of SK2 in cardiac myocytes and that the role of SK2 in this context is to accelerate repolarization of the cell following activation and calcium-mediated excitation-contraction coupling.

Unlike BK_{Ca} channels, quite a bit is known about the structural mechanism of calcium-dependent sensitivity and gating in SK_{Ca} channels. The proximal C-terminal domain of the channel binds calmodulin via novel motifs that do not conform to known Ca^{2+}-independent CaM binding motifs (such as the IQ motif) or Ca^{2+}-dependent motifs (such as the 1:5:8:14 motif). These regions instead bind calmodulin in such a way that the C-terminal lobe of calmodulin appears to mediate a Ca^{2+}-independent interaction with the channel, while the N-terminal lobe mediates Ca^{2+}-dependent changes to these interactions (Keen et al. 1999). This information is based on biochemical data and crystal structures of the SK_{Ca} Ca^{2+}-binding domain in complex with both apo (Schumacher et al. 2004) and Ca^{2+}-loaded calmodulin (Schumacher et al. 2001). Of note is the fact that in the "Ca^{2+}-loaded structure" only the N-lobe EF-hand calcium-binding sites are occupied by calcium.

Based on these structures, it appears that the binding of calcium to the N-lobe of calmodulin orders large parts of the SK_{Ca} C-terminus. At the same time, the conformation of the binding surface between the calmodulin C-lobe and the SK_{Ca} C-terminus alters

significantly, reorienting the helical residues in the interaction region (residues 430-440) by greater than 90º (Schumacher et al. 2004). Schumacher et al. propose, based on comparison of their structure with the Ca^{2+}-CaM/SK_{Ca} structure, that this rotation may directly result in gating of the channel. Since these changes occur in the proximal C-terminus, they directly affect the covalently attached inner helix gate of the channel. In their view, a rotation of this magnitude will likely cause significant conformational change in the gate, resulting in channel opening. This proposed mechanism is summarized in Figure 5.4.
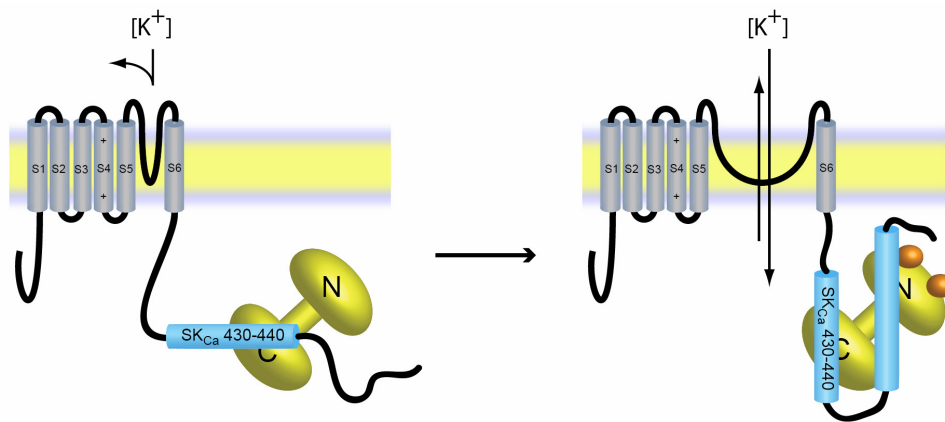
Figure 5.4: Proposed mechanism for calcium dependent activation of SK_{Ca} channels. Closed channels, at left, constitutively bind the C-lobe of calmodulin. Calcium binding causes a > 90º rotation in the 430-440 segment of the SK_{Ca} C-terminus (light blue cylinder), altering the conformation of S6 and gating the channel to the open position. Calcium binding also causes a significant ordering of other parts of the C-terminus as well; the crystal structure of Ca^{2+}-CaM with the SK_{Ca}-CTD is a domain swapped dimer with both lobes of CaM binding different parts of the SK_{Ca}-CTD.

Discussion

This dissertation has been devoted to examining and extending electrophysiological evidence that calcium regulates the cardiac voltage-gated sodium channel hH1. The

most likely explanation for our data is that calcium regulates hH1 channel function via a mechanism that links the intrinsic EF-hand calcium sensor to the extrinsic calcium sensor calmodulin. The focal point for this crosstalk is the hH1 C-terminal IQ motif, which both recruits apo-CaM and acts to raise the calcium affinity of the intrinsic calcium binding motif by approximately three orders of magnitude.
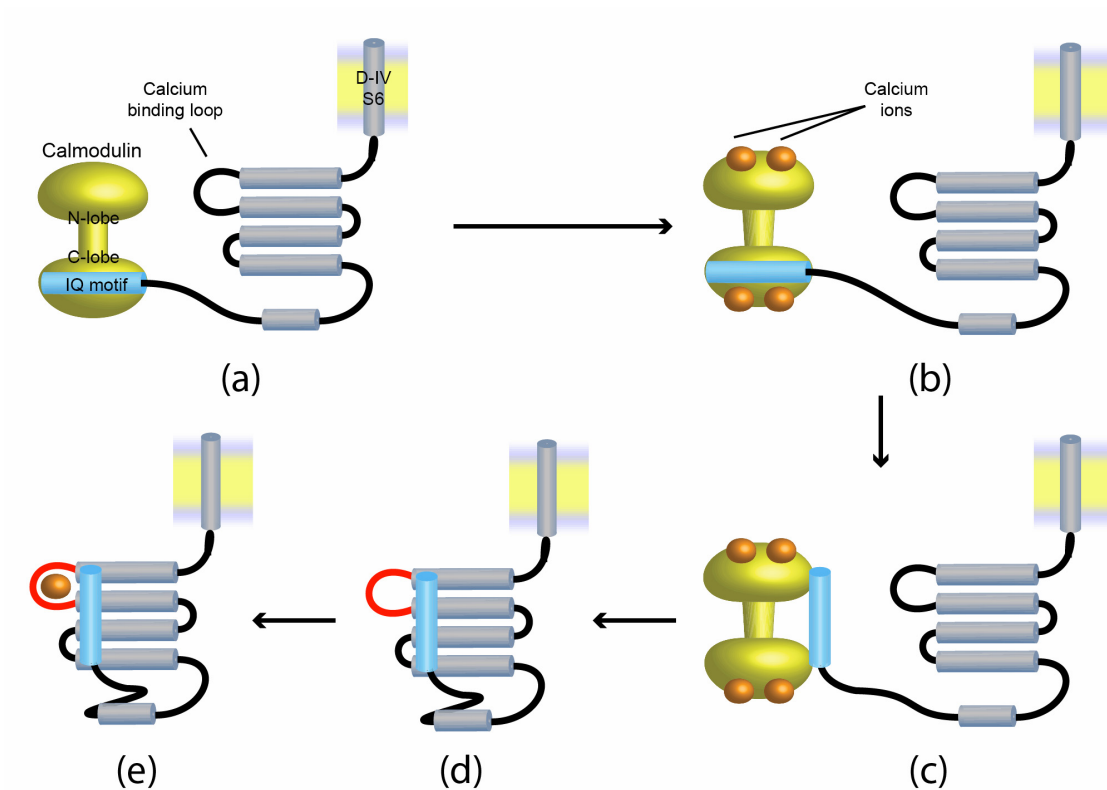
Figure 5.5: Model for the action of calcium in the hH1 C-terminus. (a) At basal levels of calcium in the cell, calmodulin is localized to the IQ motif, bound via the C-lobe. (b) As calcium levels rise, calmodulin binds calcium, which (c) weakens and alters the CaM/IQ interaction. The consequent release (d) of one or both CaM domains enables the IQ motif (light blue cylinder) to interact with the EF-hand core, raising its calcium affinity by three orders of magnitude (red calcium binding loop). (e) Calcium binds in that site.

Combining all available evidence, the following model for the mechanism of calcium-dependent regulation of hH1 is proposed (Figure 5.5). As indicated by NMR and

fluorescence titration data in Chapter IV, calmodulin is bound to the hH1 IQ motif via its C-lobe at basal calcium levels with nM affinity. Upon an increase in calcium levels, the binding of calcium to CaM causes the conformation of CaM to change, weakening and altering the CaM/IQ interaction, also demonstrated by NMR and fluorescence titration data in Chapter IV. One or both lobes of calcium-loaded calmodulin are then more readily able to dissociate. The partial or complete dissociation of CaM frees the IQ motif to bind to the EF-hand domain, as NMR data in Chapter IV shows will happen in the absence of calmodulin. This causes a concomitant calcium-dependent change in the conformation of the EF-hand domain, helping drive the equilibrium toward IQ interaction with the EF-hand domain and freeing up CaM. As shown by data in Chapters III and IV, the EF-hand domain interacting with the IQ has μM calcium affinity and will be able to bind calcium.

The sequestration of the IQ motif by CaM, and the subsequent partial or complete dissociation of CaM upon calcium loading, is central to the model presented. There is significant evidence supporting the idea that Ca^{2+}-CaM dissociates from the hH1 IQ motif during a calcium signaling event. For example, the studies described in Chapter II (Figure 2.2b) demonstrated that the addition of Ca^{2+}-CaM inhibitory peptide CaMKII-290-309 did not affect calcium-dependent changes in steady state availability. Since blocking Ca^{2+}-CaM with the peptide had no effect on steady-state availability, the implication is that the EF-hand mediates at least this aspect of calcium responsiveness. If this is the case, it is likely either that the binding mode of Ca^{2+}-CaM to the IQ is permissive of IQ/EF-hand interactions, or that one or both lobes of Ca^{2+}-CaM is recruited elsewhere.

The latter idea will be explored further in Chapter VI, where preliminary data indicating that Ca^{2+}-CaM interacts with another part of the channel is discussed.

This model bears some resemblance to the one proposed by Kim et al. for the L-type calcium channel ($Ca_V1.2$). Both pair an IQ motif with an intrinsic EF-hand in the C-terminus. However, the overall mechanism of calcium-dependent regulation is quite different. The major difference is that the proposed mechanism for $Ca_V1.2$ relies on the EF-hand domain to transduce a calcium-binding signal that occurs at CaM, whereas our proposal for $Na_V1.5$ suggests that the IQ-motif is the site of interaction between the CTD and the cytoplasmic loop. Additionally, it appears that the interaction of CaM with the Ca^{2+}-channel is mediated by a number of noncontiguous stretches of residues in the C-terminus, whereas the IQ motif is necessary and sufficient for the interaction of CaM with the Na^+-channel. Another key difference is that the intrinsic calcium binding site does not play a role in calcium-dependent properties of $Ca_V1.2$, but, as described in Chapter II, mediates calcium-dependent changes in the voltage-dependent steady state availability of hH1. Finally, the evidence in hH1 favors a model where CaM dissociates or binds elsewhere on the channel, whereas the proposed mechanism in $Ca_V1.2$ requires CaM to remain associated with the C-terminus.

As is clear from the examples described in this chapter, evolution has taken great pains to make calcium signals self-limiting. The existence of calcium-dependent feedback mechanisms in sodium, potassium, and calcium signaling underlines the importance of regulating intracellular calcium levels. The calcium-dependent alterations in the kinetic behavior of these channels likely tune the peak and trough calcium concentrations during an action potential. This effect is both direct, by modulation of calcium current,

and indirect, by providing a calcium-dependent repolarization mechanism. These processes may also provide some protection against pathological processes such as ischemia in which both extracellular and intracellular calcium concentrations rise significantly.

Calmodulin plays a significant role in many of these regulatory processes, but intrinsic calcium binding sites also regulate many of these channels as well. Further study of these systems will likely lead to new understanding of how these regulatory systems evolved and the specific biochemical reasons for why these sites were conserved. Bigger discoveries may also come from better understanding of these channels. For example, it is likely that BK_{Ca} channels are regulated by a novel calcium binding protein or contain a novel intrinsic calcium binding motif. Characterization of this motif may uncover similar motifs in other proteins not currently recognized as calcium binding proteins. A better molecular understanding of the mechanisms behind calcium-dependent control of these channels may also lead to new strategies for anti-arrhythmic and anti-epileptic therapy.

CHAPTER VI

SUMMARY AND FUTURE DIRECTIONS

Summary

The protein channel mediating the rapid depolarization of cardiac tissue during contraction, the voltage-gated sodium channel known most commonly as hH1 or $Na_V1.5$, is regulated by intracellular calcium concentrations. The studies and analyses presented in this dissertation have shown that this calcium sensitivity is mediated by both intrinsic and extrinsic calcium sensing pathways. These results strongly imply at least some level of crosstalk between these pathways. Three naturally occurring arrhythmogenic mutations, D1790G, ins1795D, and A1924T, occur in regions of the channel responsible for mediating these calcium dependent effects and have been shown to alter calcium-dependent behavior. In this chapter I examine this data in the context of the literature and other information currently available to propose future directions.

Future Directions

What is the structure of the hH1 C-terminal EF-hand? To what extent are there conformational changes associated with Ca^{2+}-binding?

In order to lay to rest many of the open questions surrounding the roles being played by calcium and by calmodulin, the three-dimensional structure of the proximal portion of the C-terminal domain at atomic resolution should be determined. This information will reveal at least four important pieces of information: a) the location of bound calcium ions and the identity of the residues that chelate the ion, b) the structure of the

87

folded globular domain, c) the location and orientation of residues whose conformation and/or electromagnetic environment are altered by the binding of calcium ion, and d) the interactions of the IQ motif with the EF-hand core that result in tuning of calcium affinity.

While some of these studies may be conducted using NMR, it is likely that an X-ray crystal structure would provide higher resolution. Comparison of ^{15}N-^{1}H HSQC data collected of hH1-CTD-93, hH1-CTD-125, hH1-CTD-148, and hH1-CTD-153 reveals that the additional residues past 125 do not result in many new resonance peaks in these correlation spectra. This likely indicates some type of chemical exchange at an intermediate timescale, and further optimization of constructs and of conditions are needed to improve these spectra further, but also may not help. In addition, it is possible that residues in the calcium binding loop are likewise in intermediate exchange, based on the fact that while some resonances shift in a calcium-dependent manner, they do not shift as dramatically as observed for other previously characterized calcium binding proteins. Attempts to date to assign the backbone of hH1-CTD-125 and of hH1-CTD-93 in our laboratory have proven to be difficult. These observations suggest that both X-ray crystallography and NMR will be challenging, but are nonetheless worth persistent effort because the end result will be extremely valuable for refining the mechanistic model to atomic resolution.

A comprehensive strategy for improving the stability and "foldedness" of the hH1-CTD constructs should be pursued. It is essential to generate additional constructs, based on hH1-CTD-153, adding or subtracting residues from the N- and C-termini. NMR will be valuable for assaying new constructs. Crystallization trials should be per-

formed for both calcium-free/apo and calcium-loaded conditions, at a few different calcium concentrations. It will also be interesting to attempt co-crystallization of these constructs with calmodulin, at first only under apo conditions. Because of the number of parameters that need to be varied, a robotic assembly capable of quickly screening a large number of conditions for a number of different samples will facilitate this process significantly. The use of a robotic assembly will also reduce the amount of protein required per condition screened. If flexibility of the protein is intrinsic and prevents the growth of crystals which diffract to high resolution, then NMR remains the method of choice for atom-level characterization of protein structure.

What is the structural mechanism of hH1 EF-hand domain function?

Even in that absence of information about the molecular-level changes associated with calcium binding in the hH1 C-terminus, it may be possible to elucidate certain molecular details about calcium-dependent channel behavior. While interactions between the hH1 EF-hand core and other regions of hH1 have not yet been identified, we do know that the conformational effect of calcium binding likely changes the binding surface presented by the EF-hand domain. Preliminary chemical shift assignments indicate that some of the peaks observed to shift upon calcium binding represent residues outside the calcium binding loop, suggesting at least a modest change in conformation. Two of the peaks that undergo fairly large shifts (~0.3 ppm in ^{1}H) have tentatively been assigned to hydrophobic residues, raising the possibility that calcium-dependent rearrangements involve a hydrophobic patch on the surface of the domain. Far less likely is the possibility that there are substantial rearrangements in the tertiary structure of the molecule; this

would result in much larger and more widespread calcium-dependent changes in the ^{15}N-^{1}H HSQC spectra.

With the goal of identifying binding partners for the hH1 EF-hand domain, it may be useful to generate a series of expression constructs covering the cytoplasmic regions of the channel to "fish" for parts of the channel that interact with the C-terminus. Another prospect for interaction with the C-terminus is the fibroblast growth factor homologous factor 1B (FHF1B). Described in Chapter I, this protein is a newly identified binding partner of the hH1 C-terminus that is known to modulate channel function. Interestingly, the D1790G mutation knocks out this interaction, raising the possibility that the EF-hand domain is directly involved and/or that the interaction between hH1 and FHF1B is calcium-dependent. We have already generated reagents for the examination of this interaction, but our preliminary binding and protease protection studies have been negative.

It is also possible that the role of the EF-hand is to capture the IQ motif, freeing calmodulin to act elsewhere in the channel. In this case, no target for the EF-hand is necessary – or, rather, the IQ motif *is* the target.

What is the role, if any, of Ca^{2+}-calmodulin in regulating channel function?

This last concept, the idea that the role of the EF-hand is to sequester the IQ motif, raises questions about the role of Ca^{2+}-loaded calmodulin in channel function. There exists no clear consensus on the role of calmodulin in modulation of channel function. As discussed in Chapter IV, a number of studies have been performed to examine the electrophysiological effects of calmodulin binding. Some have found an effect while

others have not. As the studies described in this dissertation make clear, there is no doubt that calmodulin binds to the hH1 IQ motif. The nanomolar affinity of apo-calmodulin for the motif virtually guarantees that CaM with be localized to this site. How this binding translates to biological function remains unclear. As discussed in Chapter V, we hypothesize that Ca^{2+}-loaded calmodulin, following a spike in intracellular calcium concentration, partially or completely dissociates from the IQ motif. The IQ motif then interacts with the EF-hand core. The idea that Ca^{2+}-CaM has another target on the channel is attractive, because it would be an effective means to drive the release of the IQ motif. For example, if the same molecule of CaM that is bound to the IQ motif in the apo state binds to a second site in the Ca^{2+}-loaded conformation, the presence of this second site would also ease or eliminate the energetic cost of Ca^{2+}-CaM dissociation from the IQ motif. This line of reasoning prompted a search for a Ca^{2+}-CaM "sink" in hH1 – an intramolecular binding site with high affinity for Ca^{2+}-CaM.

Calmodulin has a number of putative secondary binding sites in hH1 in addition to the known IQ motif site. These sites, as determined by submitting the hH1 sequence to the calmodulin binding site predictor (created by the laboratory of Dr. Mitsuhiko Ikura), are shown in Figure 6.1.

We have begun the process of analyzing whether these regions are actually capable of binding calmodulin. Production of each of these regions, in a manner analogous to the production of the IQ motif peptide, will be followed by calmodulin binding experiments to look for interactions and the strength of the interaction. These results may yield further clues as to the molecular mechanism by which calmodulin acts, and follow up electrophysiological studies, introducing mutations to disrupt interactions which are un-

covered, may clarify whether the interactions are physiologically relevant. We have already found, for example, that calmodulin interacts with the III-IV linker region in a calcium dependent manner (Figure 6.2).
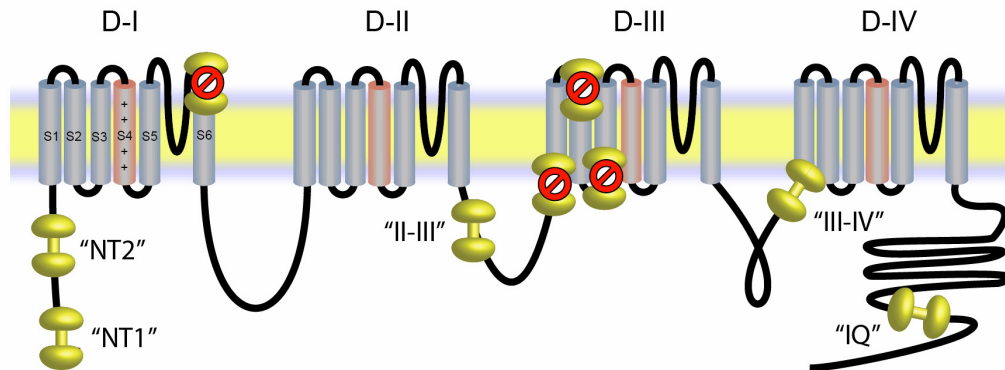
Figure 6.1: Predicted sites of calmodulin binding in hH1 based on the primary sequence. The sites are indicated by yellow dumbbells. Sites with a red circle and slash are sites which were ruled out as unrealistic calmodulin binding sites due to their predicted location relative to the cell membrane.

The III-IV linker is the cytoplasmic loop between the third and fourth transmembrane domains of the channel, and serves as the "fast inactivation particle" for hH1. The introduction of certain mutations in the III-IV linker (at the "IFM motif") prevents channels from inactivating after being gated open by a voltage pulse (McPhee et al. 1994; McPhee et al. 1995). The solution structure of the hH1 III-IV linker peptide has been determined (Rohl et al. 1999). Analysis by ^{15}N-^{1}H HSQC NMR shows that the III-IV linker peptide interacts with CaM in a calcium-dependent manner, binding strongly to Ca^{2+}-CaM but unable to bind apo-CaM with measurable affinity (Figure 6.2). The identification of a putative Ca^{2+}-CaM binding site in the III-IV linker is intriguing. It is consistent with recent reports that III-IV linker is involved in interactions with the hH1 C-

terminus and CaM (Kim, Ghosh, Liu et al. 2004; Motoike et al. 2004). However, those

studies gave no direct evidence that the same molecule of calmodulin is involved with

both IQ and III-IV interactions. Likewise, it has yet to be demonstrated that the CaM/III-

IV interaction is physiologically relevant. These findings suggest a number of future ex-

periments which need to be done in order to explore the role of CaM in this context;

calmodulin may be critically important for normal channel function if it is serving to

tether the hH1 C-terminus and the III-IV linker in some way.
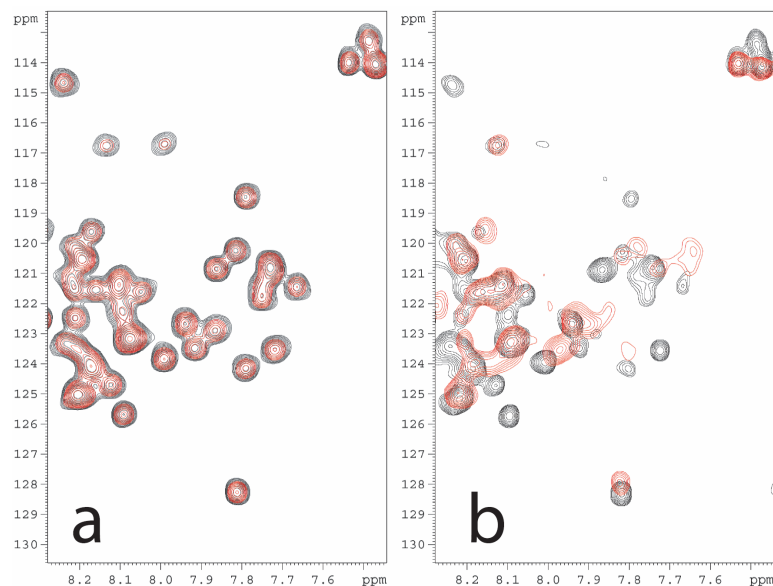
Figure 6.2: The III-IV linker interacts with calmodulin in a calcium-dependent manner. Both panels show ^{15}N-labeled III-IV linker in the absence (black) and presence (red) of unlabeled calmodulin. Panel a is under apo conditions, panel b is under calcium loaded conditions.

Does calcium regulate other sodium channels?

The studies presented here raise the interesting question of whether the type of

regulation we have reported occurs in other human voltage-gated sodium channel iso-

forms. While a number of studies have been undertaken to examine the role of

calmodulin across various isoforms, no other group has attempted to characterize the direct effect of calcium on any other voltage-gated sodium channel.

Figure 6.3: Sequence homology in the EF-hand region and the IQ-motif regions of the nine canonical members of the human voltage-gated sodium channel family. Sequences were aligned using Bioedit and BLAST. Na_X, a putative tenth member of the family, was not included in this analysis because it remains unclear whether this channel is expressed in humans, and if it is what role it is playing

An examination of the sequence homology between the members of the human sodium channel family (Figure 6.3) was interesting in this context. The sequence alignment in the vicinity of both the EF-hand and the IQ motif reveals that both regions are strongly conserved in humans. In the region of the EF-hand, positions 1, 3, 5 and 12 of the calcium binding loop all exhibit absolute conservation of acidic side-chains, and only positions 6 and 10 exhibit any nonconservative mutations. Variations in the IQ motif sequence, though modest, may be correlated with differences in calmodulin affinity essential for isoform specific functionality. The strong conservation of these regions suggests that the EF-hand and the IQ motif play an important role in basic channel function, and are likely to have deep evolutionary roots. It may be worth looking for these motifs in channels from simpler organisms in order to ascertain the evolutionary conservation of

these features, which would further support the concept of functional relevance. Such an examination may also uncover a simple model system that could facilitate future studies of the EF-hand and IQ motif.

How do these regulatory elements function in the context of normal cardiac rhythm?

An important and provocative question, applicable to both cardiac and neurological problems, is how alterations to normal channel function and regulatory processes at the molecular level (which lead to changes at the single channel and single cell level) affect the function of integrated systems at the organ level. The ability to model these processes accurately will likely aid in understanding how the perturbations caused by mutations or by drugs translate into pharmacological or pathological effects.

The nascent field of complex systems research may provide tools for conducting these modeling experiments. By building agent-based models of cellular and organ-level behavior, plugging in known kinetic and affinity information, it may be possible to understand or predict the subtle arrhythmogenic effects of alterations to channel behavior. These models may allow us to predict the types of alterations which are most and least likely to result in pathological effects, which could then in turn be used to develop improved antiarrhythmic strategies.

Is this regulatory element a viable antiarrhythmic drug target?

Further analysis is required to understand the relative importance of the Ca^{2+} effects mediated through the hH1 EF-hand and the relation to mutations causing Na^+ channel dysfunction. Ca^{2+} modulation of Na^+ channels through additional signalling path-

95

ways that involve other second messengers and cofactors, including multivalent cations and ATP, must be examined. Of particular relevance is that intracellular free Ca^{2+} rises in acquired conditions when the heart is particularly susceptible to fatal arrhythmias, such as during myocardial ischemia. Since the maintenance of Na^+ channel function appears to be a crucial determinant of survival under these conditions (Echt et al. 1991), the potential of the EF-hand as an antiarrhythmic target deserves extensive evaluation.

APPENDIX A

CALMODULIN REGULATES THE G-PROTEIN COUPLED VASOPRESSIN RE-
CEPTOR V2 IN A CALCIUM-DEPENDENT MANNER

Introduction

At approximately the time we were beginning to think about investigating the role

of the hH1 C-terminal IQ motif, described in Chapter IV, I began a collaboration with a

colleague in the Vanderbilt Medical Scientist Training Program, Hilary Nickols. The col-

laboration grew out of discussion about her tentative findings that calmodulin could bind

to the cytoplasmic C-terminal domain of the human vasopressin receptor V2R, a G-

protein coupled receptor (GPCR). These findings were published (Nickols et al. 2004)

The V2R binds the agonist arginine vasopressin (AVP) and signals through the

heterotrimeric protein G_s to promote water reabsorption and concentration of the urine in

the collecting duct of the kidney (Cabral et al. 2000). AVP, 8-arginine vasopressin, is a

cyclic nonapeptide hormone that is secreted by the posterior pituitary in response to low

urine osmolality or to decreased blood pressure. AVP binds to the V2R on the baso-

lateral surface of the principal cells of the renal collecting duct, couples to G_s, and stimu-

lates adenylyl cyclase. The subsequent increase in intracellular cAMP leads to activation

of cAMP-dependent protein kinase, phosphorylation of aquaporin-2, and the translocation

of pre-formed aquaporin-2-containing vesicles to the apical membrane of the principal

cells (van Balkom et al. 2002). This translocation appears to involve calcium in some

(Chou et al. 2000; Yip 2002) but not other (Lorenz et al. 2003) experimental conditions.

Because the calmodulin inhibitor W7 blocks the AVP-induced stimulation of water flow

in the toad urinary bladder (Levine et al. 1981) and the rat inner medullary collecting duct

(Chou et al. 2000), calmodulin may play a role in AVP-induced insertion of aquaporin 2 channels in these systems. The ultimate insertion of aquaporin 2 water channels into the apical membrane allows the renal epithelial cells to absorb water, which accounts for the antidiuretic effect of AVP.

The C-terminal region of the V2R had been shown to be important for agonist-mediated phosphorylation (Innamorati et al. 1997), receptor escape from the endoplasmic reticulum and transport to the plasma membrane (Schulein et al. 1998), sequestration and endocytosis of the receptor (Innamorati et al. 1997), and prevention of recycling (Innamorati et al. 1998) of the endocytosed V2R. In the course of exploring proteins that might interact with the V2R C-terminus in a yeast two-hybrid screen, it was discovered that calmodulin was a potential binding partner. These findings were further confirmed by immunoprecipitation assays (data not shown).

Results

The V2R C-terminus binds Ca^{2+}-calmodulin but not apo-calmodulin

To confirm and further characterize the observed interaction between the V2R C-terminal RGR motif and calmodulin, we performed a series of NMR experiments using uniformly ^{15}N-enriched calmodulin and a peptide fragment of the V2R C terminus containing the RGR motif (RGRm). For these experiments, RGRm was titrated into solutions of calmodulin, in both the absence (190 μM calmodulin) and presence (150 μM calmodulin) of calcium. As discussed elsewhere in this dissertation, the peaks in these two-dimensional spectra arise from backbone and side chain amide N-H groups, provid-

ing a minimum of one probe for each residue in the protein. The position of each peak is highly sensitive to both the structure and influences from the surrounding environment.
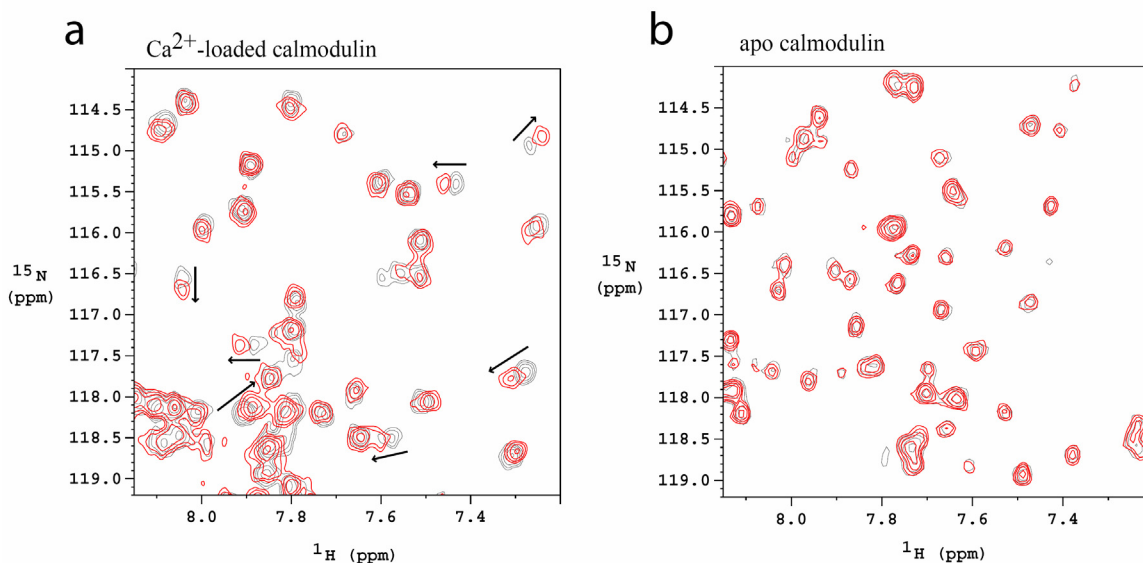
Figure A.1: A peptide fragment of the V2R C-terminus binds to calmodulin in a Ca^{2+}-dependent manner. The V2R peptide (L337-S357, RGRm) was titrated into a solution of ^{15}N-enriched calmodulin in the (*a*) presence (150μM calmodulin) and (*b*) absence (190μM calmodulin) of calcium. The panels show regions of the ^{15}N-^1H HSQC NMR spectra of free CaM (black) overlayed with spectra of CaM complexed with 1.5 molar equivalents of RGRm (red). Arrows highlight chemical shift perturbations caused by binding of the RGRm. Taken from Nickols et al. 2004.

Figure A.1a shows a selected region of the two-dimensional ^{15}N-^1H heteronuclear single quantum correlation NMR spectra obtained for Ca^{2+}-loaded calmodulin in the absence (*black*) and presence (*red*) of 1.5 molar eq of the RGRm peptide, whereas Figure A.1b shows the corresponding spectra for the apo (Ca^{2+}-free) protein. The observation that many peaks shift position when the peptide is present in Figure A.1a but not Figure A.1b reveals that RGRm binds to calmodulin in a Ca^{2+}-dependent manner, corroborating the previous findings by other methods.

The changes in NMR signals over the course of the titration of RGRm into calmodulin can be used to estimate the *in vitro* binding affinity of the peptide for Ca^{2+}-calmodulin. However, a linear change in peak position as a function of peptide concentration that saturated at a peptide:protein ratio of ~1:1 indicated that the dissociation constant (K_d) must be at least 100-fold lower than the protein concentration of 150 μM. Thus, the K_d of RGRm for calmodulin is ≤1.5 μM.

Discussion

The study presented here was performed in the course of starting to work with calmodulin for some of the other projects described in this thesis. The work done was a good introduction to performing peptide binding studies on calmodulin and helped characterize an interesting interaction. As it turns out and was described in the paper, the regulation of this GPCR by calmodulin is important for V2R-mediated calcium release.

APPENDIX B

BINDING CONSTANT CALCULATIONS

Introduction

The art of calculating binding constants from data is an old one, one which required the use of certain mathematical tricks before the advent of significant computing power at the desktop to avoid nonlinear regression analysis. This appendix explains and derives some of the basic concepts and equations involved in the calculatioin of single-site binding constants taking advantage of the computing power available to us today. While the corresponding equations for multiple site binding are substantially more complicated and not covered here, the basic approach is the same.

What is a binding constant?

It has long been recognized in chemistry that, in solution, most salts only dissociate partially in solution. Exceptions to this rule include strong acids like HCl and a few other salts like sodium chloride. For salts that do not dissociate completely, the extent of dissociation under a given set of conditions for a given concentration of salt is constant. We can therefore define for salts a dissociation constant (K_d) which for the hypothetical salt of P+ and L- is the ratio:

$$K_d = [P_{free}] [L_{free}] / [PL] \tag{1}$$

where the brackets indicate to "use the concentration of" the species inside the bracket. If you think a little bit about this equation, you will recognize that salts which remain

mostly associated in solution will have high concentrations of PL and low concentrations of free species. This makes K_d very small. Salts which are mostly dissociated, on the other hand, will have the opposite ratio of free to bound species and K_d will be large.

This hypothetical discussion of the behavior of salts is equally applicable to the interation between proteins and their interaction partners, usually referred to as their ligands. The exact same equation is used to describe their tendency to interact with each other; the K_d is a good measure of the extent of this tendency because one may easily and quantitatively compare these tendencies using their dissociation constants. Some, myself included, therefore also refer to the dissociation constant as the binding constant or the affinity of the interaction.

How does one measure K_d?

In order to experimentally ascertain the value of the dissociation constant, one needs to be able to measure the ratio of free to bound species in solution - a measurement that it is usually impossible to make directly.

Instead, a researcher investigating binding affinities will usually have some indicator of the concentration of bound species PL. For example, in this dissertation both NMR and fluorescence data were used to monitor the concentration of bound species. Since the researcher also knows how much total protein P_{tot} and ligand L_{tot} she has added, she can define P_{free} in terms of P_{tot} and PL:

$$[P_{free}] = [P_{tot}] - [PL] \tag{2}$$

and the equivalent equation for the ligand:

$$[L_{free}] = [L_{tot}] - [PL] \tag{3}$$

Substituting (2) and (3) into (1) yields:

$$K_d = ([P_{tot}] - [PL]) \, ([L_{tot}] - [PL]) \, / \, [PL] \tag{4}$$

Some simple algebraic rearrangements:

$$K_d \, [PL] = ([P_{tot}] - [PL]) \, ([L_{tot}] - [PL]) \tag{5}$$

$$K_d \, [PL] = [P_{tot}][L_{tot}] - [P_{tot}][PL] - [L_{tot}][PL] + [PL]^2 \tag{6}$$

$$[P_{tot}][L_{tot}] - [P_{tot}][PL] - [L_{tot}][PL] + [PL]^2 - K_d[PL] = 0 \tag{7}$$

$$[PL]^2 - ([P_{tot}] + [L_{tot}] + K_d)[PL] + [P_{tot}][L_{tot}] = 0 \tag{8}$$

This last rearrangement yields an equations in the form of the quadratic formula. Of the two

solutions to an equation an equation of this form, only one means something physically:

$$[PL] = -0.5 \times (\, [P_{tot}] + [L_{tot}] + K_d + \sqrt{([P_{tot}] + [L_{tot}] + K_d)^2 - 4[P_{tot}][L_{tot}]} \,) \tag{9}$$

Armed with this equation, let us now return to a discussion of the experimental

approach to the calculation of K_d. As mentioned, a researcher may use a technique like

fluorescence to measure the amount of bound species in solution. Technically, these

measurements do not give [PL] directly, but instead give a measure of the ratio of [PL] to

[P_{tot}].

For example, let us suppose that we are using fluorescence to measure the binding

of a small molecule to our favorite protein. In the absence of ligand, the protein gives a

response of 1000 fluorescence units. Call this response Q_0. Suppose that we then incre-

mentally add the small molecule ligand until the fluorescence signal no longer changes.

The response at this point is 800 fluorescence units. Call this response Q_{max}. Because the

binding of ligand to protein causes the drop in fluorescence, the fluorescence response Q

at any point during the addition of ligand reflects the ratio of bound protein to total pro-

tein. We can put this into equation form:

$$Q = Q_0 + (Q_{max} - Q_0) ([PL] / [P_{tot}]) \qquad (10)$$

Substituting [PL] from (9) into (10) and rearranging yields:

$$Q = Q_0 + (Q_0 - Q_{max})([P_{tot}]+[L_{tot}]+K_d+\sqrt{([P_{tot}]+[L_{tot}]+K_d)^2 - 4[P_{tot}][L_{tot}]})/2[P_{tot}] \qquad (11)$$

This is the equation used to calculate binding constants. After doing a full titration, a researcher will know total protein concentration P_{tot}, the response Q as he varies the ligand concentration, Q_0 from his first data point, and Q_{max} which is the response plateau. By using nonlinear regression analysis on his data set using this equation, he will be able calculate K_d.

Another very useful application of this equation is the simulation of binding curves. If a researcher knows approximately what Kd she expects the affinity of an interaction to be, she may set arbitrary values for Q_0 nd Q_{max} and simulate the expected binding curve for adding ligand to a certain concentration of protein. This will reveal how much ligand will be needed to "saturate" (reach plateau) and what the binding curve will look like.

What can cause problems in measuring K_d?

While the theoretical treatment above makes measurement of binding constants seem straightforward (if not easy), a number of issues can confound the process. It is worthwhile to explore some of these practical issues which arise from theoretical analysis of these equations.

First, it is absolutely essential to have a reasonable estimate of the protein and ligand concentrations. Without this information, it is impossible to analyze titration data because basic information is missing. I say "reasonable estimate" because, based on

simulations, altering the protein concentration ± 10% does not alter the calculated binding constant very significantly. Additionally, if the protein concentration is not known very accurately, most or all programs able to perform nonlinear regression analysis will allow the user to let the protein concentration (or any other variable in the equation, for that matter) "float" in order to optimize curve fitting.

This brings up a second point. During the fitting process, the user must be very careful to set the initial parameters for curve fitting as close as possible to the expected values. Otherwise the analysis, which is an iterative process, may get stuck in a local minimum and give some very strange results. Users should also *always* inspect the curve as compared to their data. This will immediately show whether the results of the curve fitting are way off. It may not, on the other hand, reveal if analysis was done correctly.

A third set of problems can arise from the experimental conditions picked for the titration. This is an issue that may not be obvious from a cursory inspection of the equations, but will come to light after doing a series of simulations and examining the binding curves that result from various combinations of K_d and P_{tot}. These simulations reveal that when the selected protein concentration, in units of molarity, is much larger than the binding constant, which also has units of molarity, then the binding curves become very steep and linear and saturate at 1:1 protein:ligand ratio. This makes sense in terms of the equations; small K_d means strong affinity, and at higher protein concentrations every molecule of protein will immediately bind every single molecule of ligand. This situation is not conducive to the calculation of an accurate binding constant, because the binding curves for very very strong, very strong, and strong affinities all look about the same at protein concentrations greater than 100 times K_d. Therefore, linear binding curves with

saturating response at 1:1 protein:ligand concentration are really only good for estimating an *upper limit* on the binding affinity, e.g. "the K_d is *no weaker than* --- µM."

Similarly, working with protein concentrations much smaller than the K_d can be problematic. This is because reaching saturation requires a substantial excess of ligand in this case. For example, say a protein has an affinity of 8 mM for a ligand. In order to obtain a reasonably full binding curve at a protein concentration of 64 uM, the researcher will need to get to a ligand concentration of nearly 90 mM. Under these conditions, it is possible that someone may miss an interaction during an initial test because they did not "go out far enough."

Because of these problems, it is a good idea to get an estimate of the affinity in advance of starting to make measurements in earnest. The optimal range of protein concentrations to use in affinity measurements is within an order of magnitude on either side of the K_d, e.g. for a K_d of 1 µM, work between 100 nM and 10 µM.

A final consideration is that of the experimental technique used. Each spectroscopic method has its advantages and disadvantages. NMR is useful for weaker interactions (> 100 uM) but doesn't have the sensitivity to measure stronger affinities at appropriate protein concentrations. Even if it was sensitive enough, NMR is also confounded by exchange effects; stronger interactions manifest as peaks broadened to nothing or as a new set of signals, which makes analysis of that type of data more difficult or impossible. Fluorescence, because of the intrinsically higher sensitivity of optical spectroscopic techniques, is able to measure affinities in the nM range but is subject to dilution effects and photobleaching. Also, significantly complication can arise with the use fluorescence if both binding components have the same fluorophore (e.g. both contain tryptophan).

Isothemal titration microcalorimetry (ITC) is a good technique for measuring a wide range of affinities and is also able to distinguish enthalpic and entropic contributions to binding, and also the stoichiometry of binding if this information is not known. This technique is technically challenging, however, and very sensitive to problems like buffer mismatch. The data collected in ITC experiments is an integral representing the heat released or absorbed by the binding of ligand to target. The data collected is the first derivative of data collected by other methods; there are two methods for calculation of binding constants from this data. The first option is to numerically integrate the data set and analyze it using the binding equation described above, e.g. for each addition/injection, the net "response" is the integral from 0 injections to that injection. A graph of this data will look much like a normal binding curve. The second, and better, option is to analyze the heat data directly by fitting to an equation representing the first derivative. While these equations will not be covered here, ITC equipment generally comes with software capable of performing nonlinear regression analysis directly on ITC data and additionally calculates n (stoichiometry), ΔH, ΔS, and ΔG.

APPENDIX C

MATERIALS AND METHODS

Computation

For Chapter II, multiple sequence alignments and analyses were done with AMPS and AMAS (Livingstone and Barton 1993). Threading calculations were performed usingTHREADER 3.3 (Jones et al. 1992), which identifies the known 3D structures that best accommodate a given sequence. The library of 3D structural templates (tertiary fold templates) had a representative for all unique 3D protein structures reported in the then current PDB database. The molecular graphics package MOE (2002) was used for all structure-based sequence alignments and homology modeling (Figure 2.1b,c). For the molecular models, amino acid side chains were built onto the consensus backbone (Figure 2.1b) using a systematic conformational search procedure to select optimal side chain rotamers (Soss 2002). PDB identifiers used for model generation: 1C07 (human Eps15), 1C7V (Ca^{2+}-bound C-terminal domain of calcium vector protein), 1EXR (Ca^{2+}-bound calmodulin), 1BJF (neurocalcin), and 1TRF (troponin C). The starting structure was refined with conjugate gradient energy minimization and assessed for structural integrity. The program PROCHECK was used for structure assessment (Laskowski et al. 1993).

Subcloning

All bacterial expression constructs were generated using standard molecular biology techniques to insert a PCR amplified fragment of DNA into a vector. Briefly, PCR is

used to amplify the coding region of a gene of interest from a cDNA or other template. The primers also include in-frame extensions to the coding region at the 5'- and 3'- ends, which incorporate restriction digestion sites, stop codons, and possibly other elements into the amplified fragment. Following restriction digest of the fragments and of the vector, the two pieces are mixed and briefly exposed to 65 ºC before being incubated together at 18 ºC with T4 ligase. The incubation mixture is then used to transform ultra-competent bacteria and plated onto agar with appropriate antibiotic selection depending on the antibiotic resistance gene found on the vector. Single colonies are then grown up in small volume cultures (3-5 mL LB + antibiotic) and the plasmid isolated from these cultures. The plasmid is DNA sequenced to verify the orientation and frame of the insert as well as to verify that the coding region is free of mutations resulting from PCR amplification.

Table I lists the constructs mentioned in this thesis and indicates the vector into which they were inserted, the primers used for amplification, and some other relevant information about the vector and/or construct.

CONSTRUCT	CHAPTER	VECTOR	TEMPLATE FOR PCR	PRIMERS
His-hH1-CTD-93	III,IV	pET15b (His-tag, amp)	mammalian hH1/GFP	forward:5'-GGGAATTCcatatgGAGAACTTCAGCGTGGCC reverse:5'-CGCGGATCCTCAAGACTCCCCCAGGACCC
hH1-CTD-93	III	pSV271 (no tag, kan)	mammalian hH1/GFP	forward:5'-GGGAATTCcatatgGAGAACTTCAGCGTGGCC reverse:5'-ccgCTCGAGctactaAGACTCCCCCAGGACCC
hH1-CTD-120	III	pSV271 (no tag, kan)	mammalian hH1/GFP	forward:5'-GGGAATTCcatatgGAGAACTTCAGCGTGGCC reverse:5'-ccgCTCGAGctactagatgggctcgtaggagatctt
hH1-CTD-148	III	pSV271 (no tag, kan)	mammalian hH1/GFP	forward:5'-GGGAATTCcatatgGAGAACTTCAGCGTGGCC reverse:5'-ccgCTCGAGctactaagagcgttgcagcaggtg
MBP-hH1-CTD-148	II	pSV278 (MBP-tag, kan)	mammalian hH1/GFP	forward:5'-CGCGGATCCGAGAACTTCAGCGTGGCC reverse:5'-CCGGAATTCCTAAGAGCGTTGCAGCAGGTG
MBP-hH1IQpeptide	IV	pSV278 (MBP-tag, kan, primer adds rhinovirus 3C cut site)	mammalian hH1/GFP	forward:5'-CGCGGATCCC TGGAAGTCCT GTTCCAGGGT CCGCGGCGCA AGCACGAAGA reverse:5'-CCGGAATTCCTACTAGGAGGCATGCTTCAAAGAGCG
III-IV linker	VI	pET15b (His-tag, amp)	mammalian hH1/GFP	forward:5'-GGGAATTCCA TATGGACAAC TTCAACCAAC AGAAGAAAAA GTTAG reverse:5'-CGGGATCCTACTAGTCGAATATGAAGCCCTGGTACTTG
hH1-CTD-148 IQ/AA	III	pSV271 (no tag, kan)	hH1/GFP IQ/AA	forward:5'-GGGAATTCcatatgGAGAACTTCAGCGTGGCC reverse:5'-ccgCTCGAGctactaagagcgttgcagcaggtg
MBP-hH1IQpeptide IQ/AA	IV	pSV278 (MBP-tag, kan, primer adds rhinovirus 3C cut site)	hH1/GFP IQ/AA	forward:5'-CGCGGATCCC TGGAAGTCCT GTTCCAGGGT CCGCGGCGCA AGCACGAAGA reverse:5'-CCGGAATTCTACTAGGAGGCATGCTTCAAAGAGCG

Table I: Primers used in the generation of various constructs made use of in this dissertation.

Mutagenesis

Site directed mutagenesis was used for the generation of a number of mutant constructs described in this thesis. This was generally performed using a Quikchange (Stratagene) PCR-based strategy. The strategy calls for generating ~30 bp forward and reverse primers, precisely matching the template plasmid except for the desired mutation(s) or insert. We performed low copy PCR (16-18 cycles, 55 °C anneal) using a high-fidelity thermostable DNA polymerase (*Vent; PfuUltra* may also be used). The template plasmid *must* be grown up in and purified from bacteria; this methylates the DNA. This is important because following low-copy PCR, the parental plasmid is digested by *DpnI*, which only cleaves methylated DNA. The PCR mixture is transformed into ultracompetent bacteria and plated; plasmids are purified from cultured colonies and are then sequenced to ensure the presence of the desired mutation and the absence of secondary mutations.

Table II summarizes the mutants used in these studies, and includes information about the primers and templates used in the generation of these mutants. The table only indicates one of the primers used in the generation of the mutant; in ALL cases, the reverse complement is the other primer.

MUTATION	TEMPLATE(S)	PRIMER
D1790G	hH1-CTD-93, His-hH1-CTD-93	5'–CCCCTGAGTGAAGACGGCTTCGATATGTTCTAT
F1791A	hH1-CTD-93, His-hH1-CTD-93	5'–CTGAGTGAGGACGACGCCGATATGTTCTATGAG
M1793G	hH1-CTD-93, His-hH1-CTD-93	5'–GAGGACGACTTCGATGGGTTCTATGAGATCTGG
E1799A	hH1-CTD-93, His-hH1-CTD-93	5'–TTCTATGAGATTTGGGCGAAATTTGATCCAGAG
hH1-CTD-153	hH1-CTD-148 (pSV271)	5'–CCTGCTGCAACGCTCTTTGAAGCATGCCTCCTAGTAGCTCGAGATC
A1924T	hH1-CTD-153	5'–CCTGCTGCAACGCTCTTTGAAGCATACCTCCTAGTAGCTCGAGATC
A1924T	MBP-hH1Qpeptide	5'–CGCTCTTTGAAGCATACCTCCTAGTAGAATT

Table II: Primers used in the site-directed mutagenesis of various constructs made use of in this dissertation. In all cases, both the primer and its exact reverse complement were used in the Quikchange PCR reaction.

Protein Production

hH1-CTD constructs, MBP-IQ fusion proteins, and His-III-IV linker were over-expressed in *E. coli* host BL21 (DE3) cells (Novagen). Unlabeled protein was prepared by growing cells in LB medium (10 g tryptone, 10 g NaCl, 5 g yeast extract per liter) at 37 ℃. Uniform ^{15}N-labeling for NMR was achieved by growth at 37 ℃ in M9 minimal medium containing ^{15}NH$_4$Cl as the sole nitrogen source. An exception to this was the growth of hH1-CTD-120 (Chapter III), which was grown and expressed at 30 ℃.

In all lysis steps described below, protease activity was inhibited by supplementing the lysis buffer with Roche Mini EDTA-free protease inhibitor tablets (Roche). The pH values always indicate the final adjusted pH after all components are added.

His-tagged proteins, including all MBP fusion constructs described here, were purified by NiNTA affinity chromatography (Qiagen, Valencia, CA). Briefly, the protocol called for lysis (using lysozyme and sonication) into 20 mM Tris buffer with 20 mM CaCl$_2$ and 5 mM BME at pH 7.5, 30 mL per liter of growth. The lysate was loaded onto a NiNTA column and washed with lysis buffer supplemented with 30-50 mM imidazole. Elution was achieved with a step to 300 mM imidazole.

Protein prepared for Chapter II (hH1-CTD-148 WT and mutants) were further purified as follows. NiNTA eluate was dialyzed into imidazole free lysis buffer overnight and cleaved the following day by thrombin. Thrombin was removed by passing the cleavage buffer over benzamidine sepharose and the cleaved protein was separated from MBP and other contaminants by final purification using anion exchange chromatography (MonoQ, 20 CV gradient from lysis buffer into lysis buffer + 2M NaCl, protein elution at 15-30 mS/cm conductivity, Amersham Biosciences).

For the MBP-IQpeptide fusion protein used in Chapter II, after NiNTA chroma-tography the protein was dialyzed against 50 mM Tris, 150 mM NaCl, 2 mM DTT, pH 7.5 to remove imidazole. The protein was then cleaved using rhinovirus 3C protease for 3 hours at room temperature. The cleavage reaction leaves an exogenous Gly-Pro dipep-tide at the amino terminus. The reaction mixture was adjusted to 0.1% TFA and loaded directly onto a C18 column for RP-HPLC purification in two steps. In both steps, start-ing buffer was MilliQ water + 0.05% TFA, and the final buffer was 100% ACN + 0.05% TFA. The first step was a shallow gradient on a 100 mL C18 column, eluting over a 5 CV gradient. Fractions containing peptide of interest (as determined by MALDI-TOF mass spectrometry) were pooled and loaded onto a smaller 20 mL C18 column and eluted over a 20 CV gradient. The presence of peptide was verified by MALDI-TOF MS and the purity assessed by SDS-PAGE. The peptide was then lyophilized and stored at -30 ºC for subsequent use.

The untagged constructs expressed from the pSV271 vector were purified by two different protocols, depending on whether they expressed in the soluble fraction or in in-clusion bodies. All hH1-CTD-93 constructs (His-tagged, untagged, wild-type and mu-tants) and hH1-CTD-120 expressed at 30 ºC were soluble. All hH1-CTD-148 and hH1-CTD-153 constructs were insoluble when expressed at 37 ºC; unlike the hH1-CTD-153 other constructs, the hH1-CTD-153-IQAA mutant was soluble if expressed at 30 ºC but was expressed at 37 ºC with the other hH1-CTD-153 constructs for parallel processing purposes.

Those expressing in the soluble fraction were lysed (using lysozyme and sonica-tion) into 20 mM Tris, 5 mM BME, 20 mM $CaCl_2$, 2M NaCl at pH 7.5 and loaded di-

rectly onto phenyl sepharose FF (Amersham Biosciences). After a 10 CV wash, the protein was eluted with a single step to MilliQ water. The eluted protein was loaded onto an anion exchange column (Q sepharose, Amersham Biosciences) and eluted by a 20 CV gradient from MilliQ water to lysis buffer. Fractions were analyzed by SDS-PAGE and fractions containing the protein were pooled and concentrated in Centricon devices to < 2 mL (3K MWCO for hH1-CTD-93 constructs, 5K MWCO for hH1-CTD-120). The concentrated protein was then loaded onto a 120 mL gel filtration (Superdex 75) column. Fractions analyzed by SDS-PAGE were judged to be > 95% pure; if not, a polishing step using a monodispersed anion exchange medium such a MonoQ (Amersham Biosciences) was included.

hH1-CTD proteins expressing in the insoluble fraction were purified by first isolating the inclusion bodies. Cell pellets were lysed in 20 mM Tris, 5 mM BME, 20 mM $CaCl_2$, 300 mM NaCl, 0.1% Triton-100 at pH 7.5 with lysozyme and sonication (30 mL of lysis buffer per liter of growth). Following centrifugation, the pellet was retained and resuspended in 30 mL of lysis buffer without lysozyme by sonication. Following centrifugation again, the pellet was resuspended in 30 mL of 20 mM Tris, 5 mM BME, 20 mM $CaCl_2$, 300 mM NaCl at pH 7.5 by sonication. Centrifugation yielded a thoroughly washed pellet, at about 60% purity of the target protein. The pellet was solubilized in 5 mL 6M guanidine hydrochloride and rapidly diluted to 50 mL with 20 mM Tris, 5 mM BME, 20 mM $CaCl_2$. This removed a significant fraction of contaminants, which precipitated out of solution and were removed by centrifugation and filtering. The supernatant was dialyzed against 20 mM Tris, 5 mM BME, 20 mM $CaCl_2$ pH 7.5, which removed further contaminants by precipitation, and purified via anion exchange chromatography

on a monodispersed medium over 20 CV (MonoQ, SourceQ; Amersham Biosciences). Buffers for the chromatography were 20 mM Tris, 5 mM BME, 20 mM $CaCl_2$, pH 7.5 (starting buffer) and 20 mM Tris, 5 mM BME, 20 mM $CaCl_2$, 2M NaCl, pH 7.5 (final buffer).

For the studies described in Appendix A, a peptide fragment of the V2R C termi-nus ([339]LLSSARGRTPPSLGPQDES[357] with the cysteines normally acylated in V2R (Cys-341 and Cys-342) mutated to serine) was ordered from Genemed Synthesis and sub-sequently purified by reversed-phase high pressure liquid chromatography. Removal of the single major contaminant from the eluted peptide was confirmed by electrospray ioni-zation-mass spectrometry and matrix-assisted laser desorption ionization-mass spectrome-try. The final peptide was lyophilized and resuspended at 10 mg/ml in 500 mM Tris, pH 7.0.

For the experiments in Chapter IV and Appendix A, human calmodulin was ex-pressed from a bacterial expression vector kindly provided by Eva Thulin (University of Lund, Sweden). The construct was transformed into BL21(DE3)pLysS *Escherichia coli,* and the bacteria were grown in M9 minimal media supplemented with [15]NH_4Cl. The bac-teria were grown and induced with isopropyl-β-D-thiogalactopyranoside (IPTG) as de-scribed previously. Briefly, the growth protocol calls for serial dilution of bacteria grow-ing at 30 °C, allowing the bacteria to double prior to each dilution. Following induction at 1 mM IPTG, the bacteria are incubated at 37 °C until growth stops. The protein was purified as described previously by Ca^{2+}-dependent binding of calmodulin to phenyl-Sepharose (Vogel et al. 1983). Samples were loaded in 1 mM $CaCl_2$ and eluted at 1 mM EDTA.

Electrophysiology

The following experiments were performed by Tammy Wingo, Ph.D. with the assistance of Svetlana Stepanovic in the laboratory of Jeffrey Balser, M.D., Ph.D. Cultured tsA201 cells were transiently transfected with either WT or mutant (D1790G, 4X) cDNA (1.5 µg). Green cells were selected for electrophysiological analysis 24 hours later. The cells were maintained on culture plates using Dulbecco's Minimum Essential Medium (DMEM) with FBS (10%) and 1% Pen-Strep. In experiments where both the α and β subunits were used, cultured tsA201 cells were co-transfected with a 1:1 molar ratio of the Na^+ channel β_1 subunit (provided by A. George, Vanderbilt University).

I_{Na} was recorded at 22 °C and analysed (mean ± SEM) as described previously (Tan et al. 2001). The voltage-clamp protocol used to measure steady state channel availability are described in the text or figure legends of Chapter II. A Boltzmann function $(y = [(A_1 - A_2)/(1 + e^{(x - x_0/dx)})] + A_2)$ was fitted to the availability curves to determine the membrane potential eliciting half-maximal inactivation ($V_{1/2}$), where A_1 and A_2 are initial and final values, x_0 is equivalent to $V_{1/2}$, and dx represents the time constant. All experiments were performed 4 to 6.5 minutes after membrane rupture to allow full equilibration of the pipette solutions.

The bath solution contained: 145 mM NaCl, 4 mM KCl, 1.8 mM $CaCl_2$, 1 mM $MgCl_2$, and 10 mM HEPES (pH 7.35 with CsOH). The pipette solution used to mimic Ca^{2+}-free conditions contained (in mM): NaF 10, CsF 100, CsCl 20, BAPTA 20, HEPES 10 (pH 7.35 with CsOH). For the concentrations of free Ca^{2+} used in the dose-response analysis, 20 mM BAPTA was used with 0 $CaCl_2$, 8.94 mM $CaCl_2$, 10.9 mM $CaCl_2$, and 13.4 mM $CaCl_2$ to create solutions where the free Ca^{2+} concentrations were 0, 100, 150,

and 250 nM, respectively (Bers et al. 1994). For higher (μM) Ca^{2+} concentrations, the BAPTA concentration was reduced to 1 mM to avoid precipitation of the pipette solution. For concentrations of 1 μM and 10 μM free Ca^{2+}, 1 mM BAPTA was used with 0.9 mM Ca^{2+} and 1.0 mM Ca^{2+}, respectively. The availability curves indicate a substantial portion of the voltage shift occurred between 0 and 250 nM, where the BAPTA concentration is fixed, suggesting the Ca^{2+}-dependent changes observed do not arise from lowering the BAPTA concentration to achieve high (μM) free Ca^{2+}.

Sample Preparation for Spectroscopy

In Chapter II, calcium-free hH1-CTD-148 protein samples were prepared in two ways. (1) Dialysis against: 10 mM HEPES, 1 mM BME, 10 mM EDTA, pH 8.0; followed by three further dialysis steps in EDTA-free Chelex-100 treated buffer. (2) Three steps of concentration and resuspension in: 10 mM HEPES, 1 mM BME, 1 mM BAPTA, pH 8.0; followed by three steps of concentration and resuspension in BAPTA-free Chelex-100 treated buffer.

For the studies described in Chapter III, hH1-CTD samples were decalcified, then exchanged into the following buffers: [Calcium-loaded] – 20 mM Tris, 5 mM BME, 20 mM CaCl$_2$, pH 7.5; [Apo] – 20 mM Tris, 5 mM BME, 2 mM BAPTA, pH 7.5; [EGTA] – 20 mM Tris, 5 mM BME, 2 mM EGTA, pH 7.5; [Mg^{2+}] – 20 mM Tris, 5 mM BME, 20 mM MgCl$_2$, pH 7.5. Atomic absorption was used to measure residual calcium in protein decalcified by BAPTA (Galbraith Laboratories Inc., Knoxville, TN). This analysis showed that calcium was reduced to below the detection limit (< 17 μM) by exchange into BAPTA.

Trichloroacetic acid (TCA) precipitation used in Chapters III and IV to remove calcium was performed in three rounds following the protocol of Haiech and colleagues (Haiech et al. 1981). Briefly, this protocol takes advantage of the fact that acidic residues are critical for binding calcium ions. Strong acidification of the protein solution using TCA protonates these acidic residues and prevents chelation of the calcium ion. TCA also causes the protein to precipitate. The precipitated protein can then be recovered by centrifugation and rinsed with Chelex-treated buffer. The precipitate is solubilized in 1M Tris-base and refolded by adjustment of the pH to 7.5. This process is repeated twice more to ensure complete removal of calcium. Following TCA precipitation, protein solutions were adjusted to reduce the quantity of Tris in the buffer and to add BME.

NMR titrations were performed at 150 mM Tris, 3.7 mM BME, pH 8.0 at protein concentrations varying between 100 μM and 1 mM. Intrinsic fluorescence titrations were performed at 40 mM Tris, 4.5 mM BME, pH 8.0 at a protein concentration of approximately 1 μM.

For the studies in Chapter IV and Appendix A, calmodulin was exchanged into (apo) 20 mM bis-Tris, 100 mM KCl, 1 mM DTT, 2 mM EGTA, pH 6.5 or (Ca^{2+}-loaded) 20 mM bis-Tris, 100 mM KCl, 1 mM DTT, 20 mM $CaCl_2$, pH 6.5. The calmodulin concentration was determined by A_{276}, using an extinction coefficient $\varepsilon = 3006$ M^{-1} cm^{-1}.

Intrinsic fluorescence

Steady-state fluorescence emission spectra were recorded at ambient temperature using a SPEX FLUOROMAX spectrofluorometer (Spex Instruments SA). For calcium affinity measurements, a 3.2 mL quartz cuvette was prepared by soaking in EDTA, EGTA, or BAPTA, followed by thorough rinsing with Chelex-100 treated H_2O.

Calmodulin-IQ affinity measurements in Chapter IV were likewise conducted in 1.0 mL quartz cuvettes pre-soaked in the appropriate apo or Ca^{2+} containing buffer.

In Chapter II, scanning was done from 300-375 nm (λ_{excit} = 280 nm) and 320-375 nm (λ_{excit} = 295 nm), with slit-widths set to 5 nm. Calcium-free protein in a buffer containing 10 mM HEPES and 1 mM BME at pH 7.0 was used for titrations. Protein concentration was determined by amino acid analysis. Binding constants were obtained by fitting to a standard binding equation using CaLigator 1.05 (Andre and Linse 2002).

In Chapter III, scanning was done from 320-380 nm (λ_{excit} = 295 nm) with slit-widths set to 5 nm. Calcium-free protein in a buffer containing 20 mM Tris and 5 mM BME at pH 7.5 was used for titrations performed by adding small aliquots of calcium. Binding constants and best-fit curves were obtained by fitting to a standard binding equation using CaLigator 1.05 or Mathematica 4.0 (Wolfram Research). Fits and data were plotted in Microsoft Excel.

In Chapter IV, constant wavelength analysis was used to measure calcium binding affinities, monitoring tryptophan fluorescence at 345 nm with excitation at 280 nm and 295 nm. Constant wavelength analysis was also used to measure calmodulin affinity for IQ peptides, monitoring tyrosine fluorescence at 320 nm with excitation at 277 nm.

Circular dichroism (CD)

CD spectra were recorded at ambient temperature over a range of 190-260 nm using a Jasco J-810 spectropolarimeter (Jasco, Easton, Maryland). The measurements were carried out in 1 mm quartz cuvettes prepared by soaking in EDTA, EGTA, or BAPTA, followed by thorough rinsing with Chelex-100 treated H_2O.

Nuclear magnetic resonance (NMR)

Gradient enhanced ^{15}N-^{1}H HSQC NMR spectra were recorded at 27 °C on AVANCE Bruker spectrometers operating at 500 and 600 MHz equipped with Cryo-Probes. Acquisition parameters varied, but were generally 4, 8, 16, or 32 scans per real or imaginary point in the indirect dimension, with 64 or 128 complex points (128 or 256 F.I.D.) total in the indirect dimension. Sweep width in ^{1}H was 15 ppm, and in ^{15}N increments were selected to set a sweep width of 35 ppm. Solutions for Chapter II experiments contained 0.1-1.0 mM ^{15}N-enriched protein in a buffer containing 10 mM HEPES, 1 mM BME, 1 mM $CaCl_2$, pH 8.0, 90% H_2O/10%D_2O. The NMR spectra were processed and analyzed using XWinNMR (Bruker, Germany) and Sparky (Goddard and Kneller). A sinebell squared window function and zero filling by a factor of four in the indirect dimension were generally applied prior to Fourier transform. Spectra were plotted in the programs used for data analysis.

Experiments described in Appendix A were conducted on a Bruker AVANCE 500 MHz spectrometer equipped with a CryoProbe. Two-dimensional ^{15}N-^{1}H heteronuclear single quantum correlation experiments were performed at 25 °C, acquiring four scans per increment and 512 points in the indirect (t_1) dimension. NMR data were processed and analyzed in XWinNMR (Bruker).

APPENDIX D

NMR SPECTRA

Introduction

The following ^{15}N-^{1}H HSQC NMR spectra are the full or almost full plots of spectra that, when mentioned or shown in a figure, only a zoomed part of the spectrum was shown. These zooms were chosen for various reasons. In some cases, it was to emphasize particular regions of the spectrum, such as downfield regions indicating the presence of folded protein. In other cases it was show a representative example of phenomena occurring throughout the spectrum – slow/intermediate/fast exchange during a titration, for example. Finally, in some cases spectra were not included for space or aesthetic reasons. Here, however, deference has been given to scientific content over aesthetic considerations. In some cases, spectra with poor S/N have been plotted such that noise or processing artifacts are visible. Likewise, in some of the low S/N BAPTA spectra noise ridges appear due to incomplete suppression of non-^{15}N-linked ^{1}H signals. While these ridges can be removed during processing, such removal also suppresses or removes real peaks.

Please note that many of the hH1-CTD spectra exclude a single dispersed peak which is found extremely downfield at 11.28 ppm in ^{1}H and 129.3 in ^{15}N. The decision was made to exclude the peak because plotting it generally sacrifices clarity of the rest of the spectrum.
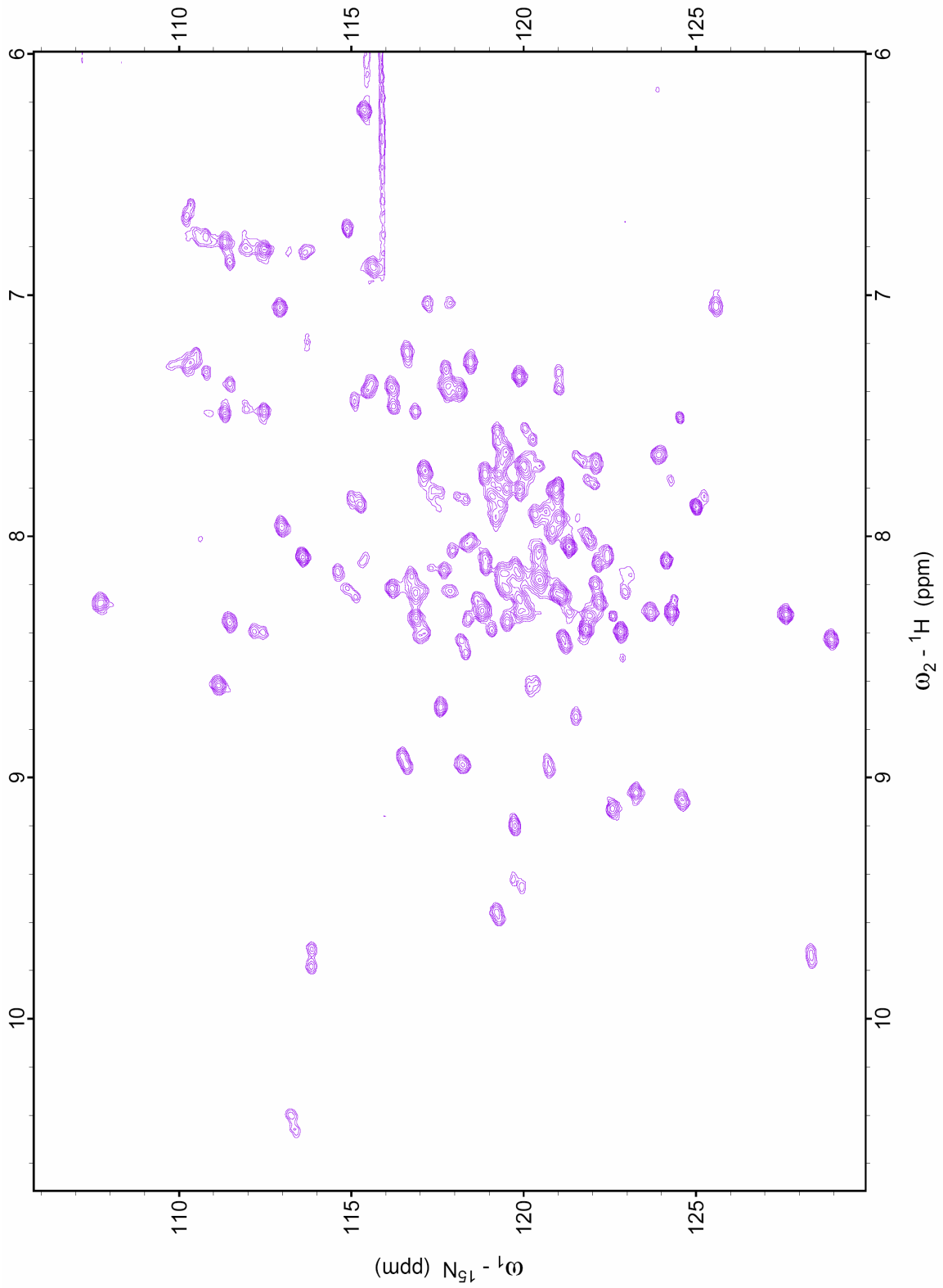
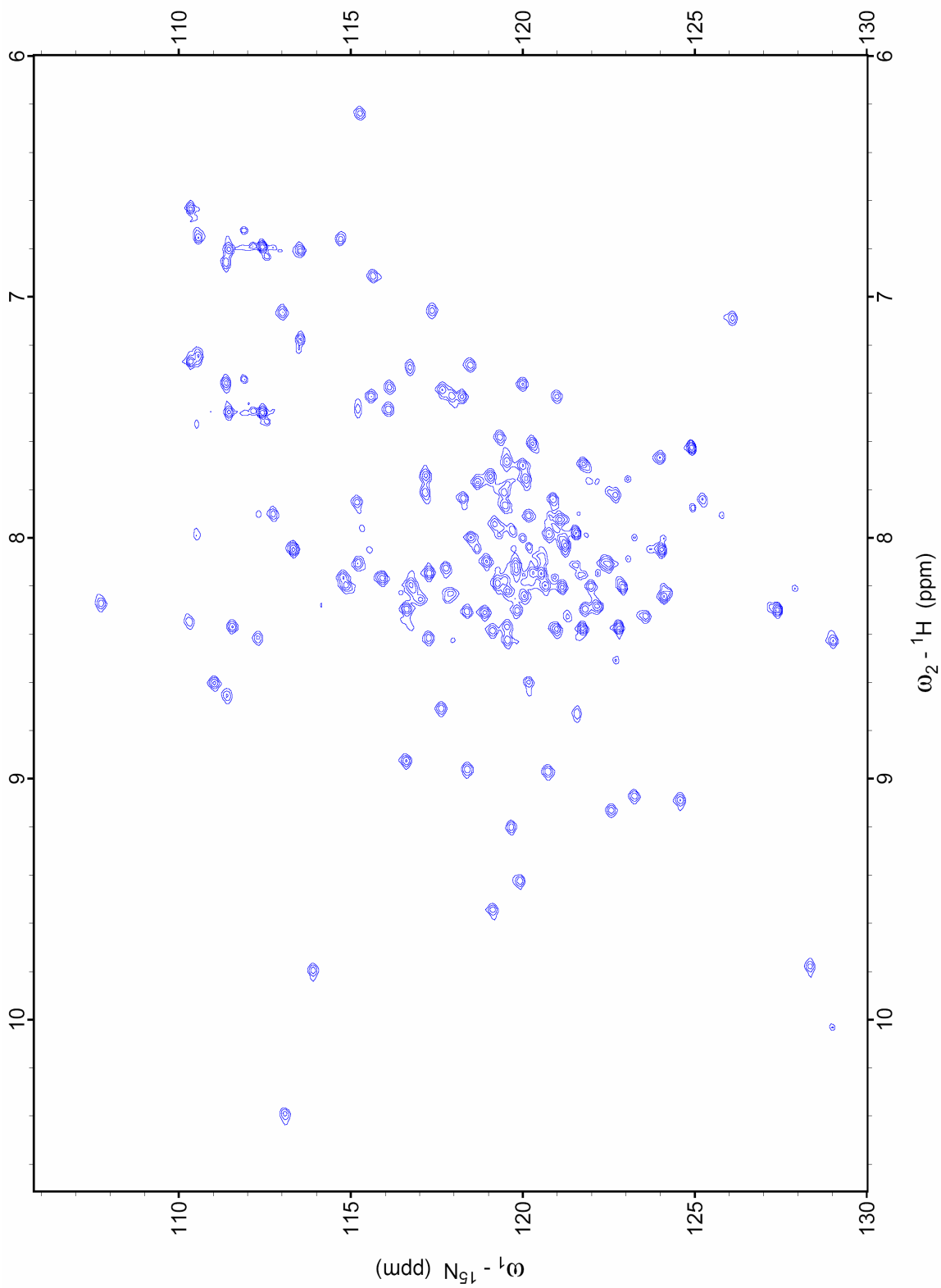**Figure D.1:** Spectrum of hH1-CTD-148. See Chapter III for details.

Figure D.2: Spectrum of hH1-CTD-120. See Chapter III for details.
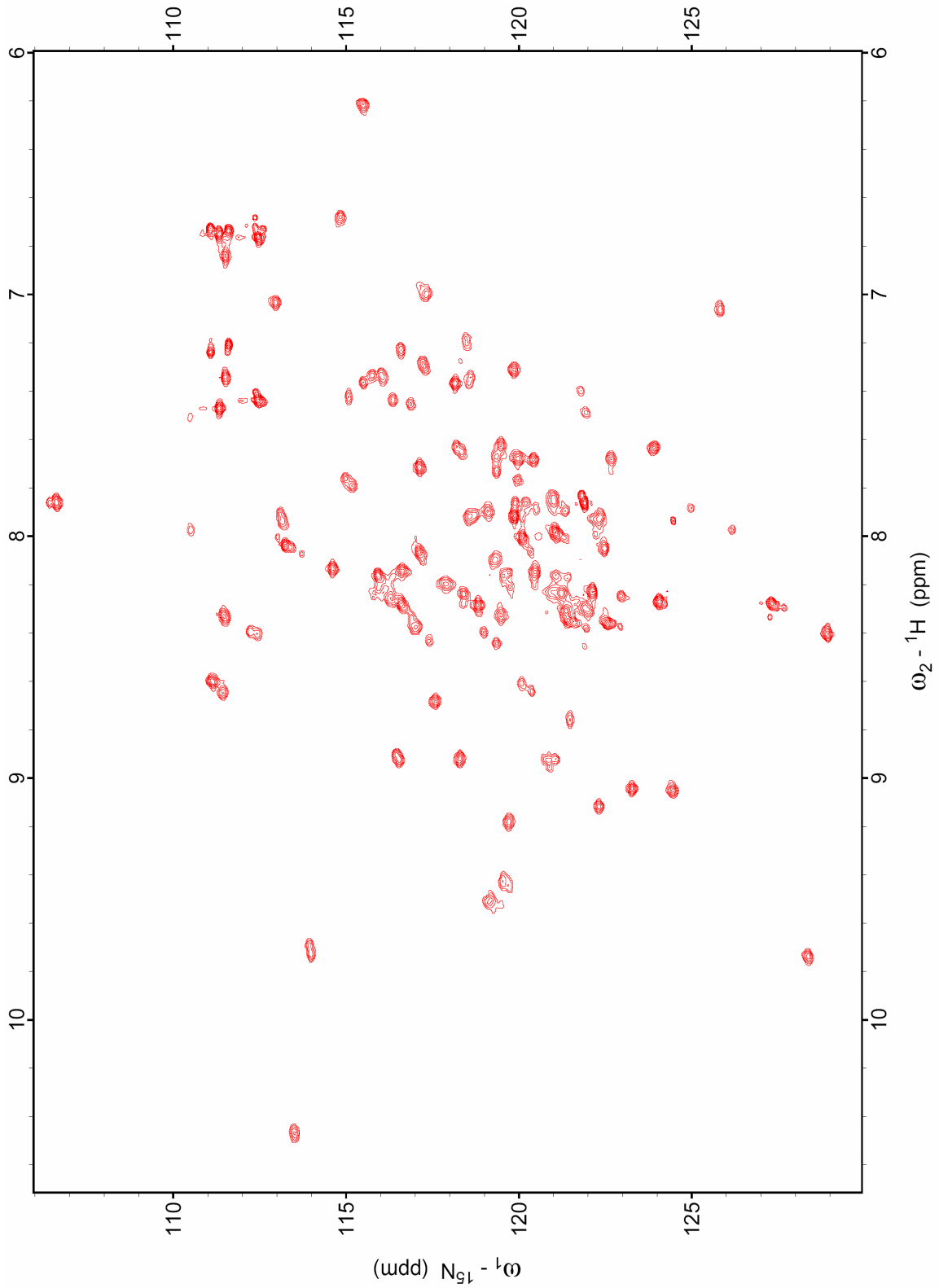
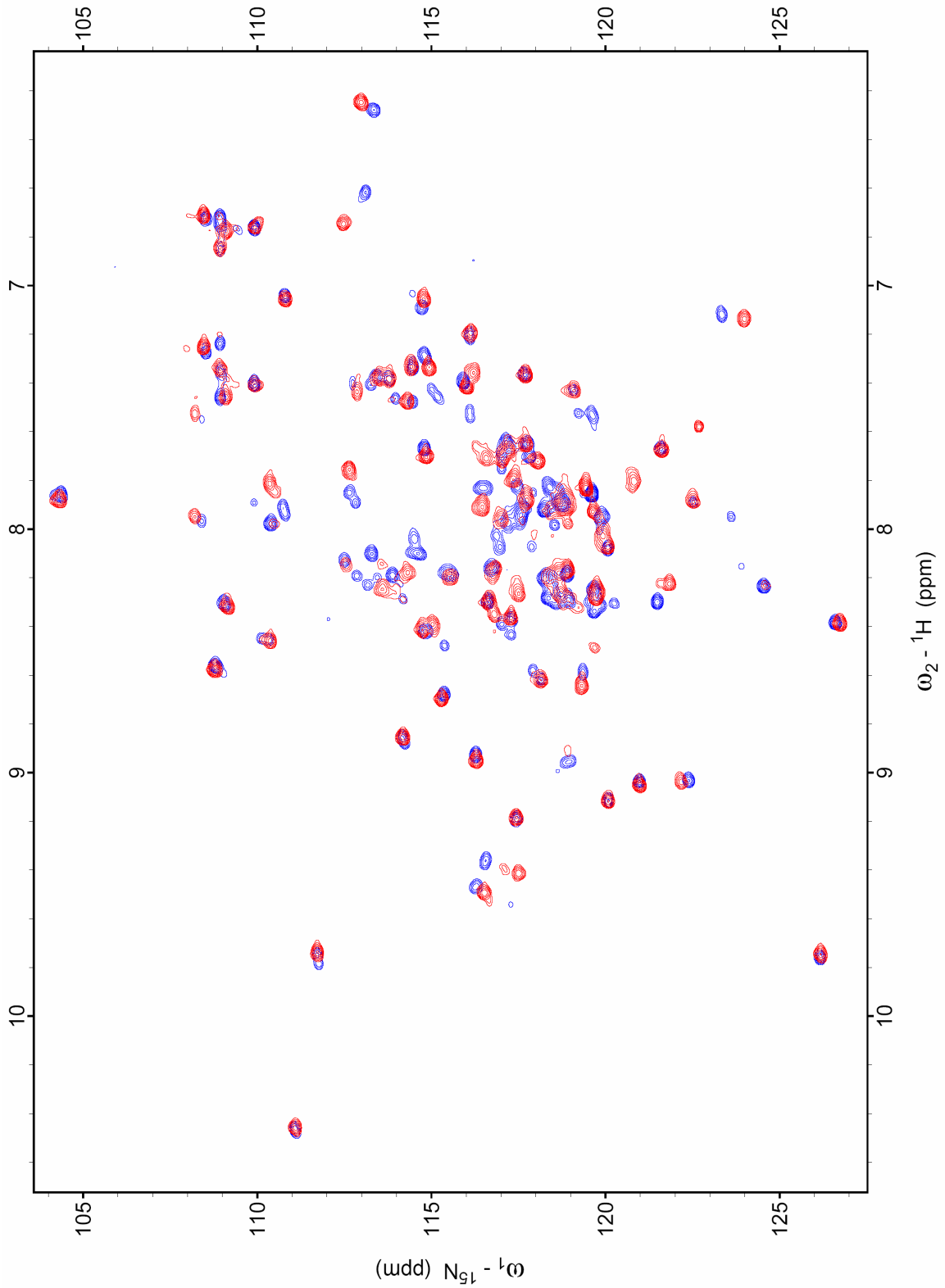**Figure D.3:** Spectrum of hH1-CTD-93. See Chapter III for details.

Figure D.4: Spectra of hH1-CTD-93, BAPTA-apo (blue) and Ca^{2+}-loaded (red). See Chapter III for details.
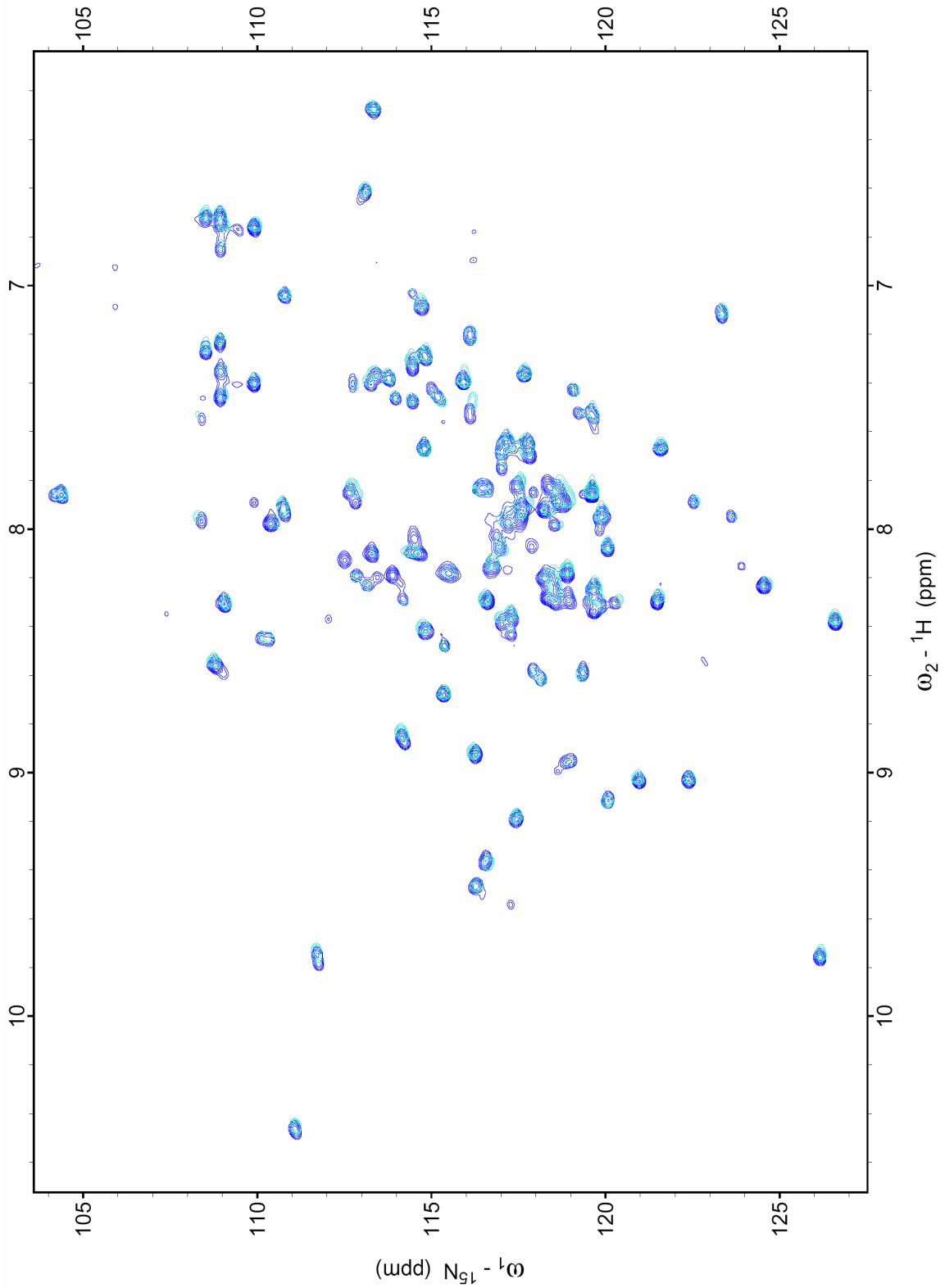
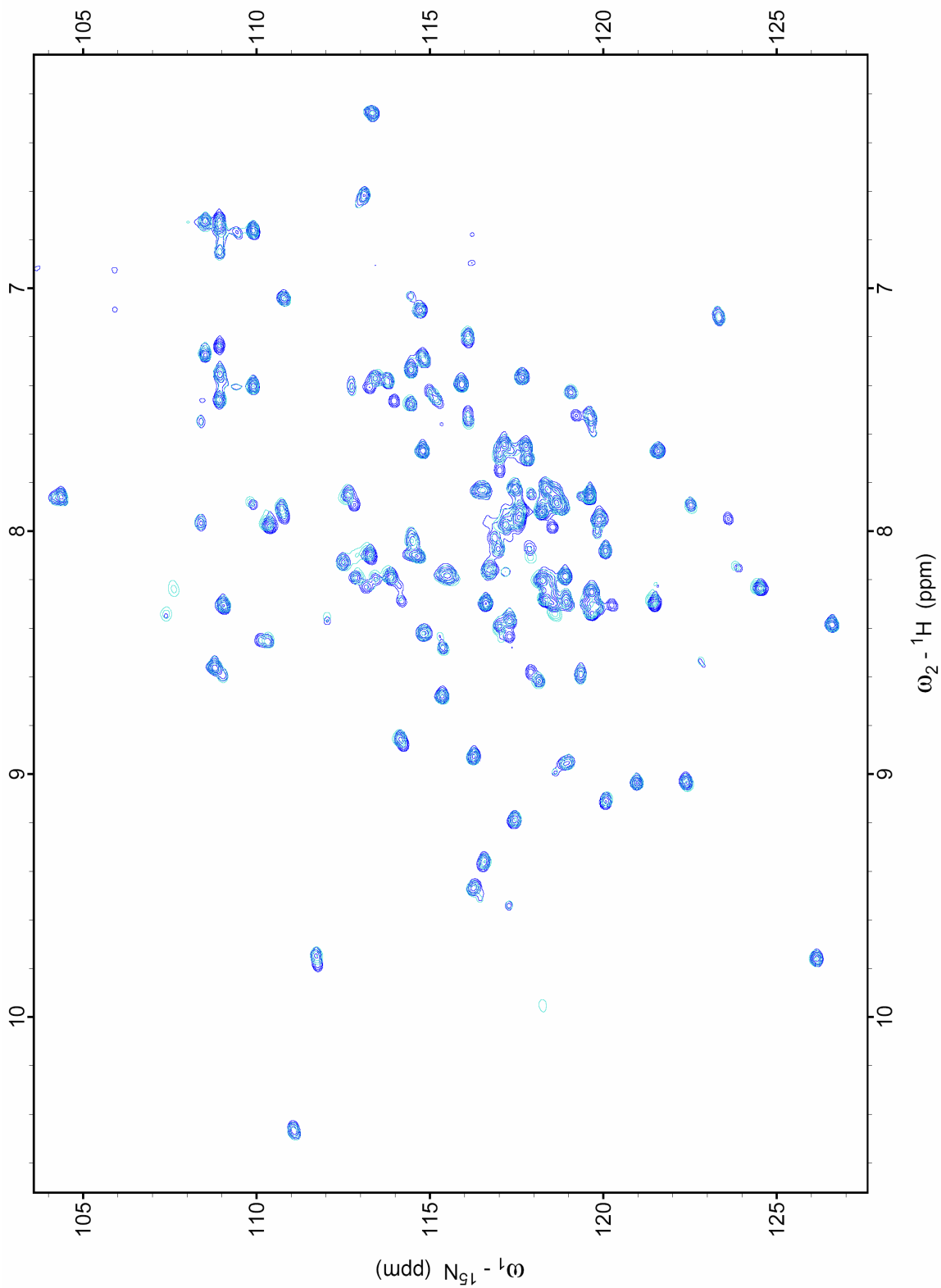**Figure D.5:** Spectra of hH1-CTD-93. BAPTA-apo (dark blue), TCA-apo (light blue). See Chapter III for details.

Figure D.6: Spectra of hH1-CTD-93. BAPTA-apo (dark blue), EGTA-apo (light blue). See Chapter III for details.
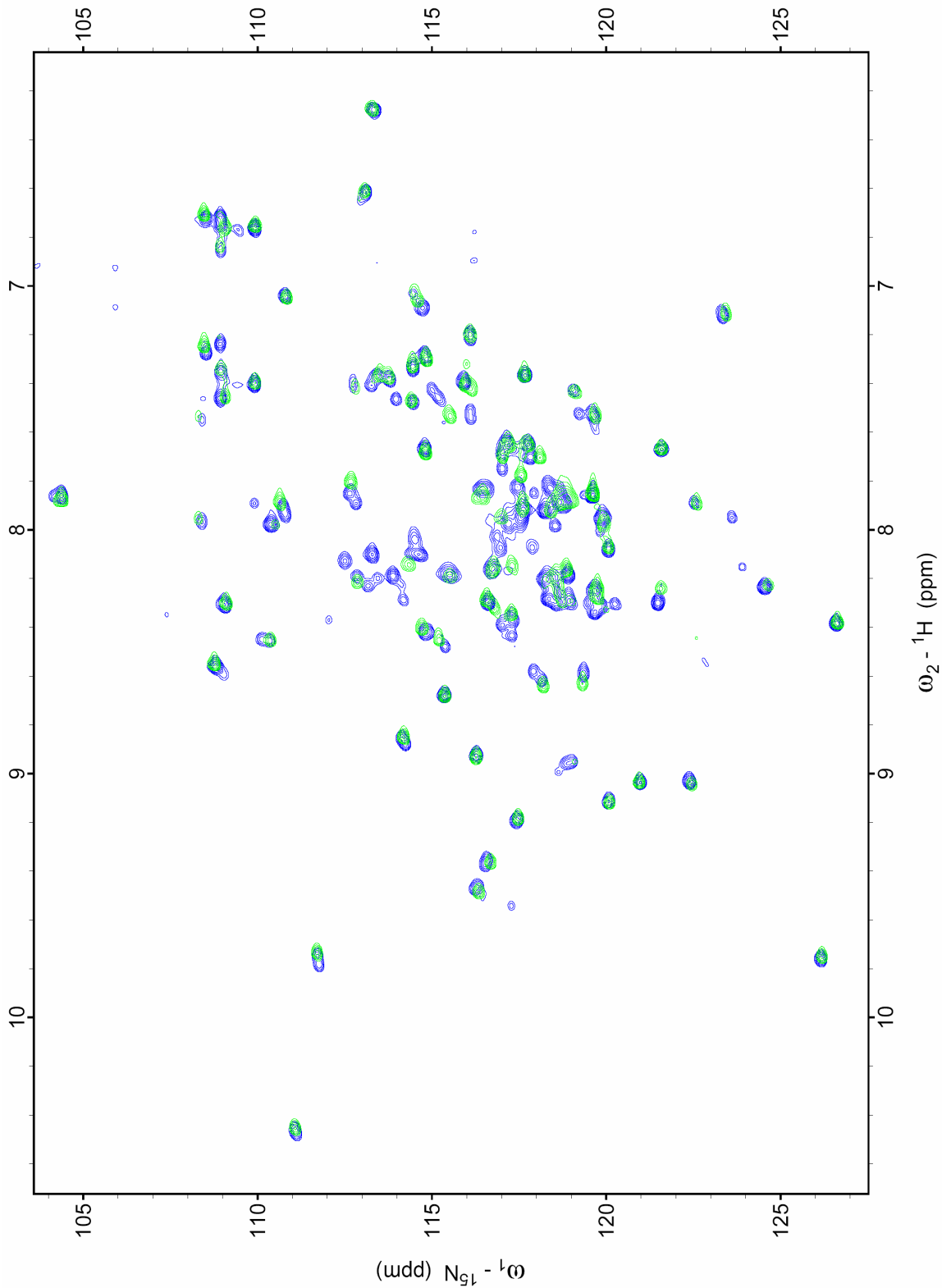
Figure D.7: Spectra of hH1-CTD-93. BAPTA-apo (dark blue), MgCl$_2$-loaded (green). See Chapter III for details.
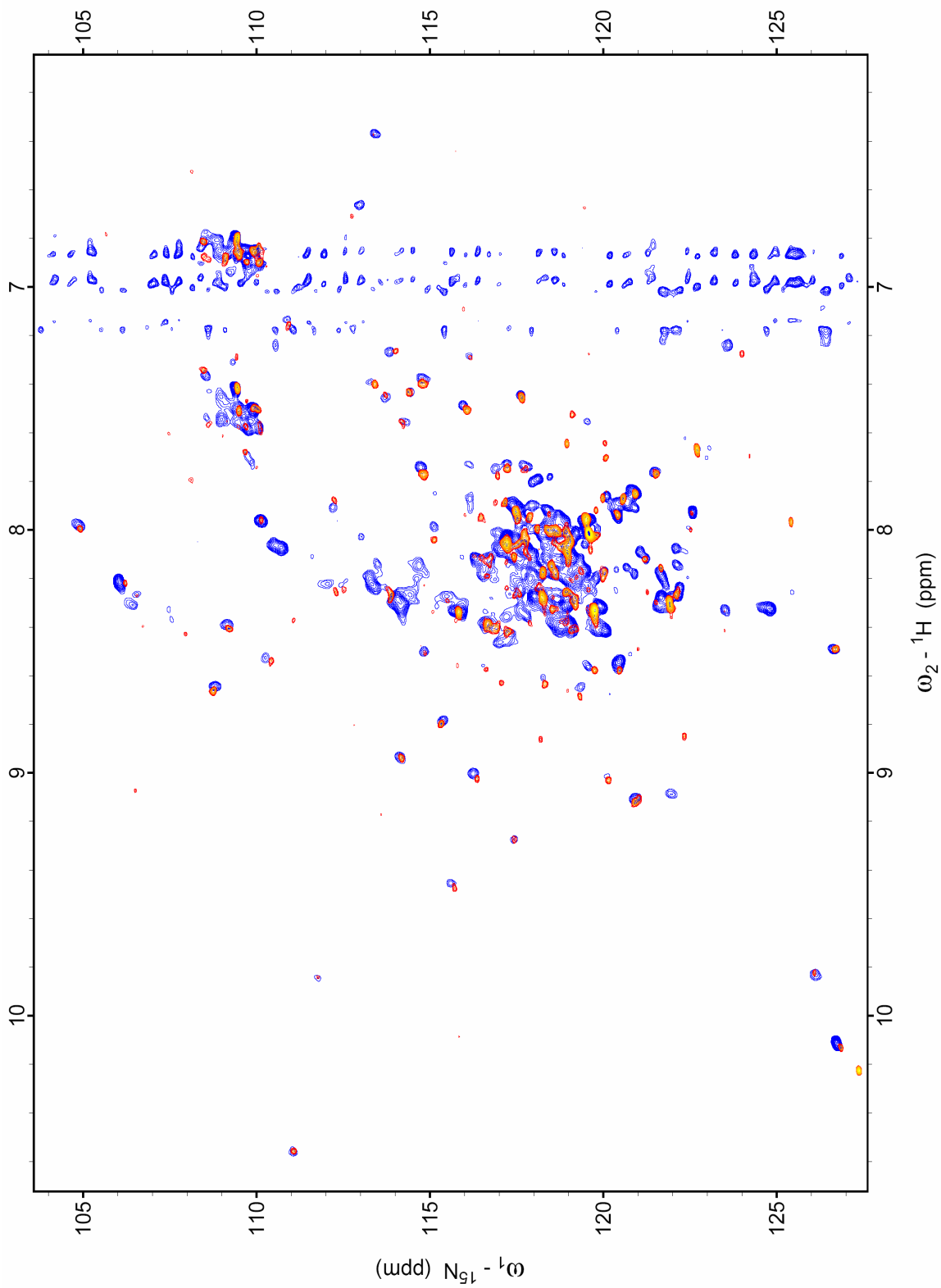
Figure D.8: Spectra of hH1-CTD-93-D1790G. BAPTA-apo (dark blue), Ca^{2+}-loaded (red-yellow). BAPTA noise ridges are visible. See Chapter III for details.
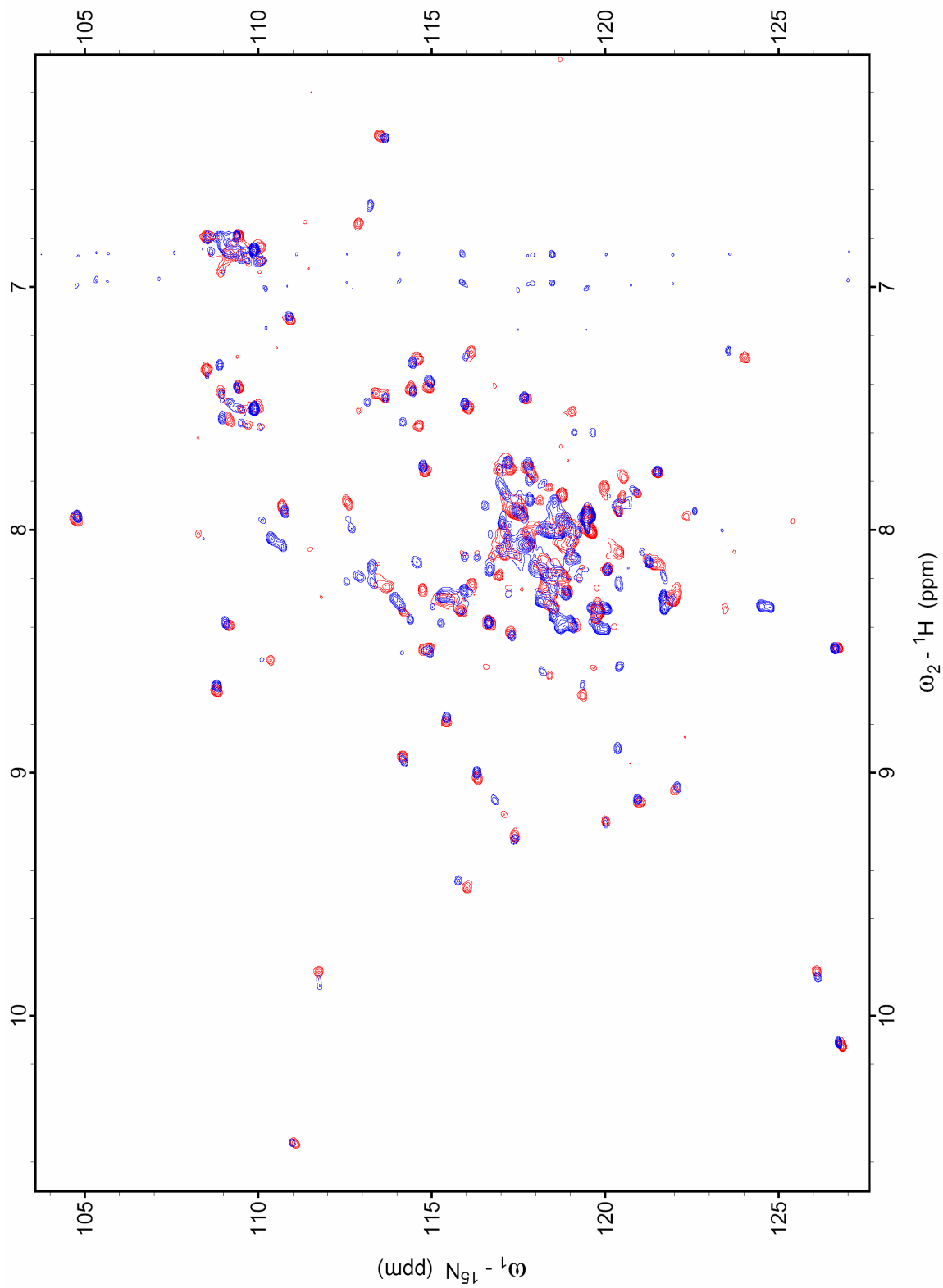
Figure D.9: Spectra of hH1-CTD-93-F1791A. BAPTA-apo (dark blue), Ca^{2+}-loaded (red-yellow). Faint BAPTA noise ridges are visible. See Chapter III for details.
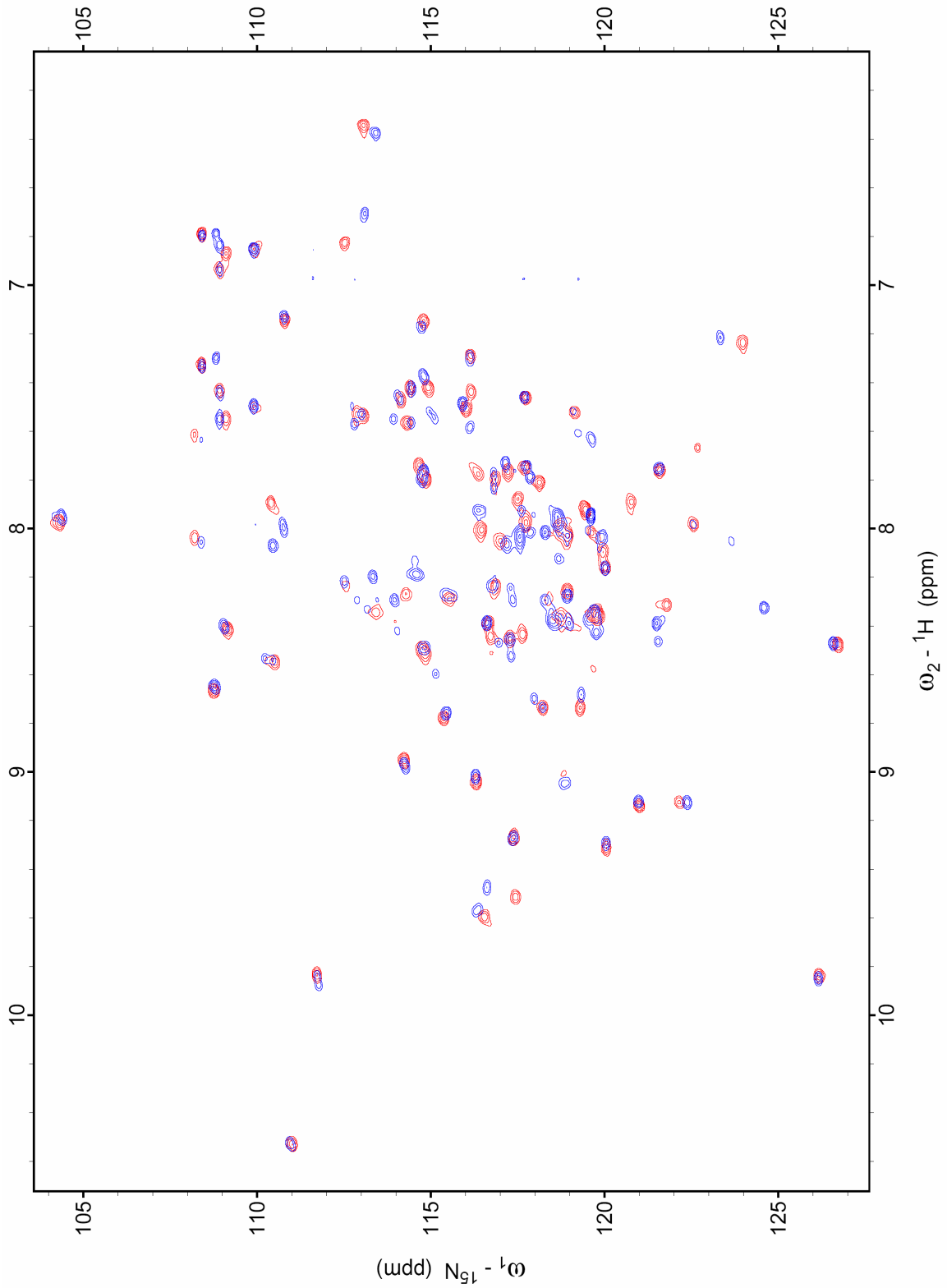
Figure D.10: Spectra of hH1-CTD-93-M1793G. BAPTA-apo (dark blue), Ca^{2+}-loaded (red-yellow). See Chapter III for details.
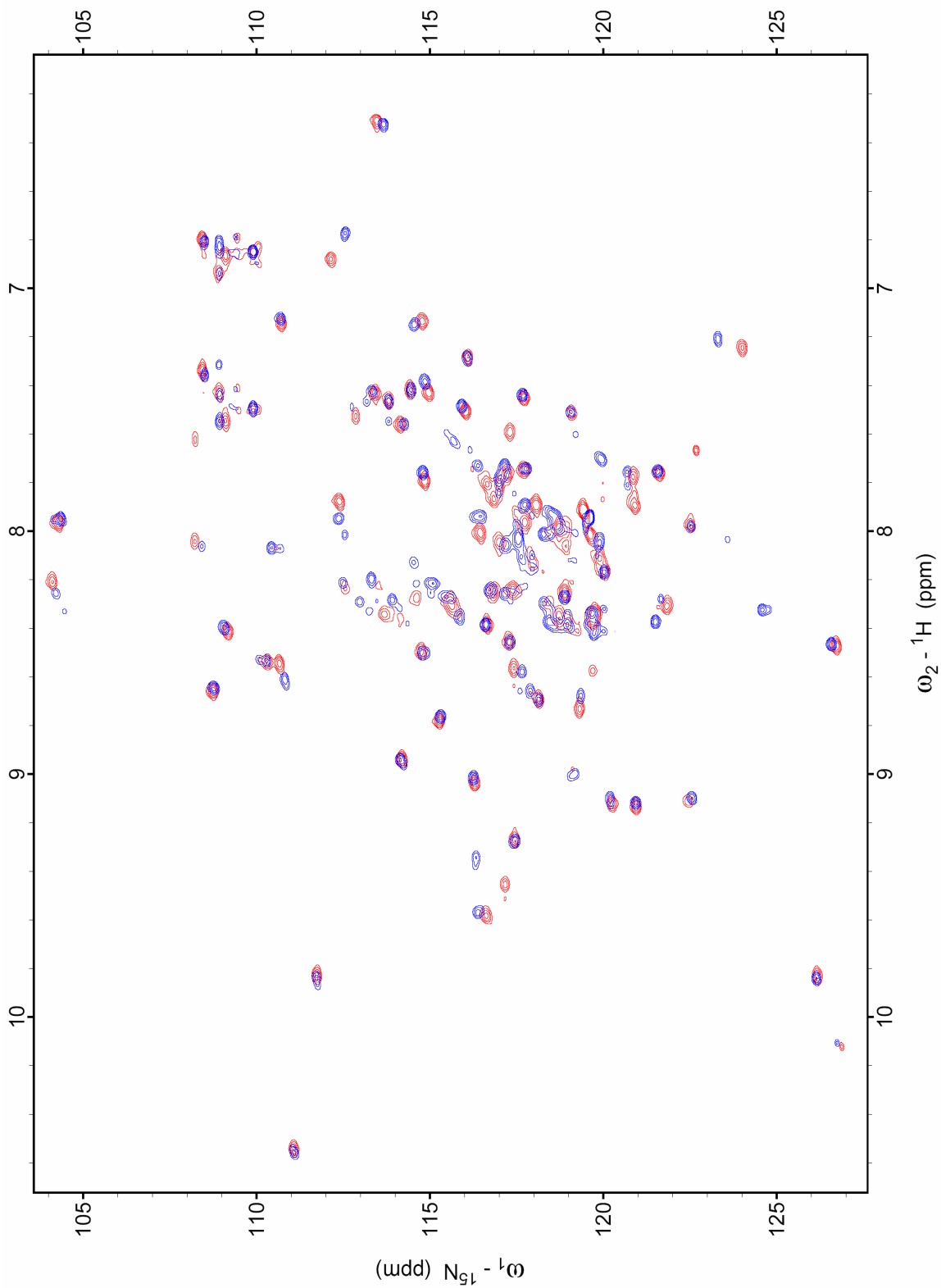
Figure D.11: Spectra of hH1-CTD-93-E1799A. BAPTA-apo (dark blue), Ca^{2+}-loaded (red-yellow). See Chapter III for details.
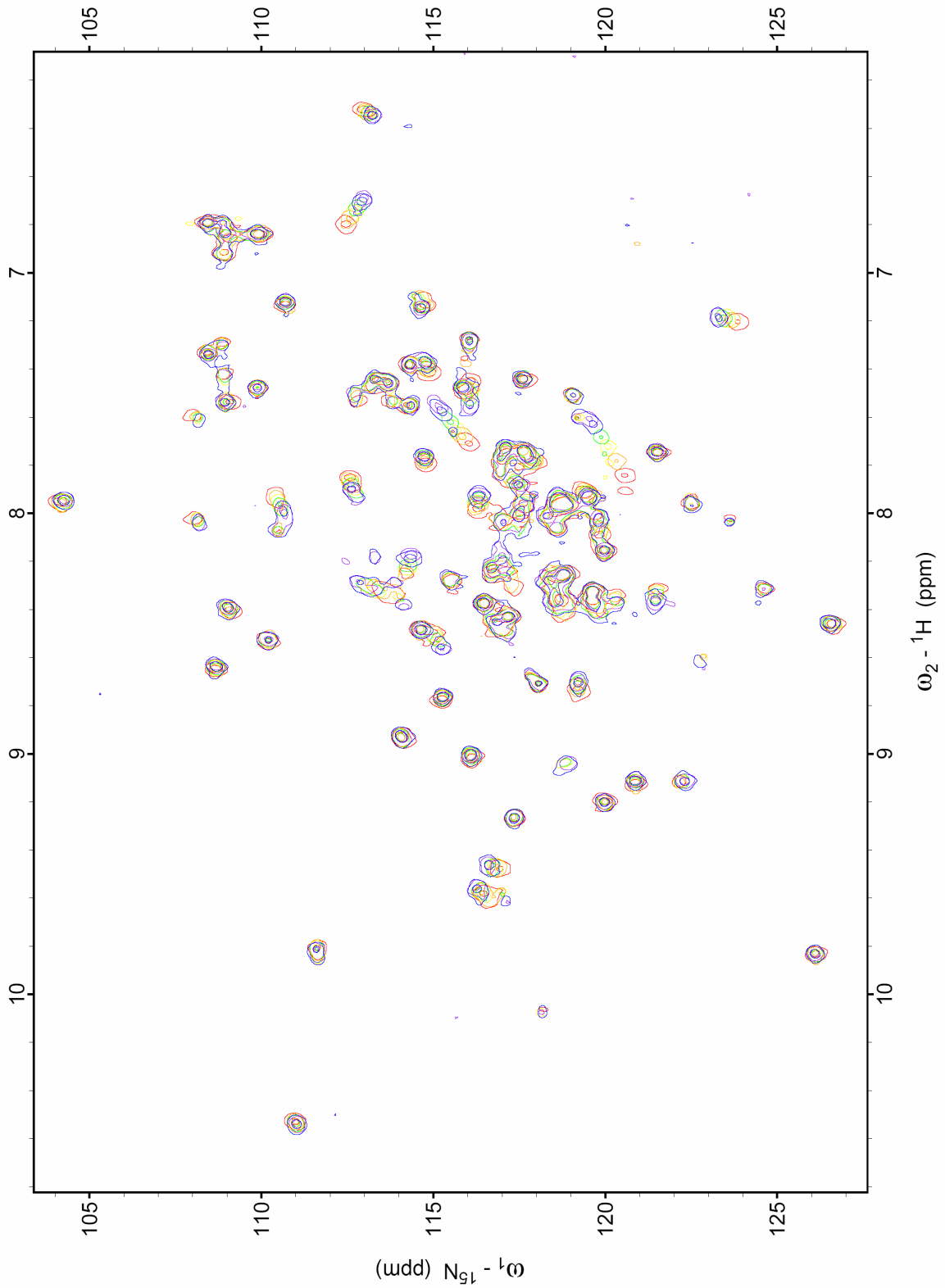
Figure D.12: Spectra of hH1-CTD-93 collected during a calcium titration. See Chapter III for details.
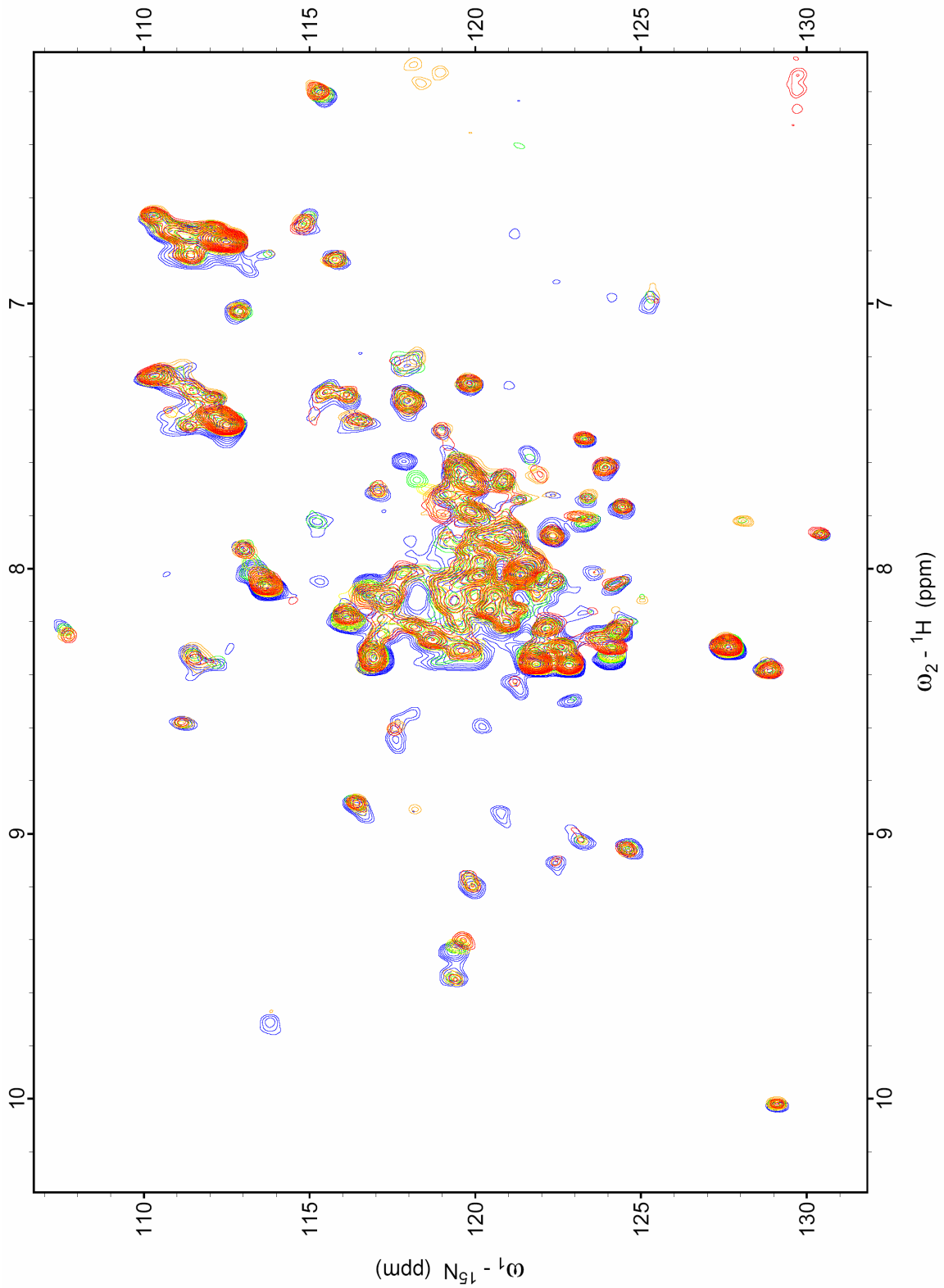
Figure D.13: Spectra of hH1-CTD-148 collected during a calcium titration. Because of μM affinity binding, intermediate exchange causes significant peak broadening. See Chapter III for details.
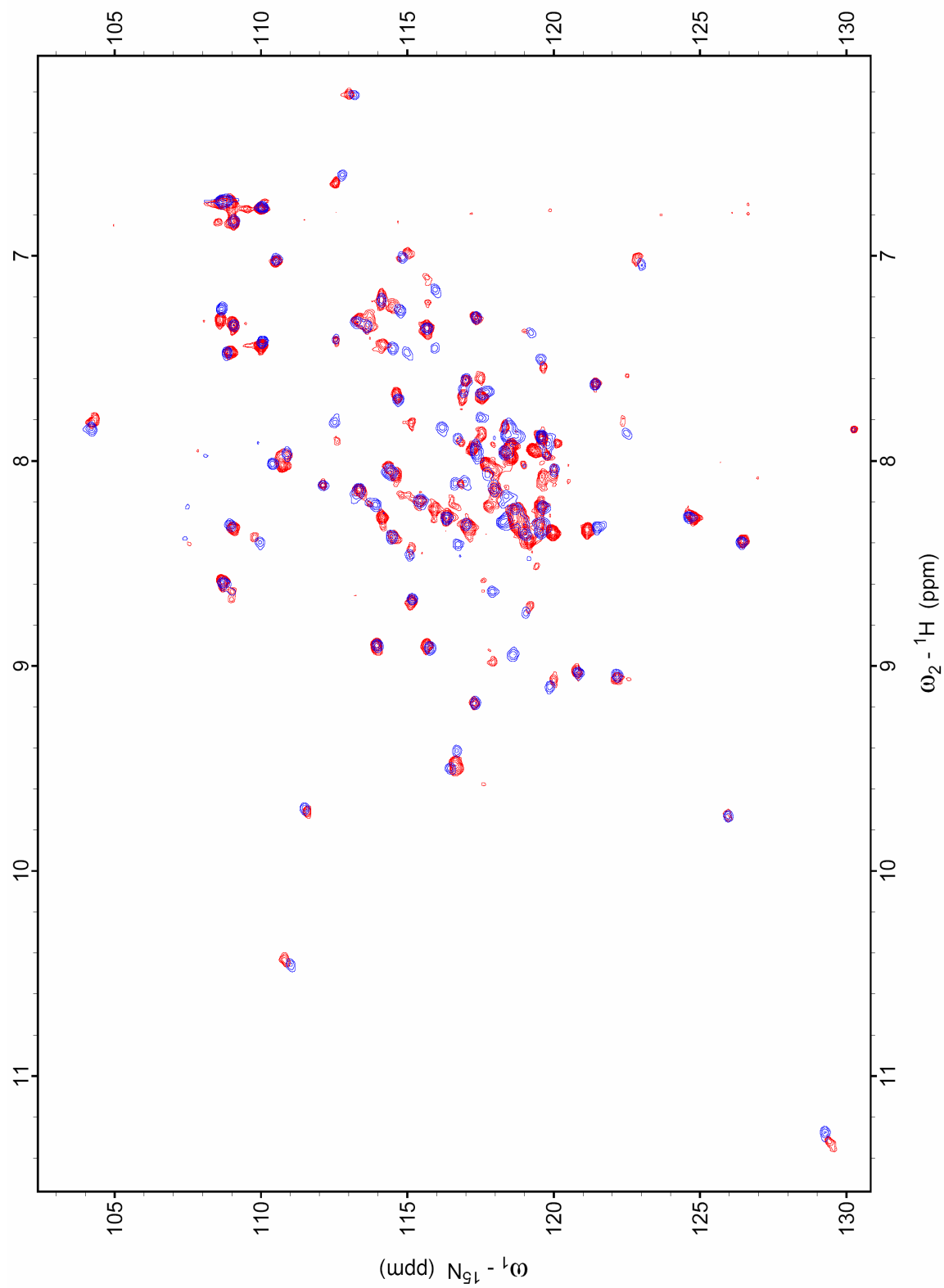
Figure D.14: Spectra of apo-hH1-CTD-93 ± IQ motif. Absence of IQ motif (blue). Plus IQ motif (red). See Chapter IV for details.
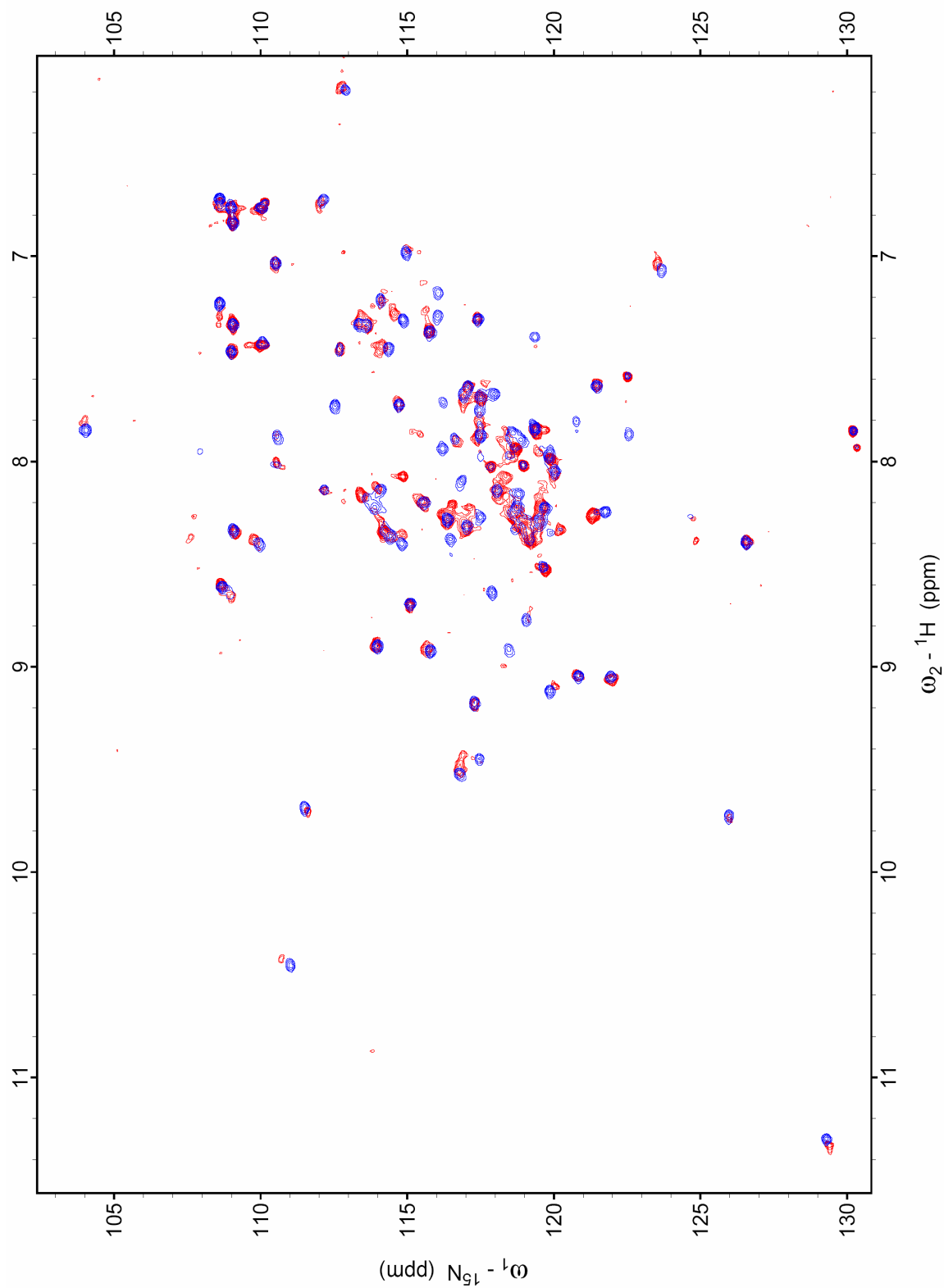
Figure D.15: Spectra of Ca^{2+}-hH1-CTD-93 $\pm$ IQ motif. Absence of IQ motif (blue). Plus IQ motif (red). See Chapter IV for details.
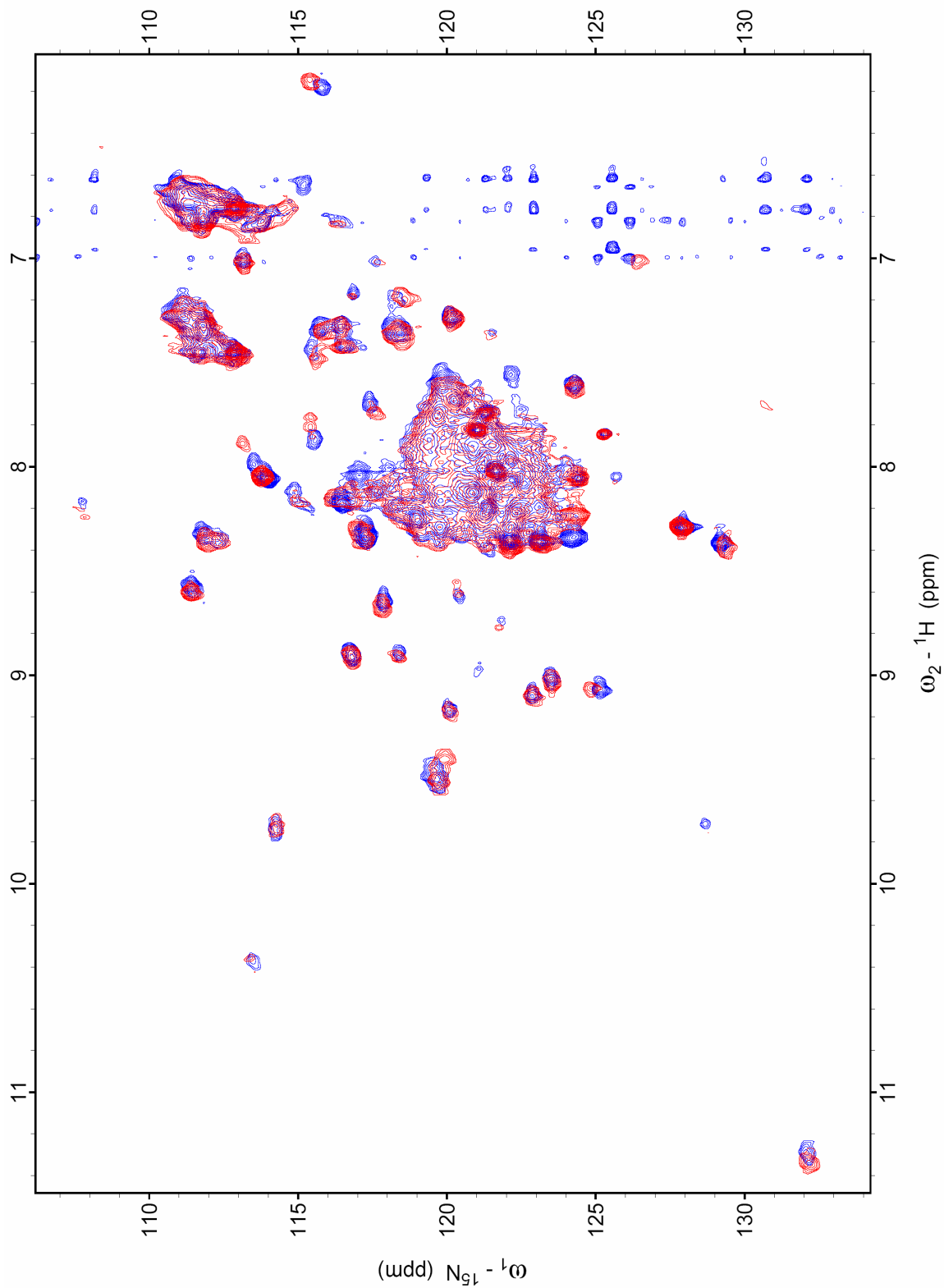
Figure D.16: Spectra of apo-hH1-CTD-153 (blue) and Ca^{2+}-hH1-CTD-153 (red). See Chapter IV for details.
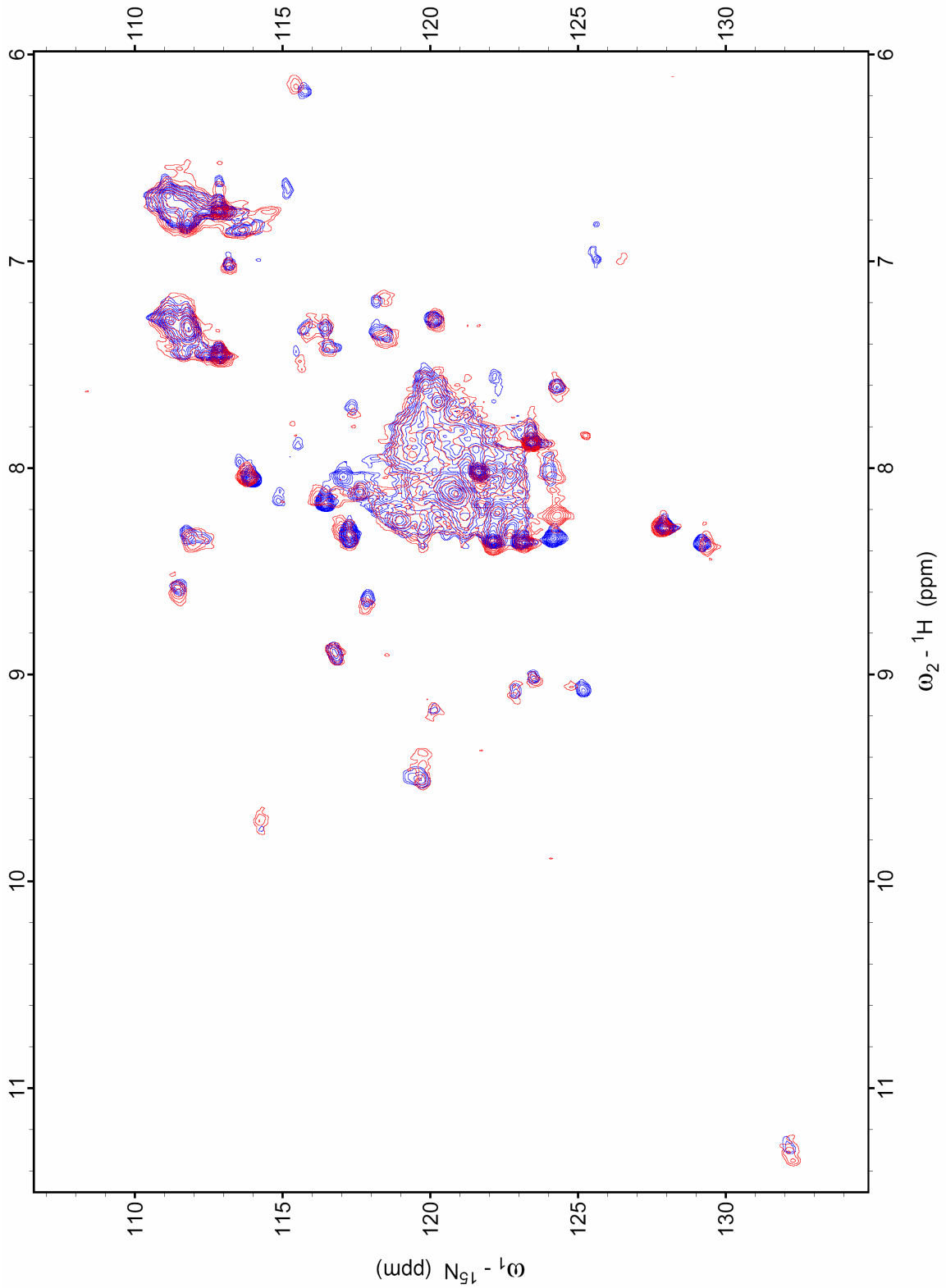
Figure D.17: Spectra of apo-hH1-CTD-153-A1924T (blue) and Ca^{2+}-hH1-CTD-153-A1924T (red). See Chapter IV for details.
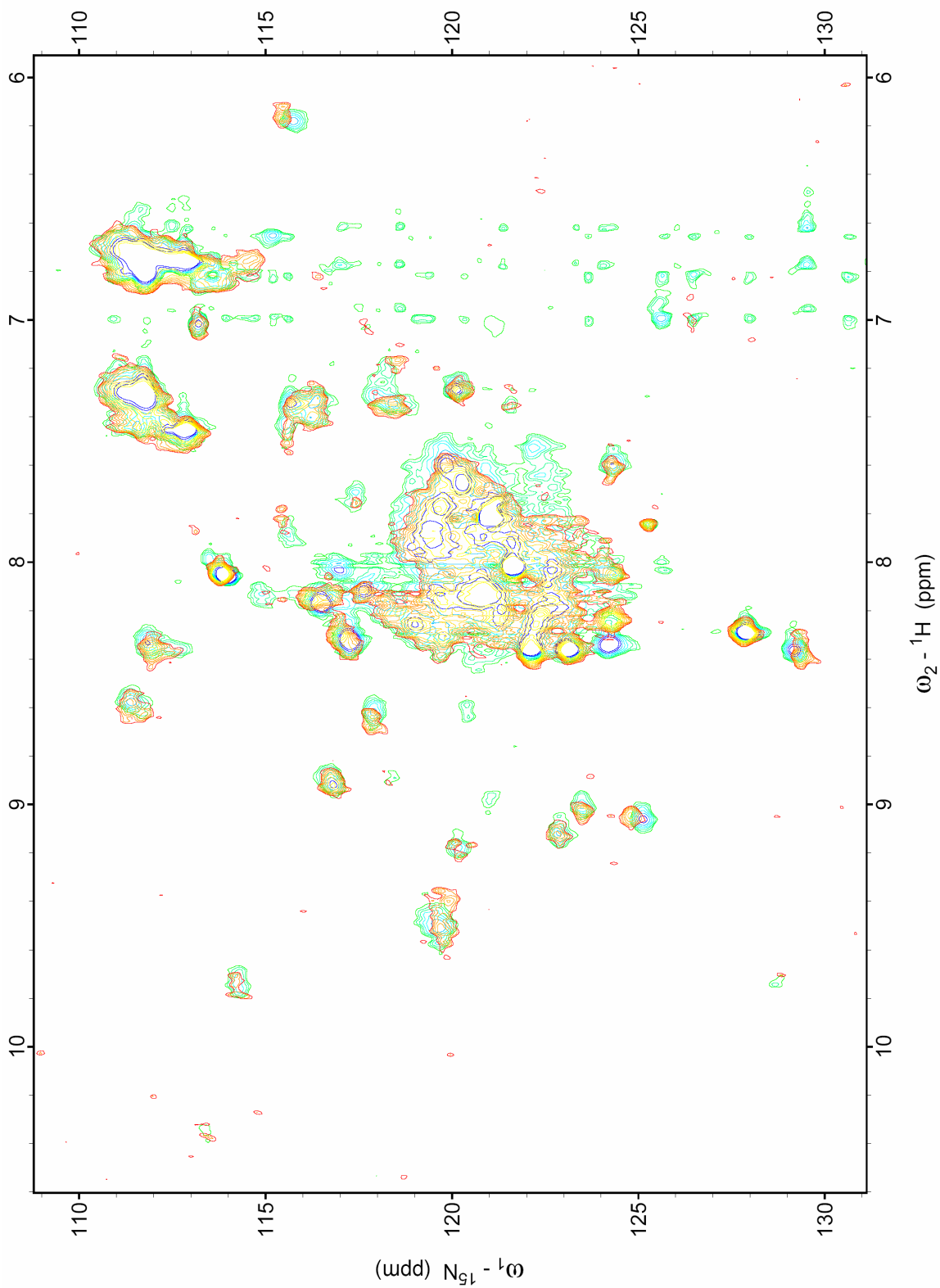
Figure D.18: Spectra of apo-hH1-CTD-153-IQ/AA (green-blue) and Ca^{2+}-hH1-CTD-153-IQ/AA (red-yellow). See Chapter IV for details.
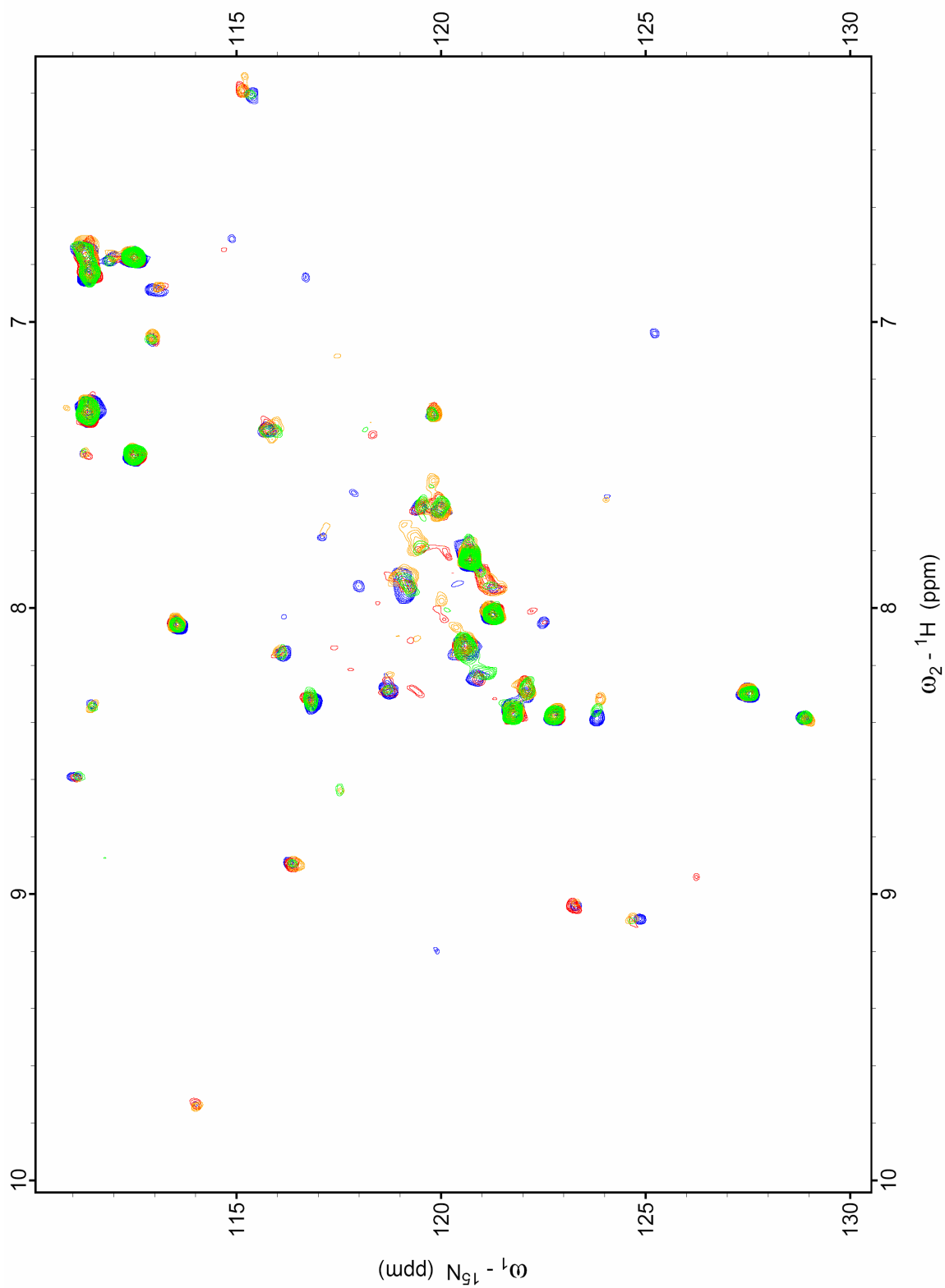
Figure D.19: Titration of calcium into TCA precipitated apo-hH1-CTD-153-IQ/AA. See Chapter IV for details.

Figure D.20: Spectra of apo-calmodulin ± IQ motif. Absence of IQ motif (blue). Plus IQ motif (red). Usable transferred assignments included. See Chapter IV for details.

142
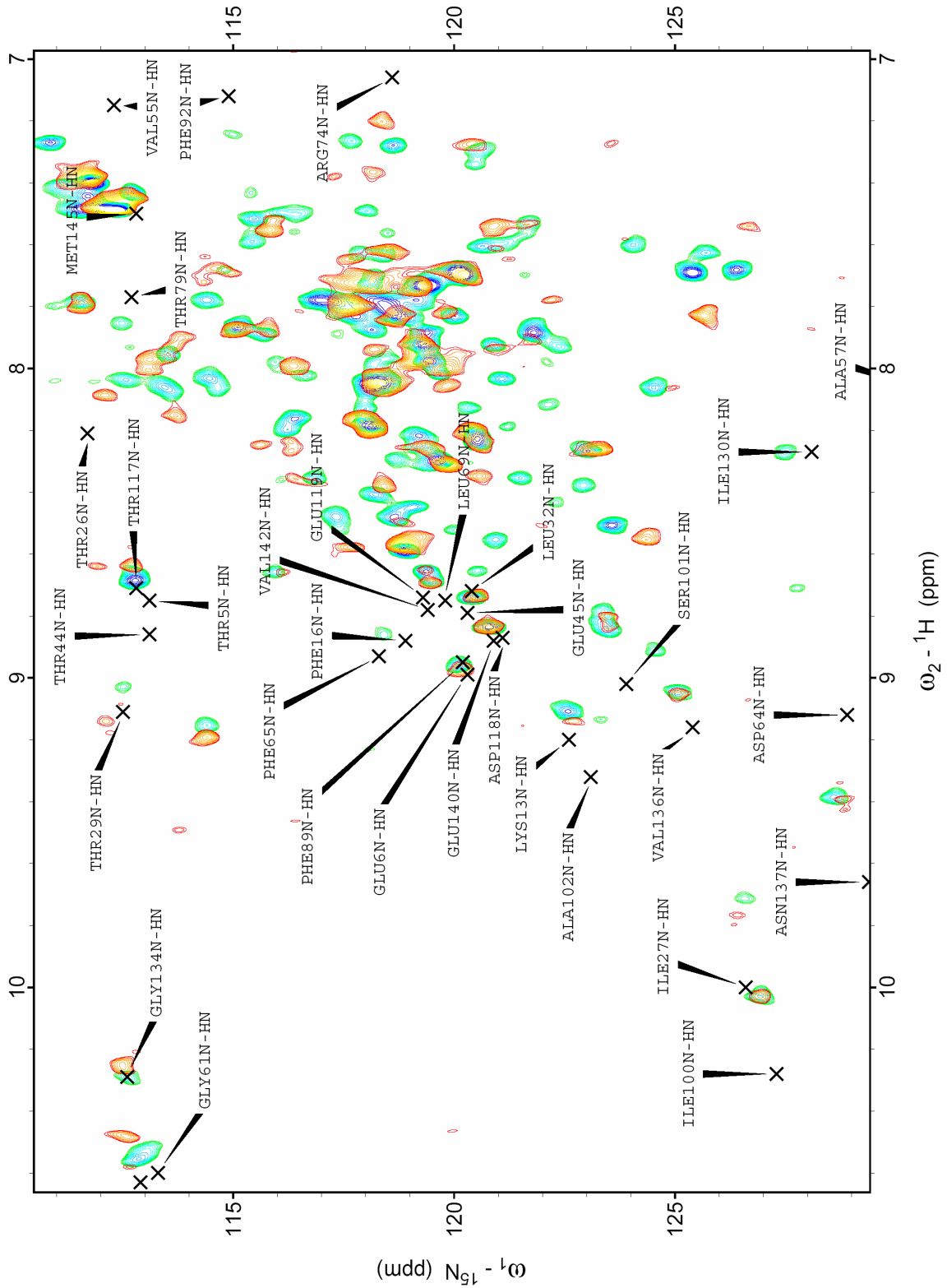
Figure D.21: Spectra of Ca^{2+}-calmodulin $\pm$ IQ motif. Absence of IQ motif (blue). Plus IQ motif (red). Some transferred assignments included. See Chapter IV for details.

REFERENCES

(2002). Molecular Operating Environment, Chemical Computing Group.

Abriel, H. and Kass, R. S. (2005). "Regulation of the voltage-gated cardiac sodium channel Nav1.5 by interacting proteins." Trends Cardiovasc Med **15**(1): 35-40.

Ackerman, M. J., Khositseth, A., Tester, D. J., Hejlik, J. B., Shen, W. K. and Porter, C. B. (2002). "Epinephrine-induced QT interval prolongation: a gene-specific paradoxical response in congenital long QT syndrome." Mayo Clin Proc **77**(5): 413-21.

Ahern, C. A. and Horn, R. (2004). "Stirring up controversy with a voltage sensor paddle." Trends in Neurosciences **27**(6): 303.

Ahluwalia, J., Tinker, A., Clapp, L. H., Duchen, M. R., Abramov, A. Y., Pope, S., Nobles, M. and Segal, A. W. (2004). "The large-conductance Ca2+-activated K+ channel is essential for innate immunity." Nature **427**(6977): 853-8.

Albrecht, D. E. and Froehner, S. C. (2002). "Syntrophins and dystrobrevins: defining the dystrophin scaffold at synapses." Neurosignals **11**(3): 123-9.

Alexander, K. A., Cimler, B. M., Meier, K. E. and Storm, D. R. (1987). "Regulation of calmodulin binding to P-57. A neurospecific calmodulin binding protein." J. Biol. Chem. **262**(13): 6108-6113.

Alexander, K. A., Wakim, B. T., Doyle, G. S., Walsh, K. A. and Storm, D. R. (1988). "Identification and characterization of the calmodulin-binding domain of neuromodulin, a neurospecific calmodulin-binding protein." J Biol Chem **263**(16): 7544-9.

Altschul, S. F., Gish, W., Miller, W., Myers, E. W. and Lipman, D. J. (1990). "Basic local alignment search tool." J Mol Biol **215**(3): 403-10.

Altschul, S. F., Madden, T. L., Schaffer, A. A., Zhang, J., Zhang, Z., Miller, W. and Lipman, D. J. (1997). "Gapped BLAST and PSI-BLAST: a new generation of protein database search programs." Nucleic Acids Res **25**(17): 3389-402.

An, R. H., Wang, X. L., Kerem, B., Benhorin, J., Medina, A., Goldmit, M. and Kass, R. S. (1998). "Novel LQT-3 mutation affects Na+ channel activity through interactions between alpha- and beta1-subunits." Circ Res **83**(2): 141-6.

Andersson, M., Malmendal, A., Linse, S., Ivarsson, I., Forsen, S. and Svensson, L. A. (1997). "Structural basis for the negative allostery between Ca(2+)- and Mg(2+)-binding in the intracellular Ca(2+)-receptor calbindin D9k." Protein Sci **6**(6): 1139-47.

Andre, I. and Linse, S. (2002). "Measurement of Ca2+-binding constants of proteins and presentation of the CaLigator software." Anal Biochem **305**(2): 195-205.

Babitch, J. (1990). "Channel hands." Nature **346**(6282): 321-2.

Bahler, M. and Rhoads, A. (2002). "Calmodulin signaling via the IQ motif." FEBS Letters **513**(1): 107.

Balser, J. R. (2001). "The cardiac sodium channel: gating function and molecular pharmacology." J Mol Cell Cardiol **33**(4): 599-613.

Bao, L., Kaldany, C., Holmstrand, E. C. and Cox, D. H. (2004). "Mapping the BKCa channel's "Ca2+ bowl": side-chains essential for Ca2+ sensing." J Gen Physiol **123**(5): 475-89.

Benhorin, J., Goldmit, M., MacCluer, J. W., Blangero, J., Goffen, R., Leibovitch, A., Rahat, A., Wang, Q., Medina, A., Towbin, J. and Kerem, B. (1998). "Identification of a new SCN5A mutation, D1840G, associated with the long QT syndrome. Mutations in brief no. 153. Online." Hum Mutat **12**(1): 72.

Bennett, P. B., Yazawa, K., Naomasa, M. and George, A. L. (1995). "Molecular mechanism for an inherited cardiac arrhythmia." Nature **376**: 683-685.

Berridge, M. J. (1997). "Elementary and global aspects of calcium signalling." J Physiol **499 (Pt 2)**: 291-306.

Bers, D. M. (2004). "Macromolecular complexes regulating cardiac ryanodine receptor function." J Mol Cell Cardiol **37**(2): 417-29.

Bers, D. M., Patton, C. W. and Nuccitelli, R. (1994). "A practical guide to the preparation of Ca2+ buffers." Methods in Cell Biology **40**: 3-29.

Bezanilla, F. (2005). "The voltage-sensor structure in a voltage-gated channel." Trends Biochem Sci **30**(4): 166-8.

Bezzina, C., Veldkamp, M. W., van Den Berg, M. P., Postma, A. V., Rook, M. B., Viersma, J. W., van Langen, I. M., Tan-Sindhunata, G., Bink-Boelkens, M. T., van Der Hout, A. H., Mannens, M. M. and Wilde, A. A. (1999). "A single Na(+)

channel mutation causing both long-QT and Brugada syndromes." <u>Circ Res</u> **85**(12): 1206-13.

Bond, C. T., Maylie, J. and Adelman, J. P. (2005). "SK channels in excitability, pacemaking and synaptic integration." <u>Curr Opin Neurobiol</u> **15**(3): 305-11.

Braveny, P. (2002). "Heart, calcium and time." <u>Experimental and Clinical Cardiology</u> **7**(1): 111-178.

Brayden, J. E. and Nelson, M. T. (1992). "Regulation of arterial tone by activation of calcium-dependent potassium channels." <u>Science</u> **256**(5056): 532-5.

Bunick, C. G., Nelson, M. R., Mangahas, S., Hunter, M. J., Sheehan, J. H., Mizoue, L. S., Bunick, G. J. and Chazin, W. J. (2004). "Designing sequence to control protein function in an EF-hand protein." <u>J Am Chem Soc</u> **126**(19): 5990-8.

Cabral, C. M., Choudhury, P., Liu, Y. and Sifers, R. N. (2000). "Processing by endoplasmic reticulum mannosidases partitions a secretion-impaired glycoprotein into distinct disposal pathways." <u>J Biol Chem</u> **275**(32): 25015-22.

Catterall, W. A., Goldin, A. L. and Waxman, S. G. (2003). "International Union of Pharmacology. XXXIX. Compendium of voltage-gated ion channels: sodium channels." <u>Pharmacol Rev</u> **55**(4): 575-8.

Cavanagh, J. (1996). <u>Protein NMR spectroscopy: principles and practice</u>. San Diego, Academic Press.

Celio, M. R., Pauls, T. L. and Schwaller, B. (1996). <u>Guidebook to the calcium-binding proteins</u>. Oxford; New York, Sambrook & Tooze Publication at Oxford University Press.

Chen, Q., Kirsch, G. E., Zhang, D., Brugada, R., Brugada, J., Brugada, P., Potenza, D., Moya, A., Borggrefe, M., Breithardt, G., Ortiz-Lopez, R., Wang, Z., Antzelevitch, C., O'Brien, R. E., Schulze-Bahr, E., Keating, M. T., Towbin, J. A. and Wang, Q. (1998). "Genetic basis and molecular mechanism for idiopathic ventricular fibrillation." <u>Nature</u> **392**: 293-296.

Cheney, R. E. and Mooseker, M. S. (1992). "Unconventional myosins." <u>Curr Opin Cell Biol</u> **4**(1): 27-35.

Chou, C. L., Yip, K. P., Michea, L., Kador, K., Ferraris, J. D., Wade, J. B. and Knepper, M. A. (2000). "Regulation of aquaporin-2 trafficking by vasopressin in the renal

collecting duct. Roles of ryanodine-sensitive Ca2+ stores and calmodulin." <u>J Biol Chem</u> **275**(47): 36839-46.

Cormier, J. W., Rivolta, I., Tateyama, M., Yang, A.-S. and Kass, R. S. (2002a). "Secondary structure of the human cardiac Na+ channel C terminus: evidence for a role of helical structures in modulation of channel inactivation." <u>Journal of Biological Chemistry</u> **277**: 9233-9241.

Cormier, J. W., Rivolta, I., Tateyama, M., Yang, A. S. and Kass, R. S. (2002b). "Secondary structure of the human cardiac Na+ channel C terminus: evidence for a role of helical structures in modulation of channel inactivation." <u>J Biol Chem</u> **277**(11): 9233-41.

Cox, D. H. (2005). "The BKCa channel's Ca2+-binding sites, multiple sites, multiple ions." <u>J Gen Physiol</u> **125**(3): 253-5.

Cuello, L. G., Cortes, D. M. and Perozo, E. (2004). "Molecular architecture of the KvAP voltage-dependent K+ channel in a lipid bilayer." <u>Science</u> **306**(5695): 491-5.

de Leon, M., Wang, Y., Jones, L., Perez-Reyes, E., Wei, X., Soong, T. W., Snutch, T. P. and Yue, D. T. (1995). "Essential Ca(2+)-binding motif for Ca(2+)-sensitive inactivation of L-type Ca2+ channels." <u>Science</u> **270**(5241): 1502-6.

Deschenes, I., Neyroud, N., DiSilvestre, D., Marban, E., Yue, D. T. and Tomaselli, G. F. (2002a). "Isoform-specific modulation of voltage-gated Na(+) channels by calmodulin." <u>Circ Res</u> **90**(4): E49-57.

Deschenes, I., Neyroud, N., DiSilvestre, D., Marban, E., Yue, D. T. and Tomaselli, G. F. (2002b). "Isoform-specific modulation of voltage-gated Na(+) channels by calmodulin." <u>Circulation Research</u> **90**(4): E49-57.

Drake, S. K., Zimmer, M. A., Kundrot, C. and Falke, J. J. (1997). "Molecular tuning of an EF-hand-like calcium binding loop. Contributions of the coordinating side chain at loop position 3." <u>J Gen Physiol</u> **110**(2): 173-84.

Dumaine, R., Wang, Q., Keating, M. T., Hartmann, H. A., Schwartz, P. J., Brown, A. M. and Kirsch, G. E. (1996). "Multiple mechanisms of Na$^+$ channel-linked long-QT syndrome." <u>Circulation Research</u> **78**: 916-924.

Echt, D. S., Liebson, P. R., Mitchell, L. B., Peters, R. W., Obias-Manno, D., Barker, A. H., Arensberg, D., Baker, A., Friedman, L., Greene, H. L., Huther, M. L., Richardson, D. W. and Investigators, t. C. (1991). "Mortality and morbidity in pa-

tients receiving encainide, flecainide, or placebo." <u>The New England Journal of Medicine</u> **324**: 781-788.

Erickson, M. G., Liang, H., Mori, M. X. and Yue, D. T. (2003). "FRET two-hybrid mapping reveals function and location of L-type Ca2+ channel CaM preassociation." <u>Neuron</u> **39**(1): 97-107.

Franzini-Armstrong, C., Protasi, F. and Ramesh, V. (1999). "Shape, size, and distribution of Ca(2+) release units and couplons in skeletal and cardiac muscles." <u>Biophys J</u> **77**(3): 1528-39.

Gee, S. H., Madhavan, R., Levinson, S. R., Caldwell, J. H., Sealock, R. and Froehner, S. C. (1998). "Interaction of muscle and brain sodium channels with multiple members of the syntrophin family of dystrophin-associated proteins." <u>J Neurosci</u> **18**(1): 128-37.

Goddard, T. D. and Kneller, D. G. Sparky 3. University of California, San Francisco.

Goldin, A. L. (2003). "Mechanisms of sodium channel inactivation." <u>Curr Opin Neurobiol</u> **13**(3): 284-90.

Haiech, J., Klee, C. B. and Demaille, J. G. (1981). "Effects of cations on affinity of calmodulin for calcium: ordered binding of calcium ions allows the specific activation of calmodulin-stimulated enzymes." <u>Biochemistry</u> **20**(13): 3890-7.

Hamada, T., Sakube, Y., Ahnn, J., Kim do, H. and Kagawa, H. (2002). "Molecular dissection, tissue localization and Ca2+ binding of the ryanodine receptor of Caenorhabditis elegans." <u>J Mol Biol</u> **324**(1): 123-35.

Henikoff, S., Greene, E. A., Pietrokovski, S., Bork, P., Attwood, T. K. and Hood, L. (1997). "Gene families: the taxonomy of protein paralogs and chimeras." <u>Science</u> **278**(5338): 609-14.

Herzog, R. I., Liu, C., Waxman, S. G. and Cummins, T. R. (2003). "Calmodulin binds to the C terminus of sodium channels Nav1.4 and Nav1.6 and differentially modulates their functional properties." <u>J Neurosci</u> **23**(23): 8261-70.

Hille, B. (1992). <u>Ionic channels of excitable membranes</u>. Sunderland, Mass., Sinauer Associates.

Hodgkin, A. L. and Huxley, A. F. (1952a). "The components of membrane conductance in the giant axon of *Loligo*." <u>*J Physiol*</u> **116**: 473-496.

Hodgkin, A. L. and Huxley, A. F. (1952b). "Currents carried by sodium and potassium ions through the membrane of the giant axon of *Loligo*." <u>J Physiol</u> **116**: 449-472.

Ikura, M., Kay, L. E. and Bax, A. (1990). "A novel approach for sequential assignment of 1H, 13C, and 15N spectra of proteins: heteronuclear triple-resonance three-dimensional NMR spectroscopy. Application to calmodulin." <u>Biochemistry</u> **29**(19): 4659-67.

Innamorati, G., Sadeghi, H., Eberle, A. N. and Birnbaumer, M. (1997). "Phosphorylation of the V2 vasopressin receptor." <u>J Biol Chem</u> **272**(4): 2486-92.

Innamorati, G., Sadeghi, H. M., Tran, N. T. and Birnbaumer, M. (1998). "A serine cluster prevents recycling of the V2 vasopressin receptor." <u>Proc Natl Acad Sci U S A</u> **95**(5): 2222-6.

Ishida, H., Nakashima, K., Kumaki, Y., Nakata, M., Hikichi, K. and Yazawa, M. (2002). "1H, 15N and 13C resonance assignments of yeast Saccharomyces cerevisiae calmodulin in the Ca2+-free state." <u>J Biomol NMR</u> **23**(4): 323-4.

Jiang, Y., Lee, A., Chen, J., Ruta, V., Cadene, M., Chait, B. T. and MacKinnon, R. (2003). "X-ray structure of a voltage-dependent K+ channel." <u>Nature</u> **423**(6935): 33-41.

Jiang, Y., Ruta, V., Chen, J., Lee, A. and MacKinnon, R. (2003). "The principle of gating charge movement in a voltage-dependent K+ channel." <u>Nature</u> **423**(6935): 42-8.

Jones, D. T., Taylor, W. R. and Thornton, J. M. (1992). "A new approach to protein fold recognition." <u>Nature</u> **358**(6381): 86-9.

Jurado, L. A., Chockalingam, P. S. and Jarrett, H. W. (1999). "Apocalmodulin." <u>Physiol. Rev.</u> **79**(3): 661-682.

Kass, R. S. and Moss, A. J. (2003). "Long QT syndrome: novel insights into the mechanisms of cardiac arrhythmias." <u>J Clin Invest</u> **112**(6): 810-5.

Keen, J. E., Khawaled, R., Farrens, D. L., Neelands, T., Rivard, A., Bond, C. T., Janowsky, A., Fakler, B., Adelman, J. P. and Maylie, J. (1999). "Domains responsible for constitutive and Ca(2+)-dependent interactions between calmodulin and small conductance Ca(2+)-activated potassium channels." <u>J Neurosci</u> **19**(20): 8830-8.

Kim, D., Lewis, D. L., Graziadei, L., Neer, E. J., Bar-Sagi, D. and Clapham, D. E. (1989). "G-protein beta gamma-subunits activate the cardiac muscarinic K+-channel via phospholipase A2." <u>Nature</u> **337**(6207): 557-60.

Kim, J., Ghosh, S., Liu, H., Tateyama, M., Kass, R. S. and Pitt, G. S. (2004). "Calmodulin mediates Ca2+ sensitivity of sodium channels." <u>J Biol Chem</u> **279**(43): 45004-12.

Kim, J., Ghosh, S., Nunziato, D. A. and Pitt, G. S. (2004). "Identification of the components controlling inactivation of voltage-gated Ca2+ channels." <u>Neuron</u> **41**(5): 745-54.

Kretsinger, R. H. and Nockolds, C. E. (1973). "Carp Muscle Calcium-binding Protein. II. STRUCTURE DETERMINATION AND GENERAL DESCRIPTION." <u>J. Biol. Chem.</u> **248**(9): 3313-3326.

Kurachi, Y., Ito, H., Sugimoto, T., Shimizu, T., Miki, I. and Ui, M. (1989). "Arachidonic acid metabolites as intracellular modulators of the G protein-gated cardiac K+ channel." <u>Nature</u> **337**(6207): 555-7.

Laskowski, R., McArthur, M., Moss, D. and Thornton, J. (1993). "PROCHECK: A program to check the stereochemical quality of protein structures." <u>Journal of Applied Crystallography</u> **26**: 283-291.

Lemaillet, G., Walker, B. and Lambert, S. (2003). "Identification of a conserved ankyrin-binding motif in the family of sodium channel alpha subunits." <u>J Biol Chem</u> **278**(30): 27333-9.

Levine, S. D., Kachadorian, W. A., Levin, D. N. and Schlondorff, D. (1981). "Effects of trifluoperazine on function and structure of toad urinary bladder. Role of calmodulin vasopressin-stimulation of water permeability." <u>J Clin Invest</u> **67**(3): 662-72.

Lewit-Bentley, A. and Rety, S. (2000). "EF-hand calcium-binding proteins." <u>Curr Opin Struct Biol</u> **10**(6): 637-43.

Li, H., Fuentes-Garcia, J. and Towbin, J. A. (2000). "Current concepts in long QT syndrome." <u>Pediatr Cardiol</u> **21**(6): 542-50.

Linse, S. and Forsen, S. (1995). "Determinants that govern high-affinity calcium binding." <u>Adv Second Messenger Phosphoprotein Res</u> **30**: 89-151.

Liu, C., Dib-Hajj, S. D. and Waxman, S. G. (2001). "Fibroblast growth factor homologous factor 1B binds to the C terminus of the tetrodotoxin-resistant sodium channel rNav1.9a (NaN)." J Biol Chem **276**(22): 18925-33.

Liu, C. J., Dib-Hajj, S. D., Renganathan, M., Cummins, T. R. and Waxman, S. G. (2003). "Modulation of the cardiac sodium channel Nav1.5 by fibroblast growth factor homologous factor 1B." J Biol Chem **278**(2): 1029-36.

Livingstone, C. D. and Barton, G. J. (1993). "Protein sequence alignments: a strategy for the hierarchical analysis of residue conservation." Comput Appl Biosci **9**(6): 745-56.

Lorenz, D., Krylov, A., Hahm, D., Hagen, V., Rosenthal, W., Pohl, P. and Maric, K. (2003). "Cyclic AMP is sufficient for triggering the exocytic recruitment of aquaporin-2 in renal epithelial cells." EMBO Rep **4**(1): 88-93.

Martonosi, A. N. and Pikula, S. (2003). "The network of calcium regulation in muscle." Acta Biochim Pol **50**(1): 1-30.

Marx, S. O., Gaburjakova, J., Gaburjakova, M., Henrikson, C., Ondrias, K. and Marks, A. R. (2001). "Coupled gating between cardiac calcium release channels (ryanodine receptors)." Circ Res **88**(11): 1151-8.

McPhee, J. C., Ragsdale, D. S., Scheuer, T. and Catterall, W. A. (1994). "A mutation in segment IVS6 disrupts fast inactivation of sodium channels." Proc Natl Acad Sci U S A **91**(25): 12346-50.

McPhee, J. C., Ragsdale, D. S., Scheuer, T. and Catterall, W. A. (1995). "A critical role for transmembrane segment IVS6 of the sodium channel alpha subunit in fast inactivation." J Biol Chem **270**(20): 12025-34.

Moczydlowski, E. G. (2004). "BK channel news: full coverage on the calcium bowl." J Gen Physiol **123**(5): 471-3.

Mohler, P. J., Rivolta, I., Napolitano, C., LeMaillet, G., Lambert, S., Priori, S. G. and Bennett, V. (2004). "Nav1.5 E1053K mutation causing Brugada syndrome blocks binding to ankyrin-G and expression of Nav1.5 on the surface of cardiomyocytes." Proc Natl Acad Sci U S A **101**(50): 17533-8.

Mori, M., Konno, T., Morii, T., Nagayama, K. and Imoto, K. (2003). "Regulatory interaction of sodium channel IQ-motif with calmodulin C-terminal lobe." Biochem Biophys Res Commun **307**(2): 290-6.

Motoike, H. K., Liu, H., Glaaser, I. W., Yang, A. S., Tateyama, M. and Kass, R. S. (2004). "The Na+ channel inactivation gate is a molecular complex: a novel role of the COOH-terminal domain." J Gen Physiol **123**(2): 155-65.

Naccarelli, G. V., Antzelevitch, C., Wolbrette, D. L. and Luck, J. C. (2002). "The Brugada syndrome." Curr Opin Cardiol **17**(1): 19-23.

Nelson, M. R. and Chazin, W. J. (1998). "Structures of EF-hand Ca(2+)-binding proteins: diversity in the organization, packing and response to Ca2+ binding." Biometals **11**(4): 297-318.

Nelson, M. R. and Chazin, W. J. (2005). "The CaBP data library. Calmodulin." from http://structbio.vanderbilt.edu/cabp_database/general/prot_pages/calmod.html.

Nelson, M. R., Thulin, E., Fagan, P. A., Forsen, S. and Chazin, W. J. (2002). "The EF-hand domain: a globally cooperative structural unit." Protein Sci **11**(2): 198-205.

Nickols, H. H., Shah, V. N., Chazin, W. J. and Limbird, L. E. (2004). "Calmodulin interacts with the V2 vasopressin receptor: elimination of binding to the C terminus also eliminates arginine vasopressin-stimulated elevation of intracellular calcium." J Biol Chem **279**(45): 46969-80.

Olsen, S. K., Garbi, M., Zampieri, N., Eliseenkova, A. V., Ornitz, D. M., Goldfarb, M. and Mohammadi, M. (2003). "Fibroblast growth factor (FGF) homologous factors share structural but not functional homology with FGFs." J Biol Chem **278**(36): 34226-36.

Ou, Y., Strege, P., Miller, S. M., Makielski, J., Ackerman, M., Gibbons, S. J. and Farrugia, G. (2003). "Syntrophin gamma 2 regulates SCN5A gating by a PDZ domain-mediated interaction." J Biol Chem **278**(3): 1915-23.

Peterson, B. Z., Lee, J. S., Mulle, J. G., Wang, Y., de Leon, M. and Yue, D. T. (2000). "Critical determinants of Ca(2+)-dependent inactivation within an EF-hand motif of L-type Ca(2+) channels." Biophys J **78**(4): 1906-20.

Piskorowski, R. and Aldrich, R. W. (2002). "Calcium activation of BK(Ca) potassium channels lacking the calcium bowl and RCK domains." Nature **420**(6915): 499-502.

Pitt, G. S., Zuhlke, R. D., Hudmon, A., Schulman, H., Reuter, H. and Tsien, R. W. (2001). "Molecular basis of calmodulin tethering and Ca2+-dependent inactivation of L-type Ca2+ channels." J Biol Chem **276**(33): 30794-802.

Putkey, J. A., Kleerekoper, Q., Gaertner, T. R. and Waxham, M. N. (2003). "A New Role for IQ Motif Proteins in Regulating Calmodulin Function." J. Biol. Chem. **278**(50): 49667-49670.

Quinton, P. M. (1990). "Cystic fibrosis: a disease in electrolyte transport." Faseb J **4**(10): 2709-17.

Robitaille, R., Garcia, M. L., Kaczorowski, G. J. and Charlton, M. P. (1993). "Functional colocalization of calcium and calcium-gated potassium channels in control of transmitter release." Neuron **11**(4): 645-55.

Rohl, C. A., Boeckman, F. A., Baker, C., Scheuer, T., Catterall, W. A. and Klevit, R. E. (1999). "Solution structure of the sodium channel inactivation gate." Biochemistry **38**(3): 855-61.

Rougier, J. S., van Bemmelen, M. X., Bruce, M. C., Jespersen, T., Gavillet, B., Apotheloz, F., Cordonier, S., Staub, O., Rotin, D. and Abriel, H. (2005). "Molecular determinants of voltage-gated sodium channel regulation by the Nedd4/Nedd4-like proteins." Am J Physiol Cell Physiol **288**(3): C692-701.

Samso, M. and Wagenknecht, T. (2002). "Apocalmodulin and Ca2+-calmodulin bind to neighboring locations on the ryanodine receptor." J Biol Chem **277**(2): 1349-53.

Schulein, R., Hermosilla, R., Oksche, A., Dehe, M., Wiesner, B., Krause, G. and Rosenthal, W. (1998). "A dileucine sequence and an upstream glutamate residue in the intracellular carboxyl terminus of the vasopressin V2 receptor are essential for cell surface transport in COS.M6 cells." Mol Pharmacol **54**(3): 525-35.

Schumacher, M. A., Crum, M. and Miller, M. C. (2004). "Crystal structures of apocalmodulin and an apocalmodulin/SK potassium channel gating domain complex." Structure (Camb) **12**(5): 849-60.

Schumacher, M. A., Rivard, A. F., Bachinger, H. P. and Adelman, J. P. (2001). "Structure of the gating domain of a Ca2+-activated K+ channel complexed with Ca2+/calmodulin." Nature **410**(6832): 1120-4.

Sharma, M. R., Penczek, P., Grassucci, R., Xin, H. B., Fleischer, S. and Wagenknecht, T. (1998). "Cryoelectron microscopy and image analysis of the cardiac ryanodine receptor." J Biol Chem **273**(29): 18429-34.

Shaw, G. S., Hodges, R. S. and Sykes, B. D. (1990). "Calcium-induced peptide association to form an intact protein domain: 1H NMR structural evidence." Science **249**(4966): 280-3.

Shaw, R. M. and Rudy, Y. (1997). "Electrophysiologic effects of acute myocardial ischemia. A mechanistic investigation of action potential conduction and conduction failure." <u>Circ Res</u> **80**(1): 124-38.

Skelton, N. J., Akke, M., Kordel, J., Thulin, E., Forsen, S. and Chazin, W. J. (1992). "15N NMR assignments and chemical shift analysis of uniformly labeled 15N calbindin D9k in the apo, (Cd2+)1 and (Ca2+)2 states." <u>FEBS Lett</u> **303**(2-3): 136-40.

Soss, M. (2002). Rotamer exploration and prediction. <u>J. Chem. Comp. Grp.</u> http://www.chemcomp.com/feature/rotexpl.htm.

Sperelakis, N. (2001). <u>Cell physiology sourcebook: a molecular approach</u>. San Diego, Academic Press.

Staub, O., Dho, S., Henry, P., Correa, J., Ishikawa, T., McGlade, J. and Rotin, D. (1996). "WW domains of Nedd4 bind to the proline-rich PY motifs in the epithelial Na+ channel deleted in Liddle's syndrome." <u>Embo J</u> **15**(10): 2371-80.

Stocker, M. (2004). "Ca(2+)-activated K+ channels: molecular determinants and function of the SK family." <u>Nat Rev Neurosci</u> **5**(10): 758-70.

Strynadka, N. C. and James, M. N. (1989). "Crystal structures of the helix-loop-helix calcium-binding proteins." <u>Annu Rev Biochem</u> **58**: 951-98.

Takeuchi, A. and Takeuchi, N. (1960). "On the permeability of end-plate membrane during the action of transmitter." <u>J Physiol (Paris)</u> **154**: 52-67.

Takeuchi, N. (1963a). "Effects of calcium on the conductance change of the end-plate membrane during the action of transmitter." <u>J Physiol</u> **167**: 141-55.

Takeuchi, N. (1963b). "Some properties of conductance changes at the end-plate membrane during the action of acetylcholine." <u>J Physiol</u> **167**: 128-40.

Tamargo, J., Caballero, R., Gomez, R., Valenzuela, C. and Delpon, E. (2004). "Pharmacology of cardiac potassium channels." <u>Cardiovasc Res</u> **62**(1): 9-33.

Tan, H. L., Bink-Boelkens, M. T., Bezzina, C. R., Viswanathan, P. C., Beaufort-Krol, G. C., van Tintelen, P. J., van den Berg, M. P., Wilde, A. A. and Balser, J. R. (2001). "A sodium-channel mutation causes isolated cardiac conduction disease." <u>Nature</u> **409**(6823): 1043-7.

Tan, H. L., Kupershmidt, S., Zhang, R., Stepanovic, S., Roden, D. M., Wilde, A. A., Anderson, M. E. and Balser, J. R. (2002a). "A calcium sensor in the sodium channel modulates cardiac excitability." Nature **415**(6870): 442-7.

Tan, H. L., Kupershmidt, S., Zhang, R., Stepanovic, S., Roden, D. M., Wilde, A. A., Anderson, M. E. and Balser, J. R. (2002b). "A calcium sensor in the sodium channel modulates cardiac excitability." Nature **415**(6870): 442-7.

Tateyama, M., Rivolta, I., Clancy, C. E. and Kass, R. S. (2003). "Modulation of cardiac sodium channel gating by protein kinase A can be altered by disease-linked mutation." J Biol Chem **18**: 18.

Tsien, R. Y. (1980). "New calcium indicators and buffers with high selectivity against magnesium and protons: design, synthesis, and properties of prototype structures." Biochemistry **19**(11): 2396-404.

van Balkom, B. W., Savelkoul, P. J., Markovich, D., Hofman, E., Nielsen, S., van der Sluijs, P. and Deen, P. M. (2002). "The role of putative phosphorylation sites in the targeting and shuttling of the aquaporin-2 water channel." J Biol Chem **277**(44): 41473-9.

van Bemmelen, M. X., Rougier, J. S., Gavillet, B., Apotheloz, F., Daidie, D., Tateyama, M., Rivolta, I., Thomas, M. A., Kass, R. S., Staub, O. and Abriel, H. (2004). "Cardiac voltage-gated sodium channel Nav1.5 is regulated by Nedd4-2 mediated ubiquitination." Circ Res **95**(3): 284-91.

Vander kooi, C. (2004). Structural basis for Prp19 function in ubiquitination and RNA splicing. Biochemistry. Nashville, TN, Vanderbilt University. **PhD:** 116.

VanScyoc, W. S., Sorensen, B. R., Rusinova, E., Laws, W. R., Ross, J. B. and Shea, M. A. (2002). "Calcium binding to calmodulin mutants monitored by domain-specific intrinsic phenylalanine and tyrosine fluorescence." Biophys J **83**(5): 2767-80.

Veldkamp, M. W., Viswanathan, P. C., Bezzina, C., Baartscheer, A., Wilde, A. A. and Balser, J. R. (2000). "Two distinct congenital arrhythmias evoked by a multidysfunctional Na(+) channel." Circ Res **86**(9): E91-7.

Vergara, C., Latorre, R., Marrion, N. V. and Adelman, J. P. (1998). "Calcium-activated potassium channels." Curr Opin Neurobiol **8**(3): 321-9.

Vogel, H. J., Lindahl, L. and Thulin, E. (1983). "Calcium-dependent hydrophobic interaction chromatography of calmodulin, troponin C and their proteolytic fragments." FEBS Lett **157**(2): 241-246.

Wagenknecht, T. and Samso, M. (2002). "Three-dimensional reconstruction of ryanodine receptors." <u>Front Biosci</u> **7**: d1464-74.

Wang, D. W., Yazawa, K., George, A. L. and Bennett, P. B. (1996). "Characterization of human cardiac Na$^+$ channel mutations in the congenital long QT syndrome." <u>PNAS</u> **93**: 13200-13205.

Wang, S. Y. and Wang, G. K. (2003). "Voltage-gated sodium channels as primary targets of diverse lipid-soluble neurotoxins." <u>Cell Signal</u> **15**(2): 151-9.

Wehrens, X. H., Abriel, H., Cabo, C., Benhorin, J. and Kass, R. S. (2000). "Arrhythmogenic mechanism of an LQT-3 mutation of the human heart Na(+) channel alpha-subunit: A computational analysis." <u>Circulation</u> **102**(5): 584-90.

Wei, A., Solaro, C., Lingle, C. and Salkoff, L. (1994). "Calcium sensitivity of BK-type KCa channels determined by a separable domain." <u>Neuron</u> **13**(3): 671-81.

Wei, J., Wang, D. W., Alings, M., Fish, F., Wathen, M., Roden, D. M. and George, A. L., Jr. (1999). "Congenital long-QT syndrome caused by a novel mutation in a conserved acidic domain of the cardiac Na+ channel." <u>Circulation</u> **99**(24): 3165-71.

West, J. W., Patton, D. E., Scheuer, T., Wang, Y., Goldin, A. L. and Catterall, W. A. (1992). "A cluster of hydrophobic amino acid residues required for fast Na(+)-channel inactivation." <u>Proc Natl Acad Sci U S A</u> **89**(22): 10910-4.

Wingo, T. L., Shah, V. N., Anderson, M. E., Lybrand, T. P., Chazin, W. J. and Balser, J. R. (2004). "An EF-hand in the sodium channel couples intracellular calcium to cardiac excitability." <u>Nat Struct Mol Biol</u> **11**(3): 219-25.

Xiong, L., Kleerekoper, Q. K., He, R., Putkey, J. A. and Hamilton, S. L. (2005). "Sites on calmodulin that interact with the C-terminal tail of Cav1.2 channel." <u>J Biol Chem</u> **280**(8): 7070-9.

Xu, W., Liu, Y., Wang, S., McDonald, T., Van Eyk, J. E., Sidor, A. and O'Rourke, B. (2002). "Cytoprotective role of Ca2+- activated K+ channels in the cardiac inner mitochondrial membrane." <u>Science</u> **298**(5595): 1029-33.

Xu, Y., Tuteja, D., Zhang, Z., Xu, D., Zhang, Y., Rodriguez, J., Nie, L., Tuxson, H. R., Young, J. N., Glatter, K. A., Vazquez, A. E., Yamoah, E. N. and Chiamvimonvat, N. (2003). "Molecular identification and functional roles of a Ca(2+)-activated K+ channel in human and mouse hearts." <u>J Biol Chem</u> **278**(49): 49085-94.

Yang, W., Lee, H. W., Hellinga, H. and Yang, J. J. (2002). "Structural analysis, identification, and design of calcium-binding sites in proteins." <u>Proteins</u> **47**(3): 344-56.

Yip, K. P. (2002). "Coupling of vasopressin-induced intracellular Ca2+ mobilization and apical exocytosis in perfused rat kidney collecting duct." <u>J Physiol</u> **538**(Pt 3): 891-9.

Zhou, J., Olcese, R., Qin, N., Noceti, F., Birnbaumer, L. and Stefani, E. (1997). "Feedback inhibition of Ca2+ channels by Ca2+ depends on a short sequence of the C terminus that does not include the Ca2+ -binding function of a motif with similarity to Ca2+ -binding domains." <u>Proc Natl Acad Sci U S A</u> **94**(6): 2301-5.

Zhou, J., Shin, H. G., Yi, J., Shen, W., Williams, C. P. and Murray, K. T. (2002). "Phosphorylation and putative ER retention signals are required for protein kinase A-mediated potentiation of cardiac sodium current." <u>Circ Res</u> **91**(6): 540-6.

Zwerling, S. J., Cohen, S. A. and Barchi, R. L. (1991). "Analysis of protease-sensitive regions in the skeletal muscle sodium channel in vitro and implications for channel tertiary structure." <u>J. Biol. Chem.</u> **266**(7): 4574-4580.